Cut finite element methods

Erik Burman

Department of Mathematics, University College London,
London, WC1E 6BT, UK
E-mail: e.burman@ucl.ac.uk

Peter Hansbo

Department of Mechanical Engineering, Jönköping University,
551 11 Jönköping, Sweden
E-mail: peter.hansbo@ju.se

Mats G. Larson

Department of Mathematics and Mathematical Statistics, Umeå University,
90187 Umeå, Sweden
E-mail: mats.larson@umu.se

Sara Zahedi

Department of Mathematics, KTH Royal Institute of Technology,
100 44 Stockholm, Sweden
E-mail: sara.zahedi@math.kth.se

Cut finite element methods (CutFEM) extend the standard finite element method to unfitted meshes, enabling the accurate resolution of domain boundaries and interfaces without requiring the mesh to conform to them. This approach preserves the key properties and accuracy of the standard method while addressing challenges posed by complex geometries and moving interfaces.

In recent years, CutFEM has gained significant attention for its ability to discretize partial differential equations in domains with intricate geometries. This paper provides a comprehensive review of the core concepts and key developments in CutFEM, beginning with its formulation for common model problems and the presentation of fundamental analytical results, including error estimates and condition number estimates for the resulting algebraic systems. Stabilization techniques for cut elements, which ensure numerical robustness, are also explored. Finally, extensions to methods involving Lagrange multipliers and applications to time-dependent problems are discussed.

CONTENTS

1. Introduction

Accurate discretization of partial differential equations (PDEs) in complex geometries or domains with interfaces is crucial for many applications. For interface problems, the governing PDEs often involve material properties and solutions that vary across the interface. Interface conditions couple the solution on both sides, and in some cases an additional physical process at the interface is described by a surface PDE. In certain applications these interfaces may deform, requiring the PDE to be discretized on evolving domains. Examples of such interfaces or boundaries include cell membranes, interfaces between immiscible fluids, or fluid–solid interfaces, such as heart valves controlling blood flow, glaciers, or an aeroplane wing undergoing shape optimization.

The standard finite element method requires boundary-conforming meshes to perform optimally when essential boundary conditions are present. However, for complex or deforming geometries, the mesh generation can be cumbersome. Therefore, discretizations that perform optimally, regardless of the position of the boundary relative to the computational mesh, are highly desirable. In such discretizations, the physical domain defined by complex geometries or interfaces is embedded within a computational domain that is easy to mesh, with the representation of the boundary or the interface independent of the computational mesh on which the PDE is discretized. Hence, regular meshes such as Cartesian grids, which are simple to generate, can be used for the discretization of the PDEs. While this simplifies mesh generation, it is not straightforward to accurately impose essential boundary and interface conditions on unfitted meshes, integrate on elements cut by the boundary, and ensure the stability and well-conditioning of the resulting linear systems. The standard finite element method requires boundary-conforming meshes to perform optimally when essential boundary conditions are present. Early examples of unfitted discretizations include the following: the immersed boundary method (McCracken and Peskin 1980, Peskin 2002), where interface conditions are

incorporated as a source term in the PDE and discontinuities are regularized; the fictitious domain method (Glowinski, Pan and Périaux 1994, Girault and Glowinski 1995), which uses Lagrange multipliers to impose essential boundary conditions; the boundary penalty method (Barrett and Elliott 1986) and the volume penalty method (Maury 2009), where Dirichlet boundary conditions are imposed weakly, either by penalty terms directly on the boundary or within the volume.

Compared to the original immersed boundary method, which regularizes discontinuities in the solution and material parameters, the penalty method in Barrett and Elliott (1986) handles discontinuities by solving separate problems in each subdomain and enforcing the interface conditions via a penalty approach. In Barrett and Elliott (1986), optimal H^1-estimates are derived for linear elements. However, the L^2-estimates are suboptimal, and the condition number of the resulting linear system scales worse than that of standard FEM due to the choice of the penalty parameter.

A different viewpoint for improving accuracy in the presence of strong or weak discontinuities is to enrich the approximation space. Examples of such methods include the *extended finite element method* (XFEM, Moës, Dolbow and Belytschko 1999, Fries and Belytschko 2010), the *immersed finite element method* (IFEM, Zhang, Gerstenberger, Wang and Liu 2004) and the *cut finite element method* (CutFEM, Burman *et al.* 2015*b*). In XFEM, the approximation space is locally enriched to capture the discontinuity, with different enrichments for weak and strong discontinuities. In the immersed finite element method, special basis functions that satisfy the interface conditions are constructed on elements intersected by the interface.

In CutFEM, the requirement for conforming approximation spaces is released. Inspired by discontinuous Galerkin methods, the approximation space is enriched (independent of the type of discontinuity) on elements cut by the unfitted interface. This is achieved by defining active meshes that cover each subdomain separated by the interface, with finite element spaces defined on these active meshes. Interface conditions are imposed weakly, either using a consistent penalty method such as Nitsche's method (Nitsche 1971, Becker, Hansbo and Stenberg 2003, Hansbo and Hansbo 2002, Hansbo, Hansbo and Larson 2003, Hansbo and Hansbo 2004, Hansbo 2005) or through a Lagrange multiplier method (Burman and Hansbo 2010*a*). These methods are related, as shown by Stenberg (1995), where Nitsche's method is derived from a stabilized multiplier method.

Since the PDE is defined in the physical domain but the approximation space in CutFEM is defined on the active mesh (which may not conform to the physical domain), some control over the solution on the entire active mesh is desirable and often necessary. To prove stability, independent of the boundary's position relative to the computational mesh, stabilization terms are often added to the weak form. These stabilization terms also guarantee that the condition number of the linear system resulting from the cut finite element discretization scales similarly to that of the body-fitted discretization. For early contributions in this direction, see

e.g. Burman (2010), Burman and Hansbo (2012), Burman and Zunino (2012) and Wadbro, Zahedi, Kreiss and Berggren (2013).

Unfitted discretizations, depending on the relative position of the unfitted boundary to the computational mesh, can lead to severely ill-conditioned linear systems. In XFEM, strategies to address this include removing basis functions with very small support (Reusken 2008) and preconditioning (Lehrenfeld and Reusken 2017, Gross and Reusken 2023). In CutFEM, in addition to adding stabilization terms, other techniques have been employed, such as using agglomeration of elements or extension operators (Huang, Wu and Xiao 2017, Badia, Verdugo and Martín 2018, Burman, Hansbo and Larson 2022c), both aiming at extending the approximate solution from the interior of the domain to the cut elements. The idea of agglomerating elements for stability was first introduced in the context of unfitted discontinuous Galerkin methods by Johansson and Larson (2013).

Cut finite element discretizations require accurate integration on cut elements, and standard quadrature rules cannot be directly applied to such elements. When the unfitted boundary is represented piecewise linearly, integration on a cut element is straightforward. However, for high-order approximations of the geometry, several strategies exist. For example, when the boundary is implicitly defined by a level set function (Osher and Fedkiw 2001, Sethian 2001), high-order quadrature schemes on hyperrectangles, based on one-dimensional Gaussian quadrature rules, have been proposed by Saye (2015, 2022). Lehrenfeld (2016) introduced an algorithm based on an isoparametric mapping to perform integration on a piecewise linear approximation of the boundary. Another strategy, proposed in Burman, Hansbo and Larson (2018b) within the CutFEM framework, drawing on ideas from Bramble, Dupont and Thomée (1972), involves transforming the boundary condition at curved boundaries to conditions on a piecewise linear approximation of the boundary. Unfitted methods that avoid explicit integration on cut elements also exist. Examples include the *transfer path method* (Cockburn and Solano 2012), the *shifted boundary method* (Main and Scovazzi 2018) and ϕ-FEM (Duprez, Lleras and Lozinski 2023). In these methods, integration is not carried out on cut elements; instead, integration is performed on elements that are entirely inside the physical domain or on full elements that cover the physical domain. When boundary conditions are transferred from the physical boundary to the boundary of the computational mesh, there is often an underlying assumption regarding the rate at which the distance between the mesh boundary and the exact physical boundary should decrease.

Another unfitted discretization is the *finite cell method* (Parvizian, Düster and Rank 2007), where the equations are extended outside the physical domain using a scalar parameter that rapidly switches from being one in the physical domain to a small positive number in the fictitious domain. The choice of this parameter is a trade-off between accuracy and the condition number that can be tolerated. This extension, with the discontinuous parameter, introduces other challenges, such as accurate integration on cut elements. To reduce integration errors, all cells cut by

the unfitted boundary are adaptively refined, and integration is performed on the finer mesh. Dirichlet boundary conditions are enforced weakly, for example using Nitsche's method (Ruess *et al.* 2013).

The basic ideas of CutFEM. The basic ideas behind CutFEM can be summarized as follows.

- *Mesh.* The domain of interest is covered by an 'active mesh'. This active mesh is typically created by embedding the physical domain into a computational domain, which is equipped with a quasi-uniform mesh, referred to as the background mesh. The elements in the background mesh that intersect the domain of interest define the active mesh. For interface problems, a separate active mesh is associated with each subdomain.

- *Spaces.* Finite element spaces are defined on the active mesh.

- *Weak form.* Essential interface and boundary conditions are imposed weakly in the variational formulation, typically using either a consistent penalty method, such as Nitsche's method, or a Lagrange multiplier method.

- *Robustness with respect to the geometry's position relative to the mesh.* A common strategy for extending the control of the approximate solution from the physical domain (where the PDE is defined) to the active mesh is to add stabilization terms in the weak form. An alternative approach is to use extension operators. Agglomeration of elements can be used in combination with both stabilization and extension, or as an independent strategy. Preconditioning can be used to improve on the condition number of the linear systems.

- *Integration on cut elements.* When the unfitted boundary is represented by a piecewise linear approximation, integration is typically carried out on the cut elements. For higher-order approximations of the boundary, various strategies for handling the integration are available.

The same principles used for bulk domains can also be applied to approximating PDEs on interfaces or manifolds. This was first proposed by Olshanskii, Reusken and Grande (2009), and the method is referred to as the *trace finite element method* (TraceFEM), as detailed in Reusken (2015). The original contribution proposed an unstabilized unfitted discretization on the surface, but later work extended the method to elements cut by the surface by incorporating stabilization terms into the weak form. For stabilization terms specific to linear finite elements, see Burman, Hansbo and Larson (2015*c*) and Burman *et al.* (2016*b*). For stabilization terms that provide a uniform bound on the condition number even when higher-order elements are used, refer to Olshanskii and Reusken (2017), Zahedi (2017), Grande, Lehrenfeld and Reusken (2018), Burman, Hansbo, Larson and Massing (2018*c*) and Larson and Zahedi (2019).

The presented strategy applies to both stationary domains and evolving interfaces and boundaries; see e.g. Hansbo, Larson and Zahedi (2015a, 2016) and Lehrenfeld and Olshanskii (2019). In this paper we focus on model problems based on second-order elliptic PDEs. To keep the exposition concise, we discretize the equations using standard continuous finite elements away from the interface. However, the methods are largely agnostic to the choice of discretization in the bulk, and there is a large body of literature on unfitted methods based on the discontinuous Galerkin method; see e.g. Johansson and Larson (2013), Massjung (2012), Bastian and Engwer (2009), Burman and Ern (2018), Cangiani, Dong and Georgoulis (2021), Gürkan and Massing (2019), Burman, Hansbo, Larson and Massing (2017b) and Cangiani *et al.* (2021). There is also a host of work dedicated to first-order hyperbolic problems utilizing cut cells, usually employing finite volume or discontinuous Galerkin approaches.

Additional references and topics not covered in this review. There is a growing body of literature addressing both theoretical and applied aspects of cut finite element methods. A collection of articles on both theoretical and applied aspects was presented in Bordas, Burman, Larson and Olshanskii (2017). While a comprehensive discussion of all these developments is beyond the scope of the present review, we provide some pointers to works on various topics below.

- *Elliptic interface problems with high-order methods and geometry approximation.* See Huang *et al.* (2017), Ji, Wang and Chen (2017), Lehrenfeld and Reusken (2018), de Prenter, Lehrenfeld and Massing (2018), Wu and Xiao (2019) and Burman, Cicuttin, Delay and Ern (2021a).

- *A posteriori error estimation and adaptivity.* Discussed in Chen, Li and Xiang (2021), Burman, He and Larson (2022f), Chen and Liu (2023) and Chen and Liu (2024). Associated flux recovery techniques are covered in Capatina and He (2021) and Tchinda Ngueyong and Urquiza (2024).

- *Numerical integration on cut cells.* See Olshanskii and Safin (2016), Garhuom and Düster (2022) and Aulisa and Loftin (2023).

- *Efficient linear solvers.* Covered in Ludescher, Gross and Reusken (2020), Kothari and Krause (2022) and Gross and Reusken (2023).

- *Recent work on moving domains.* See Burman, Frei and Massing (2022b), Lou and Lehrenfeld (2022), von Wahl, Richter and Lehrenfeld (2022), Heimann, Lehrenfeld and Preuß (2023) and Badia, Martorell and Verdugo (2024).

- *Linear elasticity.* See Hansbo, Larson and Larsson (2017b) and Yang (2024).

- *Biharmonic problems, plates and higher order elliptic problems.* The boundary value problem was discussed in Burman, Hansbo and Larson (2020a) and Burman *et al.* (2022c) and the interface problem in Cai, Chen and Wang (2021).

- *Non-linear solid mechanics.* Covered in Badia, Caicedo, Martín and Principe (2021) and Poluektov and Figiel (2022).

- *Contact problems.* Discussed in Fabre, Pousin and Renard (2016), Burman and Hansbo (2017), Claus and Kerfriden (2018), Claus, Bigot and Kerfriden (2018) and Claus *et al.* (2021).

- *Incompressible flow problems with interfaces.* Covered in Court (2019), Cáceres, Guzmán and Olshanskii (2020), Burman, Delay and Ern (2021*b*), Olshanskii, Quaini and Sun (2021) and Garcke, Nürnberg and Zhao (2023). Other complex fluid models such as Oseen's equations, three-field Stokes' equations or non-Newtonian fluids, were considered in Burman, Claus and Massing (2015*a*), Massing, Schott and Wall (2018), Winter, Schott, Massing and Wall (2018), Ahlkrona and Elfverson (2021) and Anselmann and Bause (2022).

- *Fluid–structure interaction.* See Burman and Fernández (2014), Massing, Larson, Logg and Rognes (2015), Zonca, Vergara and Formaggia (2018), Schott, Ager and Wall (2019), Ager, Schott, Winter and Wall (2019), Fernández and Landajuela (2020), Dunn, Lui and Sarkis (2021), Fernández and Gerosa (2021), Liu (2021) and Burman, Fernández and Gerosa (2023*a*).

- *Shape and topology optimization.* Discussed in Burman *et al.* (2017*a*), Villanueva and Maute (2017), Bernland, Wadbro and Berggren (2018), Burman *et al.* (2019*a*), Dilgen, Jensen and Aage (2021), Dilgen *et al.* (2021) and Bretin, Chapelat, Outtier and Renard (2022).

- *Wave equations.* The scalar wave equation is considered in Sticko and Kreiss (2016, 2019), Burman, Hansbo and Larson (2022*d*) and Burman, Duran and Ern (2022*a*), the elastic wave equation in Sticko, Ludvigsson and Kreiss (2020), and Maxwell's equations in Guo, Lin and Zou (2023), Chen, Li, Lyu and Xiang (2024) and Yang and Xie (2024).

- *Mixed-dimensional problems, flow in fractures and in fractured porous media.* See Giovanardi, Formaggia, Scotti and Zunino (2017), Burman, Hansbo, Larson and Samvin (2019*c*), Odsæter, Kvamsdal and Larson (2019), Köppel, Martin, Jaffré and Roberts (2019*b*), Köppel, Martin and Roberts (2019*a*), Kerfriden, Claus and Mihai (2020), Burman, Hansbo and Larson (2020*b*) and Chernyshenko and Olshanskii (2020).

- *Solidification and phase change problems.* Discussed in Olshanskii, Palzhanov and Quaini (2023) and Tchinda Ngueyong, Urquiza and Martin (2024*a*,*b*).

- *Biomedical applications.* See Bui, Tomar and Bordas (2019), Farina *et al.* (2021) and Berre, Rognes and Massing (2024).

- *Inverse problems with interfaces.* Covered in Burman, He and Larson (2021*c*) and Burman and Preuss (2023).

- *Reduced order models and multiscale modelling.* See Karatzas, Nonino, Ballarin and Rozza (2022), Mikaeili, Claus and Kerfriden (2022) and Zhang, Deng and Wu (2024).

- *CutFEM/TraceFEM for surface PDE.* Discussed in Olshanskii and Reusken (2014), Hansbo, Larson and Zahedi (2015b), Cenanovic, Hansbo and Larson (2016), Olshanskii and Reusken (2017), Hansbo, Jonsson, Larson and Larsson (2017a), Jonsson, Larson and Larsson (2017), Olshanskii, Quaini, Reusken and Yushutin (2018), Hansbo, Larson and Larsson (2020), Olshanskii *et al.* (2023) and Fries and Kaiser (2023).

- *First-order hyperbolic problems.* See Berger (2017), May and Berger (2017), Engwer, May, Nüßing and Streitbürger (2020), Gürkan, Sticko and Massing (2020), Fu and Kreiss (2021) Fu, Frachon, Kreiss and Zahedi (2022), May and Laakmann (2024) and Fu, Kreiss and Zahedi (2024).

Outline. The paper is organized as follows. In Section 2 we introduce the basic concepts of CutFEM for several model problems of varying complexity. In Section 3 we present the basic analysis of CutFEM in a more abstract setting, discussing stability, convergence and conditioning of the discrete system. The analysis is then applied to the model problems. In Section 4 we explore different stabilization methods needed to control the conditioning of the discrete system; in Section 5 we give further details for the case of an embedded surface. In Section 6 we analyse strong stability through an extension procedure, where unstable degrees of freedom are eliminated, and show the connection to the weak stabilization methods introduced in Section 4. Section 7 focuses on Lagrange multiplier methods, and we demonstrate how stable and accurate methods can be developed within the CutFEM framework. In Section 8 we give further examples of problems addressed using Lagrange multipliers and discuss hybridization methods, leading back to the methods introduced in Section 2. Finally, in Section 9, we introduce CutFEM for time-dependent problems with moving domains.

2. CutFEM for basic model problems

In this section we construct cut finite element methods for stationary model problems. We consider several types of problems: a boundary value problem, an interface problem, an interface problem coupled with a surface PDE at the interface, and the Stokes equations.

2.1. A boundary value problem

The continuous problem. Let $\Omega \subset \mathbb{R}^d$ be a domain with a smooth boundary $\partial\Omega$, and let $u \colon \Omega \to \mathbb{R}$ be the solution to the boundary value problem

$$-\nabla \cdot (\alpha \nabla u) = f \quad \text{in } \Omega, \quad u = g \quad \text{on } \partial\Omega, \tag{2.1}$$
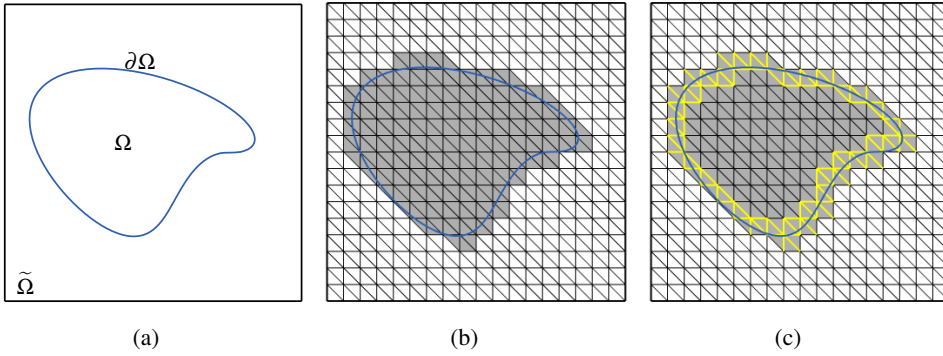
Figure 2.1. (a) The domain $\Omega \subset \mathbb{R}^2$ and the background domain $\widetilde{\Omega}$. (b) The background mesh $\widetilde{\mathcal{T}}_h$, the active mesh $\mathcal{T}_h$, (consisting of the grey triangles), and the active domain Ω_h (the grey region). (c) Edges marked in yellow illustrate the edges in the set $\mathcal{F}_h$, where the stabilization defined in equation (2.14) applies.

where $\alpha \in \mathbb{R}$ is a positive constant, and f and g are given functions. Typically, $d \in \{1, 2, 3\}$. The corresponding weak formulation is as follows: find $u \in V_g$ such that

$$a(u, v) = l(v) \quad \text{for all } v \in V_0, \tag{2.2}$$

where the forms are defined as

$$a(v, w) = (\alpha \nabla v, \nabla w)_\Omega, \quad l(v) = (f, v)_\Omega \tag{2.3}$$

with $(v, w)_\omega = \int_\omega vw$, equipped with the appropriate measure, and the spaces are

$$V_g = \{v \in H^1(\Omega) \mid v = g \text{ on } \partial\Omega\}, \quad V_0 = \{v \in H^1(\Omega) \mid v = 0 \text{ on } \partial\Omega\}. \tag{2.4}$$

Assume $f \in L^2(\Omega)$ and $g \in H^{1/2}(\partial\Omega)$. It follows from the Lax–Milgram lemma that there is a unique solution to the weak formulation (2.2).

The cut finite element method based on Nitsche's method. Let $\widetilde{\Omega} \subset \mathbb{R}^d$ be a polytopal domain such that $\Omega \subset \widetilde{\Omega}$, and let $\widetilde{\mathcal{T}}_h$ be a quasi-uniform partition of $\widetilde{\Omega}$ into shape-regular elements, with mesh parameter $h \in (0, h_0]$.

Let

$$\mathcal{T}_h = \{T \in \widetilde{\mathcal{T}}_h \mid T \cap \Omega \neq \emptyset\}, \quad \Omega_h = \bigcup_{T \in \mathcal{T}_h} T. \tag{2.5}$$

We refer to $\widetilde{\Omega}$ as the background domain, $\widetilde{\mathcal{T}}_h$ as the background mesh, $\mathcal{T}_h$ as the active mesh, and Ω_h as the active domain. Note that the background mesh is not required to conform to the domain Ω, meaning the boundary $\partial\Omega$ typically intersects the mesh elements, giving rise to so-called cut elements. An illustration for a domain $\Omega \subset \mathbb{R}^2$ is provided in Figure 2.1.

Let $V_h \subset C(\Omega_h)$ be a finite element space defined on the active mesh $\mathcal{T}_h$. To derive the method, we start from (2.1), multiply by $v \in V_h$, and apply Green's formula:

$$
\begin{aligned}
(f, v)_\Omega &= -(\nabla \cdot (\alpha \nabla u), v)_\Omega \\
&= (\alpha \nabla u, \nabla v)_\Omega - (n \cdot \alpha \nabla u, v)_{\partial\Omega} \\
&= (\alpha \nabla u, \nabla v)_\Omega - (n \cdot \alpha \nabla u, v)_{\partial\Omega} \\
&\quad \underbrace{- (u - g, n \cdot \alpha \nabla v)_{\partial\Omega}}_{=0} + \underbrace{\beta h^{-1}(u - g, v)_{\partial\Omega}}_{=0}, \quad (2.6)
\end{aligned}
$$

where we have added a symmetrizing term and a penalty term, both of which vanish for the exact solution and thus do not affect consistency. Here $\beta := \beta_0 \alpha$, with β_0 a dimensionless penalty parameter. This leads to the following Nitsche method: find $u_h \in V_h$ such that

$$
a_h(u_h, v) = l_h(v) \quad \text{for all } v \in V_h, \quad (2.7)
$$

where the forms are defined as

$$
\begin{aligned}
a_h(v, w) &= (\alpha \nabla v, \nabla w)_\Omega - (n \cdot \alpha \nabla v, w)_{\partial\Omega} \\
&\quad - (v, n \cdot \alpha \nabla w)_{\partial\Omega} + \beta h^{-1}(v, w)_{\partial\Omega}, \quad (2.8) \\
l_h(w) &= (f, w)_\Omega - (g, n \cdot \alpha \nabla w)_{\partial\Omega} + \beta h^{-1}(g, w)_{\partial\Omega}. \quad (2.9)
\end{aligned}
$$

To prove coercivity of the form a_h, we need the inverse inequality

$$
h^{1/2} \|\alpha^{1/2} \nabla v\|_{\partial\Omega} \lesssim \|\alpha^{1/2} \nabla v\|_\Omega, \quad v \in V_h. \quad (2.10)
$$

Here and below, we will use the notation $a \lesssim b$ to mean $a \leq cb$, with c being a constant independent of the mesh size h and the way the interface intersects the mesh. However, the bound (2.10) does not hold in general due to the presence of cut elements. This is because, for a cut element T, the intersection $T \cap \Omega$ can have an arbitrarily small measure in $\mathbb{R}^d$ while $|T \cap \partial\Omega| \propto h$, and the hidden constant in (2.10) depends on the ratio between these two measures. Therefore, to ensure coercivity, we assume the existence of a stabilizing form $s_h : V_h \times V_h \to \mathbb{R}$ such that

$$
h^{1/2} \|\alpha^{1/2} \nabla v\|_{\partial\Omega} \lesssim \|\alpha^{1/2} \nabla v\|_\Omega + \|\alpha^{1/2} v\|_{s_h}, \quad v \in V_h, \quad (2.11)
$$

where $\|v\|_{s_h}^2 = s_h(v, v)$. Thus we consider the following cut finite element method: find $u_h \in V_h$ such that

$$
A_h(u_h, v) = l_h(v) \quad \text{for all } v \in V_h, \quad (2.12)
$$

where

$$
A_h(v, w) = a_h(v, w) + \tau s_h(v, w), \quad (2.13)
$$

and the positive constant $\tau \propto \alpha$.

A stabilizing form. For continuous piecewise linear finite elements on triangles, a common stabilizing form s_h is the *ghost penalty* (Burman 2010), defined as

$$s_h(v, w) = \sum_{F \in \mathcal{F}_h} h([\nabla_n v], [\nabla_n w])_F, \qquad (2.14)$$

where $v, w \in V_h$, $\mathcal{F}_h$ consist of interior faces in the active mesh $\mathcal{T}_h$ that are associated with cut elements (see Figure 2.1(c)), and $[\nabla_n v]$ is the jump in the normal derivative across the face F.

The ghost penalty term is motivated by the estimate

$$\|\nabla v\|_{T_1}^2 \lesssim \|\nabla v\|_{T_2}^2 + h\|[\nabla_n v]\|_F^2, \qquad (2.15)$$

where $T_1, T_2 \in \mathcal{T}_h$ are adjacent elements with $T_1 \cap T_2 = F$.

Assuming that a non-cut element in Ω can be reached from a cut element by passing through a sequence of faces in $\mathcal{F}_h$, we can apply (2.15) repeatedly to derive the following bound:

$$\|\nabla v\|_{\Omega_h}^2 \lesssim \|\nabla v\|_{\Omega}^2 + \|v\|_{s_h}^2. \qquad (2.16)$$

This shows that the stabilization form provides an extended control (in this case, in the H^1-seminorm) of finite element functions from the physical domain Ω to the active domain Ω_h, where they are defined. Equation (2.11) follows from this, and since for $v \in V_h$ and $T \in \mathcal{T}_h$, the following inverse trace inequality holds:

$$\|\nabla v\|_{T \cap \partial \Omega} \lesssim h^{-1/2}\|\nabla v\|_T. \qquad (2.17)$$

For more details on this inverse trace inequality, see Section 3.3.

We will return to the precise requirements for the stabilizing form and present various stabilization forms in Section 4.

2.2. An interface problem

The continuous problem. Let $\Omega \subset \mathbb{R}^d$ be a domain with a smooth boundary $\partial \Omega$, and let Ω_0 be a smooth, closed hypersurface residing in the interior of Ω. The hypersurface Ω_0 divides Ω into two subdomains, $\Omega = \Omega_1 \cup \Omega_2$, where Ω_2 is the domain enclosed by the interface Ω_0. See Figure 2.2(a) for an illustration in $\mathbb{R}^2$.

We consider the following problem: find $u \colon \Omega \to \mathbb{R}$ such that

$$-\nabla \cdot (\alpha_i \nabla u) = f_i \quad \text{in } \Omega_i, i = 1, 2, \qquad (2.18)$$
$$[u] = g_0 \quad \text{on } \Omega_0, \qquad (2.19)$$
$$[n \cdot \alpha \nabla u] = f_0 \quad \text{on } \Omega_0, \qquad (2.20)$$
$$u = 0 \quad \text{on } \partial \Omega, \qquad (2.21)$$

where $\alpha_i > 0$ are positive constants, and $f_i \colon \Omega_i \to \mathbb{R}$ $(i = 1, 2)$, $f_0 \colon \Omega_0 \to \mathbb{R}$ and $g_0 \colon \Omega_0 \to \mathbb{R}$ are given functions. Assume $f_i \in L^2(\Omega_i)$ and $g_0 \in H^{1/2}(\Omega_0)$. The restriction of u to Ω_i is denoted by u_i, and we define the jump conditions at the

interface as

$$[u] = u_1 - u_2, \quad [n \cdot \alpha \nabla u] = n_1 \cdot \alpha_1 \nabla u_1 + n_2 \cdot \alpha_2 \nabla u_2, \qquad (2.22)$$

where n_i is the unit normal vector on Ω_0, outward-directed with respect to Ω_i. For simplicity, we assume a homogeneous Dirichlet boundary condition on $\partial\Omega$.

Let

$$V_1 = \{v \in H^1(\Omega_1) \mid v = 0 \text{ on } \partial\Omega\}, \quad V_2 = H^1(\Omega_2). \qquad (2.23)$$

In the derivation of a weak formulation, the following jump and average operators across the interface Ω_0 will be convenient.

- For a scalar function v, where $v_i = v|_{\Omega_i}$, $i = 1, 2$, we define the jump and average operators as

$$[v] = v_1 - v_2, \quad \langle v \rangle = \eta_1 v_1 + \eta_2 v_2, \quad \langle v \rangle_* = \eta_2 v_1 + \eta_1 v_2, \qquad (2.24)$$

where $\eta_1 + \eta_2 = 1$ and $\eta_1, \eta_2 \in [0, 1]$.

- For the normal flux,

$$[n \cdot \alpha \nabla v] = n_1 \cdot \alpha_1 \nabla v_1 + n_2 \cdot \alpha_2 \nabla v_2 \qquad (2.25)$$

and

$$\langle n \cdot \alpha \nabla v \rangle = \eta_1 n_1 \cdot \alpha_1 \nabla v_1 - \eta_2 n_2 \cdot \alpha_2 \nabla v_2, \qquad (2.26)$$

$$\langle n \cdot \alpha \nabla v \rangle_* = \eta_2 n_1 \cdot \alpha_1 \nabla v_1 - \eta_1 n_2 \cdot \alpha_2 \nabla v_2. \qquad (2.27)$$

We then have the identity

$$[n \cdot a \nabla v w] = \langle n \cdot a \nabla v \rangle [w] + [n \cdot a \nabla v] \langle w \rangle_*. \qquad (2.28)$$

For $i = 1, 2$, we multiply (2.18) by $v_i \in V_i$, integrate over Ω_i, and apply Green's identity:

$$\begin{aligned}
\sum_{i=1}^{2} (f_i, v_i)_{\Omega_i} &= \sum_{i=1}^{2} (-\nabla \cdot (\alpha_i \nabla u_i), v_i)_{\Omega_i} \\
&= \sum_{i=1}^{2} (\alpha_i \nabla u_i, \nabla v_i)_{\Omega_i} - (n_i \cdot \alpha_i \nabla u_i, v_i)_{\Omega_0} \\
&= \sum_{i=1}^{2} (\alpha_i \nabla u_i, \nabla v_i)_{\Omega_i} - (\langle n \cdot \alpha \nabla u \rangle, [v])_{\Omega_0} - ([n \cdot \alpha \nabla u], \langle v \rangle_*)_{\Omega_0} \\
&= \sum_{i=1}^{2} (\alpha_i \nabla u_i, \nabla v_i)_{\Omega_i} - (\langle n \cdot \alpha \nabla u \rangle, [v])_{\Omega_0} - (f_0, \langle v \rangle_*)_{\Omega_0}. \qquad (2.29)
\end{aligned}$$

Here we also used the interface condition $[n \cdot \alpha \nabla u] = f_0$ on Ω_0.

In the case $g_0 = 0$, the solution remains in $V = H_0^1(\Omega)$, so we can take $v_i = v|_{\Omega_i}$ for $v \in V$ and set $v_1|_{\Omega_0} = v_2|_{\Omega_0} = v_0$. Thus the weak formulation is as follows: find $u \in V$ such that

$$a(u, v) = l(v) \quad \text{for all } v \in V, \tag{2.30}$$

where the forms are defined as

$$a(v, w) = \sum_{i=1}^{2} (\alpha_i \nabla u_i, \nabla v_i)_{\Omega_i}, \tag{2.31}$$

$$l(v) = \sum_{i=1}^{2} (f_i, v_i)_{\Omega_i} + (f_0, \langle v \rangle_*)_{\Omega_0} = \sum_{i=0}^{2} (f_i, v_i)_{\Omega_i}. \tag{2.32}$$

Observe that when $g_0 = 0$, the interface is present in the weak formulation (2.30) through the jump in the coefficients α_1 and α_2. Since the solution remains in $H^1(\Omega)$, the existence of a unique solution to the weak formulation (2.30) follows from the Lax–Milgram lemma. However, the jump in the coefficient α results in a discontinuity in the normal component of the gradient across the interface. As a result, the solution is no longer in $H^2(\Omega)$, and a naive discretization using finite elements that does not account for the interface will lead to a loss of accuracy in the approximate solution.

In the case $g_0 \neq 0$, a weak formulation can be obtained by introducing a Lagrange multiplier λ to replace $-\langle n \cdot \alpha \nabla u \rangle$. The weak formulation then becomes: find $(u_1, u_2, \lambda) \in V_1 \times V_2 \times \Lambda$ such that

$$a(u, v) + b(\lambda, v) = l(v), \tag{2.33}$$
$$b(\mu, u) = (g_0, \mu), \tag{2.34}$$

for all $(v_1, v_2, \mu) \in V_1 \times V_2 \times \Lambda$. Here the bilinear form a is as in (2.31) and

$$b(\lambda, v) = (\lambda, [v])_{\Omega_0}, \tag{2.35}$$

$$l(v) = \sum_{i=1}^{2} (f_i, v_i)_{\Omega_i} + (f_0, \langle v \rangle_*)_{\Omega_0}. \tag{2.36}$$

Note that the trace of a function in $H^1(\Omega_i)$ on Ω_0 belongs to $H^{1/2}(\Omega_0)$. Therefore λ must be sought in the dual of $H^{1/2}(\Omega_0)$, i.e. in $\Lambda := H^{-1/2}(\Omega_0)$. The well-posedness of the weak formulation (2.33)–(2.34) follows from Brezzi (1974). We will formulate cut finite element methods based on discretizing this well-posed weak formulation.

For $g_0 \neq 0$, a variational formulation can also be obtained by following Nitsche's strategy to enforce the interface conditions. Starting from equation (2.29), we obtain the following:

$$\sum_{i=1}^{2}(f_i, v_i)_{\Omega_i} = \sum_{i=1}^{2}(\alpha_i \nabla u_i, \nabla v_i)_{\Omega_i} - (\langle n \cdot \alpha \nabla u \rangle, [v])_{\Omega_0} - (f_0, \langle v \rangle_*)_{\Omega_0}.$$

$$= \sum_{i=1}^{2}(\alpha_i \nabla u_i, \nabla v_i)_{\Omega_i} - (\langle n \cdot \alpha \nabla u \rangle, [v])_{\Omega_0}$$

$$\underbrace{- ([u] - g_0, \langle n \cdot \alpha \nabla v \rangle)_{\Omega_0}}_{=0} + \underbrace{\beta([u] - g_0, [v])_{\Omega_0}}_{=0} - (f_0, \langle v \rangle_*)_{\Omega_0}.$$

$$\text{(2.37)}$$

Here we used the interface condition $[u] = g_0$, and introduced a symmetrizing term and a penalty term, where $\beta \in L^{\infty}(\Omega_0)$ is a penalty parameter. Both of these terms vanish for the exact solution. Although a well-posed weak formulation cannot be obtained directly from this approach, we note that any solution to (2.18)–(2.21) such that $u_i \in V_i \cap H^{3/2+\epsilon}(\Omega_i)$, $\epsilon > 0$, for $i = 1, 2$, also satisfies the formulation (2.37). Therefore this formulation can serve as a starting point for deriving accurate cut finite element methods. If the exact solution has insufficient regularity, one may nevertheless show that approximations obtained using (2.37) converge optimally (Burman, Hansbo and Larson 2024b).

The cut finite element method based on Nitsche's method. We first derive a cut finite element method based on the formulation (2.37), where Nitsche's method is used to impose the interface conditions weakly. Let $\widetilde{\Omega}$ be a polytopal domain such that $\Omega \subseteq \widetilde{\Omega}$, equipped with a background mesh $\widetilde{\mathcal{T}}_h$. For simplicity, in order to focus on the interface, we assume that $\partial\widetilde{\Omega} = \partial\Omega$. We define the active meshes and corresponding active domains associated with the subdomains Ω_i, $i = 1, 2$, as follows:

$$\mathcal{T}_{h,i} = \{T \in \widetilde{\mathcal{T}}_h \mid T \cap \Omega_i \neq \emptyset\}, \quad \Omega_{h,i} = \bigcup_{T \in \mathcal{T}_{h,i}} T. \quad \text{(2.38)}$$

An illustration of these domains and meshes is provided in Figure 2.2.

Next, let $V_{h,i} \subset C(\Omega_{h,i})$ be finite element spaces defined on the active meshes $\mathcal{T}_{h,i}$, for $i = 1, 2$, with the condition that $v_1 = 0$ on $\partial\Omega$ for $v_1 \in V_{h,1}$. Define the space

$$W_h = V_{h,1} \oplus V_{h,2}. \quad \text{(2.39)}$$

We then arrive at the following cut finite element method: find $u_h \in W_h$ such that

$$A_h(u_h, v) = l_h(v) \quad \text{for all } v \in W_h, \quad \text{(2.40)}$$
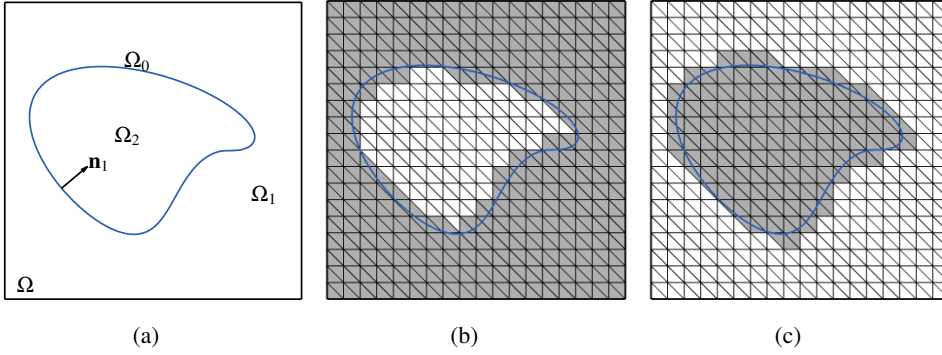
Figure 2.2. (a) The subdomains Ω_i, $i = 1, 2$, the interface Ω_0 and the domain Ω. The background domain $\widetilde{\Omega}$ coincides in this case with the physical domain Ω. (b) The background mesh $\widetilde{\mathcal{T}}_h$, the active mesh $\mathcal{T}_{h,1}$ (consisting of the grey triangles) and the active domain $\Omega_{h,1}$ (the grey region). (c) The active mesh $\mathcal{T}_{h,2}$ (consisting of the grey triangles) and the active domain $\Omega_{h,2}$ (the grey region).

where the forms are defined as

$$A_h(v, w) = a_h(v, w) + s_h(v, w), \tag{2.41}$$

$$a_h(v, w) = \sum_{i=1}^{2} (\alpha_i \nabla v_i, \nabla w_i)_{\Omega_i}$$
$$- (\langle n \cdot \alpha \nabla v \rangle, [w])_{\Omega_0} - ([v], \langle n \cdot \alpha \nabla w \rangle)_{\Omega_0} + (\beta h^{-1}[v], [w])_{\Omega_0}, \tag{2.42}$$

$$s_h(v, w) = \sum_{i=1}^{2} \tau_i s_{h,i}(v_i, w_i), \tag{2.43}$$

$$l_h(v) = \sum_{i=1}^{2} (f_i, v_i)_{\Omega_i} + (f_0, \langle v \rangle_*)_{\Omega_0} - (g_0, \langle n \cdot \alpha \nabla v \rangle)_{\Omega_0} + (\beta h^{-1} g_0, [v])_{\Omega_0}. \tag{2.44}$$

Here τ_i are non-negative constants, and the penalty parameter

$$\beta := \beta_0 \frac{\alpha_1 \alpha_2}{\alpha_1 + \alpha_2}, \tag{2.45}$$

where β_0 must be chosen sufficiently large to ensure coercivity (see Section 3.7). Note that the solution $u_h \in W_h$ consists of a pair of functions, i.e. $u_h = (u_{h,1}, u_{h,2})$, where $u_{h,i} \in V_{h,i}$ for $i = 1, 2$. Since the two active meshes $\mathcal{T}_{h,i}$, for $i = 1, 2$, overlap on the cut elements, u_h is double-valued on these elements, as illustrated in Figure 2.3 for a one-dimensional case with continuous piecewise linear finite element spaces $V_{h,i}$. As an approximation to the interface problem, we define $\tilde{u}_h$
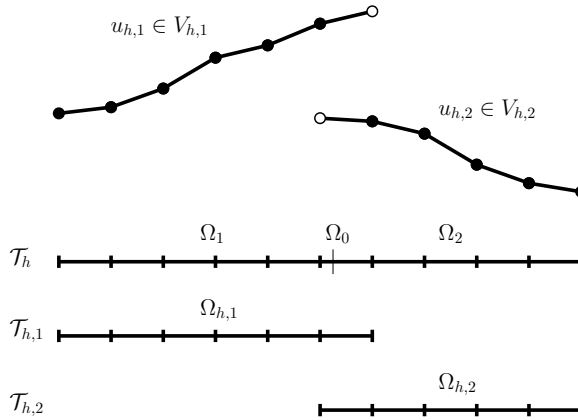
Figure 2.3. An illustration in one space dimension of how a solution $u_h \in W_h$ from the cut finite element method (2.40) might look. Note that $u_h = (u_{h,1}, u_{h,2})$, where $u_{h,i} \in V_{h,i}$ for $i = 1, 2$, with $V_{h,i}$ here consisting of continuous piecewise linear finite elements.

as follows:

$$\tilde{u}_h(x) = \begin{cases} u_{h,1} & \text{if } x \in \Omega_1, \\ u_{h,2} & \text{if } x \in \Omega_2. \end{cases} \tag{2.46}$$

One way to minimize the required penalty β is by carefully selecting the weights η_i. We will see in Section 3.7 that by choosing the weights as

$$\eta_1 = \frac{\alpha_2}{\alpha_1 + \alpha_2}, \quad \eta_2 = \frac{\alpha_1}{\alpha_1 + \alpha_2}, \tag{2.47}$$

which correspond to the harmonic average of α_1 and α_2 (Dryja 2003), we can minimize the global penalty parameter β. This choice is also known to make the error in the approximation of the fluxes robust with respect to the contrast in the diffusion coefficients (Burman, Guzmán, Sánchez and Sarkis 2018a).

In the original formulation by Hansbo and Hansbo (2002), the finite element space $V_{h,i}$ was defined as the restriction of a finite element space on the background mesh to the subdomain Ω_i, rather than to the active mesh and the active subdomain $\Omega_{h,i}$. In this case the stabilization term s_h was not included (i.e. $\tau_i = 0$), and coercivity was instead ensured by choosing the weights as

$$\eta_i|_T = \frac{|T \cap \Omega_i|}{|T|} \tag{2.48}$$

for each cut element, i.e. $T \in \mathcal{T}_{h,0}$. However, the condition number of the resulting linear system was found to be sensitive to the position of the interface relative to the background mesh.

For moderate ratios of the parameters α_i, $i = 1, 2$, this choice of the weights η_i ensures stability with $\tau_i = 0$ and with a constant penalty parameter β, as we will illustrate in a numerical example in Section 2.5. However, without the stabilization form (i.e. with $\tau_i = 0$), stability cannot be guaranteed independently of both the position of the interface and the parameters α_i, $i = 1, 2$. Optimal choices of parameters have been proposed by several authors (Barrau, Becker, Dubach and Luce 2012, Annavarapu, Hautefeuille and Dolbow 2012, Wadbro *et al.* 2013). The problem of ill-conditioning with respect to the position of the interface in the presence of high (even infinite) contrast was solved for the fictitious domain problem, the interface problem and PDEs on surfaces by introducing a penalty operator extending coercivity from the physical domain to the whole mesh domain (Burman 2010, Burman and Hansbo 2012, Burman and Zunino 2012, Burman *et al.* 2015c). A different approach with the same objective was introduced in Wadbro *et al.* (2013). Stability is a critical aspect in the design of cut finite element methods, as it influences both the accuracy of the approximation and the conditioning of the resulting linear system. To ensure stability and robustness, the common strategy in CutFEM, first proposed in Burman and Zunino (2012), is to add stabilization terms $s_{h,i}$ and to choose the weights independently of the cut configuration, but depending on the parameters α_i as in (2.47).

A cut finite element method based on Lagrange multipliers. In addition to the active meshes and the active finite element spaces associated with the bulk subdomains Ω_1 and Ω_2, as defined in equations (2.38) and (2.39), we now introduce an active mesh for the Lagrange multiplier, which is associated with the hypersurface Ω_0, along with a corresponding finite element space on this mesh. Specifically, let

$$\mathcal{T}_{h,0} = \{T \in \widetilde{\mathcal{T}}_h \mid T \cap \Omega_0 \neq \emptyset\}, \quad \Omega_{h,0} = \bigcup_{T \in \mathcal{T}_{h,0}} T, \tag{2.49}$$

and let $\Lambda_h \subset L^2(\Omega_{h,0})$ denote an appropriate finite element space for the Lagrange multiplier on the active mesh $\mathcal{T}_{h,0}$. We refer to Section 7 for more details of how to choose the space Λ_h.

Cut finite element methods can be constructed by directly discretizing the weak formulation in equations (2.33)–(2.34) and adding stabilization forms. This results in the following weak formulation: find $(u_h, \lambda_h) \in W_h \times \Lambda_h$ such that

$$A_h(u_h, v) + b(\lambda_h, v) = l(v), \tag{2.50}$$

$$b(\mu_h, u_h) - \tau_0 s_{h,0}(\mu_h, \lambda_h) = (g_0, \mu_h), \tag{2.51}$$

for all $(v, \mu_h) \in W_h \times \Lambda_h$, where the bilinear form A_h is defined as

$$A_h(v, w) = a(v, w) + s_h(v, w). \tag{2.52}$$

Here a is the bilinear form defined in equation (2.31), b is defined in equation (2.35), l is the linear form defined in equation (2.36) and s_h is the stabilization form
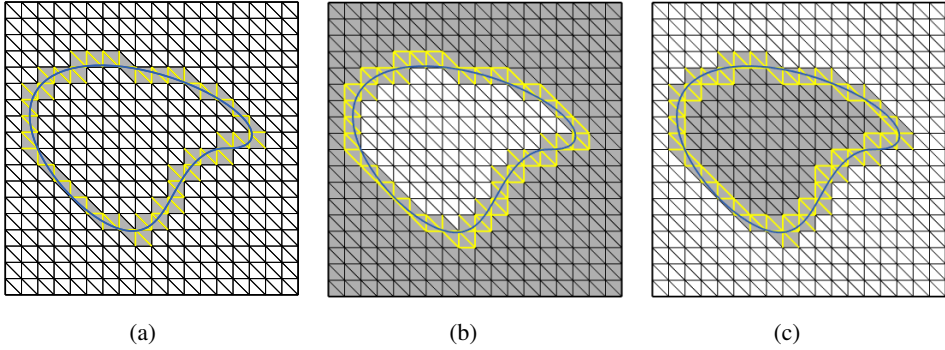
Figure 2.4. The active mesh $\mathcal{T}_{h,i}$ (consisting of the grey triangles), which are the elements from the background mesh $\widetilde{\mathcal{T}}_h$ that intersect the subdomain Ω_i. The edges marked in yellow indicate the faces where stabilization is active. Here (a) $i = 0$, (b) $i = 1$, (c) $i = 2$.

as given in equation (2.43), with each form $s_{h,i}$ stabilizing the operator associated with Ω_i, and the constants τ_i are positive constants.

An example of the stabilization form $s_{h,i}$ for $i = 1, 2$, in the case of continuous piecewise linear finite elements, is the ghost penalty stabilization introduced in equation (2.14):

$$s_{h,i}(v, w) = \sum_{F \in \mathcal{F}_{h,i}} h([\nabla_n v], [\nabla_n w])_F. \tag{2.53}$$

For $i = 0$ and discontinuous piecewise linear finite elements, an example is

$$s_{h,0}(v, w) = \sum_{F \in \mathcal{F}_{h,0}} h([v], [w])_F + h^3([\nabla v], [\nabla w])_F. \tag{2.54}$$

Note that the scaling with h in the stabilization differs for $i = 1, 2$ compared to $i = 0$, as it depends on the operator being stabilized by the stabilization form. The set $\mathcal{F}_{h,i}$ consists of interior faces in the active mesh $\mathcal{T}_{h,i}$ that are associated with cut elements. Thus each face in $\mathcal{F}_{h,i}$ is shared by two elements in the active mesh $\mathcal{T}_{h,i}$, with at least one of the elements being a cut element. Note that boundary edges are excluded from $\mathcal{F}_{h,i}$. For an illustration, see the yellow edges in Figure 2.4.

2.3. An interface problem coupled to a surface problem at the interface

The continuous problem. Using the same notation as in the previous subsection for the interface problem, we now consider the following problem: find $u : \Omega \to \mathbb{R}$ such that

$$-\nabla \cdot (\alpha_i \nabla u) = f_i \qquad\qquad \text{in } \Omega_i, i = 1, 2, \tag{2.55}$$
$$-n_i \cdot \alpha_i \nabla u_i = [bu]_i \qquad\qquad \text{on } \Omega_0, i = 1, 2, \tag{2.56}$$

$$-\nabla_0 \cdot (\alpha_0 \nabla_0 u_0) = f_0 - [n \cdot \alpha \nabla u] \quad \text{on } \Omega_0, \tag{2.57}$$

$$u = 0 \qquad\qquad \text{on } \partial\Omega. \tag{2.58}$$

Here the jump operators are defined by

$$[bv]_i = b_i v_i - b_0 v_0, \quad [n \cdot \alpha \nabla v] = n_1 \cdot \alpha_1 \nabla v_1 + n_2 \cdot \alpha_2 \nabla v_2, \tag{2.59}$$

$\alpha_i \in \mathbb{R}$ and $b_i \in \mathbb{R}$ are positive constants, $f_i : \Omega_i \to \mathbb{R}$, are given functions, assume $f_i \in L^2(\Omega_i)$, and ∇_0 denotes the surface gradient.

Now let $V_0 = H^1(\Omega_0)$, and let V_1, V_2 be defined as in equation (2.23). Define

$$W = V_0 \oplus V_1 \oplus V_2. \tag{2.60}$$

We multiply equation (2.55) by $b_i v_i$ with $v_i \in V_i$, for $i = 1, 2$, integrate over Ω_i, apply Green's identity, and use the interface conditions to obtain

$$\sum_{i=1}^{2} (f_i, b_i v_i)_{\Omega_i} = \sum_{i=1}^{2} -(\nabla \cdot (\alpha_i \nabla u_i), b_i v_i)_{\Omega_i} \tag{2.61}$$

$$= \sum_{i=1}^{2} b_i (\alpha_i \nabla u_i, \nabla v_i)_{\Omega_i} - (n_i \cdot \alpha_i \nabla u_i, b_i v_i)_{\Omega_0}$$

$$= \sum_{i=1}^{2} b_i (\alpha_i \nabla u_i, \nabla v_i)_{\Omega_i} - (n_i \cdot \alpha_i \nabla u_i, b_i v_i - b_0 v_0)_{\Omega_0} - ([n \cdot \alpha \nabla u], b_0 v_0)_{\Omega_0}$$

$$= \sum_{i=1}^{2} b_i (\alpha_i \nabla u_i, \nabla v_i)_{\Omega_i} + \sum_{i=1}^{2} ([bu]_i, [bv]_i)_{\Omega_0} - (\nabla_0 \cdot (\alpha_0 \nabla_0 u_0) + f_0, b_0 v_0)_{\Omega_0}$$

$$= \sum_{i=1}^{2} b_i (\alpha_i \nabla u_i, \nabla v_i)_{\Omega_i} + \sum_{i=1}^{2} ([bu]_i, [bv]_i)_{\Omega_0} + b_0 (\alpha_0 \nabla_0 u_0, \nabla_0 v_0)_{\Omega_0} - (f_0, b_0 v_0)_{\Omega_0}.$$

We thus have the following weak formulation: find $u \in W$ such that

$$a(u, v) = l(v) \quad \text{for all } v \in W, \tag{2.62}$$

where the forms are defined as

$$a(v, w) = b_0 (\alpha_0 \nabla_0 u_0, \nabla_0 v_0)_{\Omega_0} + \sum_{i=1}^{2} (b_i (\alpha_i \nabla u_i, \nabla v_i)_{\Omega_i} + ([bu]_i, [bv]_i)_{\Omega_0}), \tag{2.63}$$

$$l(v) = \sum_{i=0}^{2} b_i (f_i, v_i)_{\Omega_0}. \tag{2.64}$$

Existence, uniqueness and stability of the formulation (2.62) follow from the Lax–Milgram lemma.

The cut finite element method. Let $\widetilde{\Omega}$ be a polygonal domain such that $\Omega \subset \widetilde{\Omega}$, equipped with a background mesh $\widetilde{\mathcal{T}}_h$. We define the active meshes and the active

domains associated with the subdomains Ω_i, for $i = 0, 1, 2$, as follows:

$$\mathcal{T}_{h,i} = \{T \in \widetilde{\mathcal{T}}_h \mid T \cap \Omega_i \neq \emptyset\}, \quad \Omega_{h,i} = \bigcup_{T \in \mathcal{T}_{h,i}} T. \tag{2.65}$$

Next, let $V_{h,i} \subset C(\Omega_{h,i})$ be finite element spaces defined on the active meshes $\mathcal{T}_{h,i}$ for $i = 0, 1, 2$, with the condition that $v_1 = 0$ on $\partial\Omega$ for $v_1 \in V_{h,1}$. Define

$$W_h = V_{h,0} \oplus V_{h,1} \oplus V_{h,2}. \tag{2.66}$$

In this case we can base the cut finite element method directly on the weak formulation (2.62), adding a stabilizing form. This leads to the following formulation: find $u_h \in W_h$ such that

$$A_h(u_h, v) = l(v) \quad \text{for all } v \in W_h, \tag{2.67}$$

where l is the linear form defined in (2.63) and

$$A_h(v, w) = a(v, w) + s_h(v, w), \tag{2.68}$$

with a defined in equation (2.63). The stabilizing form is defined as

$$s_h(v, w) = \sum_{i=0}^{2} \tau_i s_{h,i}(v_i, w_i), \tag{2.69}$$

where each form $s_{h,i}$ stabilizes the operator associated with Ω_i, and τ_i are positive constants.

An example of the stabilization form $s_{h,i}$, in the case of continuous piecewise linear finite elements, is the ghost penalty stabilization:

$$s_{h,i}(v, w) = \sum_{F \in \mathcal{F}_{h,i}} h^k([\nabla_n v], [\nabla_n w])_F, \tag{2.70}$$

where $k = 0$ for $i = 0$ (the surface problem: see the work by Burman *et al.* 2015*c*), and $k = 1$ as in (2.14) for $i = 1, 2$. As before, the set $\mathcal{F}_{h,i}$ consists of interior faces in the active mesh $\mathcal{T}_{h,i}$ that are shared by at least one cut element. We will discuss stabilization terms for bulk problems in more detail in Section 4, while stabilization for surface problems will be addressed in Section 5.

2.4. The Stokes interface problem

The continuous problem. Let $\Omega \subset \mathbb{R}^d$, where $d = 2$ or 3, be a domain with a polygonal boundary $\partial\Omega$. The domain Ω contains two incompressible immiscible fluids, separated by the interface Ω_0. Each fluid, with viscosity μ_i, occupies a subdomain $\Omega_i \subset \Omega$, $i = 1, 2$. We seek the velocity $\boldsymbol{u} \colon \Omega \to \mathbb{R}^2$ and the pressure $p \colon \Omega \to \mathbb{R}$ such that

$$-\nabla \cdot (\mu \boldsymbol{\epsilon}(\boldsymbol{u}) - p\boldsymbol{I}) = \boldsymbol{f}_i \qquad \text{in } \Omega_i, i = 1, 2, \tag{2.71}$$

$$\nabla \cdot \boldsymbol{u} = 0 \qquad \text{in } \Omega_i, i = 1, 2, \tag{2.72}$$

$$[\boldsymbol{u}] = \boldsymbol{0} \qquad \text{on } \Omega_0, \tag{2.73}$$

$$[\boldsymbol{n} \cdot (\mu \boldsymbol{\epsilon}(\boldsymbol{u}) - p\boldsymbol{I})] = \sigma \kappa \boldsymbol{n} \quad \text{on } \Omega_0, \tag{2.74}$$

$$\boldsymbol{u} = \boldsymbol{0} \qquad \text{on } \partial\Omega. \tag{2.75}$$

Here $\boldsymbol{\epsilon}(\boldsymbol{u}) = (\nabla \boldsymbol{u} + (\nabla \boldsymbol{u})^\top)/2$ is the strain rate tensor, μ is the viscosity function, defined by $\mu = 2\mu_i$ in Ω_i, σ is the surface tension coefficient, $\kappa \boldsymbol{n}$ is the mean curvature vector, and $\boldsymbol{f}_i \colon \Omega_i \to \mathbb{R}^d$ is a given external force field (e.g. the gravitational force). We assume homogeneous Dirichlet boundary conditions, but other types of suitable boundary conditions on $\partial\Omega$ are also possible. In particular, we may have $\boldsymbol{u} = \boldsymbol{u}_B$, where $\boldsymbol{u}_B$ is a given function, and by Gauss's integral theorem, this function satisfies

$$\int_{\partial\Omega} \boldsymbol{u}_B \cdot \boldsymbol{n}_B \, \mathrm{d}s = \int_\Omega \nabla \cdot \boldsymbol{u} \, \mathrm{d}x = 0, \tag{2.76}$$

where $\boldsymbol{n}_B$ denotes the unit outward-directed normal vector on the boundary $\partial\Omega$. Note that the pressure p is determined from equations (2.71)–(2.75) only up to an additive constant. This constant is typically fixed by requiring $\int_\Omega p \, \mathrm{d}x = 0$.

Let

$$V = \{\boldsymbol{v} \in [H^1(\Omega)]^d \mid v = 0 \text{ on } \partial\Omega\}, \quad Q = \left\{q \in L^2(\Omega) \mid \int_\Omega q \, \mathrm{d}x = 0\right\}. \tag{2.77}$$

Take $\boldsymbol{v}_i = v|_{\Omega_i}$ for $v \in V$ and set $\boldsymbol{v}_1|_{\Omega_0} = \boldsymbol{v}_2|_{\Omega_0} = \boldsymbol{v}_0$. For $i = 1, 2$, we multiply equation (2.71) by $v \in V$, integrate over Ω_i, and apply Green's identity:

$$\sum_{i=1}^2 (\boldsymbol{f}_i, \boldsymbol{v}_i)_{\Omega_i} = \sum_{i=1}^2 (-\nabla \cdot (\mu \boldsymbol{\epsilon}(\boldsymbol{u}) - p\boldsymbol{I}), \boldsymbol{v})_{\Omega_i}$$

$$= \sum_{i=1}^2 (\mu \boldsymbol{\epsilon}(\boldsymbol{u}), \boldsymbol{\epsilon}(\boldsymbol{v}))_{\Omega_i} - (p, \nabla \cdot \boldsymbol{v})_{\Omega_i} + \sum_{i=1}^2 -(\mu \boldsymbol{\epsilon}(\boldsymbol{u})\boldsymbol{n}_i, \boldsymbol{v})_{\Omega_0} + (p, \boldsymbol{n}_i \cdot \boldsymbol{v})_{\Omega_0}$$

$$= \sum_{i=1}^2 (\mu \boldsymbol{\epsilon}(\boldsymbol{u}), \boldsymbol{\epsilon}(\boldsymbol{v}))_{\Omega_i} - (p, \nabla \cdot \boldsymbol{v})_{\Omega_i} - (\sigma \kappa \boldsymbol{n}, \boldsymbol{v}_0)_{\Omega_0}, \tag{2.78}$$

where $\boldsymbol{n}_i$ is the unit normal vector on Ω_0, outward-directed with respect to Ω_i, and we used the interface condition (2.74).

Further, let $q_i = q|_{\Omega_i}$ for $q \in Q$. Multiplying (2.72) by $q \in Q$ and integrating over Ω_i we arrive at the following weak formulation: find $\boldsymbol{u} \in V$ and $p \in Q$ such that

$$a(\boldsymbol{u}, \boldsymbol{v}) + b(\boldsymbol{v}, p) = l(\boldsymbol{v}) \quad \text{for all } \boldsymbol{v} \in V, \tag{2.79}$$

$$b(\boldsymbol{u}, q) = 0 \qquad \text{for all } q \in Q, \tag{2.80}$$

where the forms are defined as

$$a(\boldsymbol{v}, \boldsymbol{w}) = \sum_{i=1}^{2} (2\mu_i \boldsymbol{\epsilon}(\boldsymbol{v}), \boldsymbol{\epsilon}(\boldsymbol{w}))_{\Omega_i}, \tag{2.81}$$

$$b(\boldsymbol{v}, q) = -\sum_{i=1}^{2} (q, \nabla \cdot \boldsymbol{v})_{\Omega_i}, \tag{2.82}$$

$$l(\boldsymbol{v}) = \sum_{i=0}^{2} (\boldsymbol{f}_i, \boldsymbol{v}_i)_{\Omega_i}, \tag{2.83}$$

with $\boldsymbol{f}_0 = \sigma \kappa \boldsymbol{n}$. We next formulate a cut finite element discretization based on Nitsche's method.

The cut finite element method based on Nitsche's method. We use the same notation as in Section 2.2. Let $\widetilde{\Omega}$ be a polytopal domain such that $\Omega \subset \widetilde{\Omega}$, equipped with a background mesh $\widetilde{\mathcal{T}}_h$. For simplicity, we assume that $\partial\widetilde{\Omega} = \partial\Omega$. We define the active meshes and corresponding active domains associated with the subdomains Ω_i, $i = 1, 2$, as before:

$$\mathcal{T}_{h,i} = \{T \in \widetilde{\mathcal{T}}_h \mid T \cap \Omega_i \neq \emptyset\}, \quad \Omega_{h,i} = \bigcup_{T \in \mathcal{T}_{h,i}} T. \tag{2.84}$$

An illustration of these domains and meshes is provided in Figure 2.4. On the active mesh $\mathcal{T}_{h,i}$, we define finite element spaces $V_{h,i}$ for the velocity and $Q_{h,i}$ for the pressure. These pairs of spaces $(V_{h,i}, Q_{h,i})$ are chosen to be either inf-sup stable pairs or pairs that are stable with some pressure stabilization. Examples include the stabilized P1-P0 pair (Becker, Burman and Hansbo 2009), the P1 iso P2 elements (linear elements both for the velocity and the pressure but on different meshes) (Hansbo, Larson and Zahedi 2014), the Taylor–Hood elements (Kirchhart, Gross and Reusken 2016) and the Scott–Vogelius pair (Liu, Neilan and Olshanskii 2023). See also the work by Guzmán and Olshanskii (2018) for inf-sup stability of various element pairs in the context of cut finite element discretizations.

Define

$$\boldsymbol{W}_h = \boldsymbol{V}_{h,1} \oplus \boldsymbol{V}_{h,2}, \quad Q_h = Q_{h,1} \oplus Q_{h,2}, \tag{2.85}$$

with $Q_h \subset Q$.

Similar to the derivation of the weak formulation for the interface problem in Section 2.2, we can obtain a weak formulation by integrating by parts in each subdomain and imposing interface conditions weakly using Nitsche's method. For $i = 1, 2$, we multiply (2.71) by $\boldsymbol{v}_h = (\boldsymbol{v}_{h,1}, \boldsymbol{v}_{h,2}) \in \boldsymbol{W}_h$, where $\boldsymbol{v}_{h,i} \in \boldsymbol{V}_{h,i}$, integrate over Ω_i, apply Green's identity, use the identity (2.28), and apply the interface

conditions. This results in the following formulation:

$$\sum_{i=1}^{2}(\boldsymbol{f}_i, \boldsymbol{v}_{h,i})_{\Omega_i} = \sum_{i=1}^{2}(-\nabla \cdot (\mu\boldsymbol{\epsilon}(\boldsymbol{u}) - p\boldsymbol{I}), \boldsymbol{v}_h)_{\Omega_i}$$

$$= \sum_{i=1}^{2}(\mu\boldsymbol{\epsilon}(\boldsymbol{u}), \boldsymbol{\epsilon}(\boldsymbol{v}_h))_{\Omega_i} - (p, \nabla \cdot \boldsymbol{v}_h)_{\Omega_i} + \sum_{i=1}^{2} -(\mu\boldsymbol{\epsilon}(\boldsymbol{u})\boldsymbol{n}_i, \boldsymbol{v}_h)_{\Omega_0} + (p, \boldsymbol{n}_i \cdot \boldsymbol{v}_h)_{\Omega_0}$$

$$= \sum_{i=1}^{2}(\mu\boldsymbol{\epsilon}(\boldsymbol{u}), \boldsymbol{\epsilon}(\boldsymbol{v}_h))_{\Omega_i} - (p, \nabla \cdot \boldsymbol{v}_h)_{\Omega_i} - (\langle(\mu\varepsilon(\boldsymbol{u}) - p\boldsymbol{I})\boldsymbol{n}\rangle, [\boldsymbol{v}_h])_{\Omega_0}$$

$$- (\sigma\kappa\boldsymbol{n}, \langle\boldsymbol{v}_h\rangle_*)_{\Omega_0}$$

$$= \sum_{i=1}^{2}(\mu\boldsymbol{\epsilon}(\boldsymbol{u}), \boldsymbol{\epsilon}(\boldsymbol{v}_h))_{\Omega_i} - (p, \nabla \cdot \boldsymbol{v}_h)_{\Omega_i} + (\langle p\rangle, [\boldsymbol{n} \cdot \boldsymbol{v}_h])_{\Omega_0} - (\langle\mu\varepsilon(\boldsymbol{u})\boldsymbol{n}\rangle, [\boldsymbol{v}_h])_{\Omega_0}$$

$$- ([\boldsymbol{u}], \langle\mu\varepsilon(\boldsymbol{v}_h)\boldsymbol{n}\rangle)_{\Omega_0} + (\beta h^{-1}[\boldsymbol{u}], [\boldsymbol{v}_h])_{\Omega_0} - (\sigma\kappa\boldsymbol{n}, \langle\boldsymbol{v}_h\rangle_*)_{\Omega_0}. \tag{2.86}$$

Note that in the derivation we rewrote the interface term and used the interface condition (2.74) as

$$\int_{\Omega_0} [((\mu\varepsilon(\boldsymbol{u}) - p\boldsymbol{I})\boldsymbol{n})\boldsymbol{v}_h] = \int_{\Omega_0} \langle(\mu\varepsilon(\boldsymbol{u}) - p\boldsymbol{I})\boldsymbol{n}\rangle[\boldsymbol{v}_h] + \int_{\Omega_0} \underbrace{[(\mu\varepsilon(\boldsymbol{u}) - p\boldsymbol{I})\boldsymbol{n}]}_{\sigma\kappa\boldsymbol{n}}\langle\boldsymbol{v}_h\rangle_*,$$

$$\tag{2.87}$$

while the condition $[\boldsymbol{u}] = \boldsymbol{0}$ at Ω_0 is enforced by introducing both a symmetrizing term and a penalty term in equation (2.86), both of which vanish for the exact solution $\boldsymbol{u}$. We also multiply (2.72) by $q_h = (q_{h,1}, q_{h,2}) \in Q_h$, and to obtain a skew-symmetric coupling, we introduce the term $(\langle q_h\rangle, [\boldsymbol{u} \cdot \boldsymbol{n}])_{\Omega_0}$, which vanishes for the exact solution.

Based on this derivation, we can now state the following cut finite element formulation: find $\boldsymbol{u}_h \in W_h$ and $p_h \in Q_h$ such that

$$A(\boldsymbol{u}_h, \boldsymbol{v}_h) + b_h(\boldsymbol{v}_h, p_h) = l(\boldsymbol{v}_h), \tag{2.88}$$

$$b_h(\boldsymbol{u}_h, q_h) - S_b = 0, \tag{2.89}$$

for all $\boldsymbol{v}_h \in W_h$ and $q_h \in Q_h$. Here

$$A_h(\boldsymbol{v}, \boldsymbol{w}) = a_h(\boldsymbol{v}, \boldsymbol{w}) + S_a, \tag{2.90}$$

$$a_h(\boldsymbol{v}, \boldsymbol{w}) = \sum_{i=1}^{2}(2\mu_i\boldsymbol{\epsilon}(\boldsymbol{v}), \boldsymbol{\epsilon}(\boldsymbol{w}))_{\Omega_i} - (\langle\mu\varepsilon(\boldsymbol{v})\boldsymbol{n}\rangle, [\boldsymbol{w}])_{\Omega_0}$$

$$- ([\boldsymbol{v}], \langle\mu\varepsilon(\boldsymbol{w})\boldsymbol{n}\rangle)_{\Omega_0} + \beta h^{-1}([\boldsymbol{v}], [\boldsymbol{w}])_{\Omega_0}, \tag{2.91}$$

$$b_h(\boldsymbol{v}, q) = -\sum_{i=1}^{2} (q, \nabla \cdot \boldsymbol{v})_{\Omega_i} + (\langle q \rangle, [\boldsymbol{v} \cdot \boldsymbol{n}])_{\Omega_0}, \qquad (2.92)$$

$$l_h(\boldsymbol{v}) = \sum_{i=1}^{2} (\boldsymbol{f}_i, \boldsymbol{v})_{\Omega_i} + (\sigma \kappa \boldsymbol{n}, \langle \boldsymbol{v} \rangle_*)_{\Omega_0}. \qquad (2.93)$$

Note that in the derivation of the weak formulation in equation (2.86) we added the term $-([\boldsymbol{u}], \langle \mu\varepsilon(\boldsymbol{v}_h)\boldsymbol{n}\rangle)_{\Omega_0}$ in order to obtain a symmetric bilinear form, a_h. If we had instead added $([\boldsymbol{u}], \langle \mu\varepsilon(\boldsymbol{v}_h)\boldsymbol{n}\rangle)_{\Omega_0}$, we would have arrived at an anti-symmetric version of Nitsche's method, for which coercivity of a_h can be established more easily. Boiveau and Burman (2015) studied a finite element method based on the non-symmetric version of Nitsche's method for incompressible linear elasticity, and showed that the penalty term can be eliminated. However, obtaining optimal *a priori* error estimates in the L^2-norm can be more challenging for the anti-symmetric formulation, due to the lack of adjoint consistency.

In early work, Becker *et al.* (2009) proposed a stabilized formulation using piecewise affine approximation for the velocities and piecewise constant approximation for the pressure. Pressure stability was ensured by a term S_b penalizing the jump of the pressure across all interior element faces in the active mesh, thereby enabling optimal error estimates independent of the boundary's position relative to the mesh. The stabilization form S_a was not used, meaning uniform control of the condition number was not achieved. The advantage of adding both stabilization forms to the weak formulation is that they ensure stability and well-posed linear systems, regardless of the position of the interface or the boundary relative to the mesh, as discussed in Hansbo *et al.* (2014). We also refer to Burman and Hansbo (2014) and Massing, Larson, Logg and Rognes (2014) for the Stokes fictitious domain problem.

In most studies, ghost penalty stabilization has been used to stabilize both the velocity and the pressure, with $S_a = s_{h,\boldsymbol{u}}(\boldsymbol{v}, \boldsymbol{w})$ and $S_b = s_{h,p}(p, q)$. For instance, in the case of P1 iso P2 elements (continuous piecewise linear elements for both the velocity and pressure, but on different meshes), the stabilization terms take the form (Hansbo *et al.* 2014)

$$s_{h,\boldsymbol{u}}(\boldsymbol{v}, \boldsymbol{w}) = \sum_{l=1}^{d} \sum_{i=1}^{2} \tau_{\boldsymbol{u},i} \sum_{F \in \mathcal{F}_{h,i}} h([\nabla v_i^l \cdot \boldsymbol{n}_F], [\nabla w_i^l \cdot \boldsymbol{n}_F])_F, \qquad (2.94)$$

$$s_{h,p}(p, q) = \sum_{i=1}^{2} \tau_{p,i} \sum_{F \in \mathcal{F}_{h,i}} h^3([\nabla p \cdot \boldsymbol{n}_F], [\nabla q \cdot \boldsymbol{n}_F])_F, \qquad (2.95)$$

where $\boldsymbol{n}_F$ is the normal vector associated with the face F. The scaling with h differs for the velocity and the pressure, as it depends on the operator being stabilized by the stabilization form.

Recently, Liu *et al.* (2023) and Frachon, Hansbo, Nilsson and Zahedi (2024*a*) demonstrated that, with the stabilization $s_{h,p}(p,q)$, cut finite element discretizations cannot guarantee pointwise divergence-free velocity field approximations, even when the underlying finite element pair satisfies the divergence-free property. To address this issue, Frachon *et al.* (2024*a*) propose a modified stabilization approach for the bilinear form b_h, where they choose $S_b = s_{h,p}(\text{div } \boldsymbol{u}_h, q)$ for element pairs such that $\nabla \cdot V_{h,i} = Q_{h,i}$.

Cut finite element methods that produce pointwise divergence-free velocity approximations for the Stokes problem in domains with unfitted boundaries, where boundary conditions are imposed weakly, have recently been developed by Burman, Hansbo and Larson (2024*a*) and by Frachon, Nilsson and Zahedi (2024*b*). In Burman *et al.* (2024*a*), a CutFEM framework for divergence-free elements using Lagrange multipliers is proposed, and optimal *a priori* error estimates are derived without the need for stabilization forms; for well-conditioning of the resulting linear systems, a ghost penalty term for the velocity may be added. This approach was extended to the case of Darcy flow in Lehrenfeld, van Beeck and Voulis (2023). In contrast, Frachon *et al.* (2024*b*) investigate compatible cut finite element discretizations that rely on stabilization, emphasizing the importance of selecting appropriate stabilization forms to avoid polluting the divergence condition. They stress ensuring that the condition

$$\int_{\partial\Omega} \boldsymbol{u}_h \cdot \boldsymbol{n} \, \mathrm{d}s = 0 \tag{2.96}$$

holds when imposing the boundary conditions weakly, and caution against introducing terms such as $(\langle q_h \rangle, [\boldsymbol{u}_h \cdot \boldsymbol{n}])_{\Omega_0}$ into the weak form of the mass continuity equation. These factors are essential for ensuring robust, pointwise divergence-free unfitted discretizations.

Frachon *et al.* (2024*b*) have developed cut finite element methods based on the Brezzi–Douglas–Marini (BDM) and Raviart–Thomas (RT) spaces, both families of $\boldsymbol{H}^{\text{div}}$-conforming finite element spaces. By combining the ideas from Frachon *et al.* (2024*b*) with the cut finite element method based on Nitsche's method and the Scott–Vogelius pair proposed in Liu *et al.* (2023), robust, pointwise divergence-free cut finite element discretizations can be obtained.

For extensions of the presented cut finite element discretization to two-phase Navier–Stokes flows and insoluble surfactants, see Claus and Kerfriden (2019) and Frachon and Zahedi (2019, 2023).

2.5. Numerical illustration

We first present some numerical solutions to the interface problem (2.18)–(2.21) to demonstrate the performance of CutFEM based on (2.40), using the parameters $\beta = 10^2$ and $\tau_i = 10^{-1}$, with $P1$ triangular elements. In Figure 2.5 we show the two subdomains Ω_i, $i = 1, 2$. We apply zero boundary conditions strongly on the outer boundary of Ω_1.
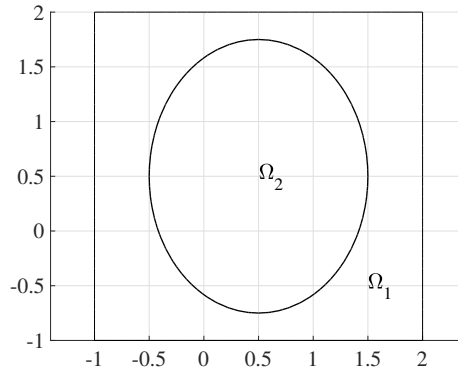
Figure 2.5. The domains Ω_1 and Ω_2 used for the numerical examples of the interface problem (2.18)–(2.21).
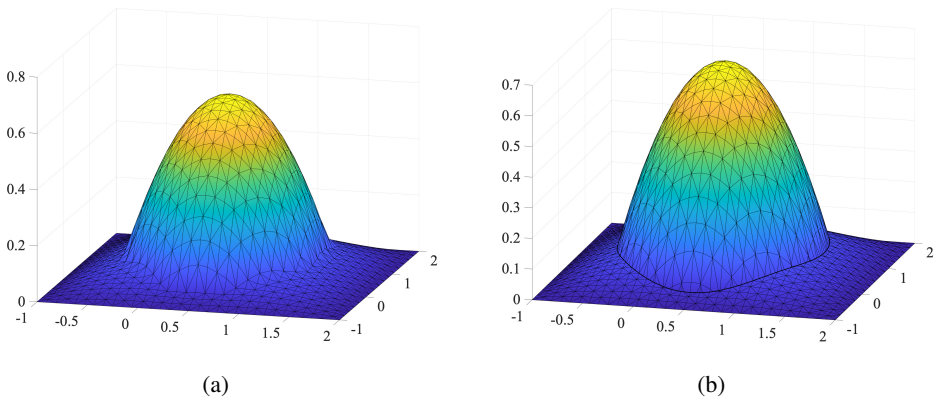

(a)

(b)

Figure 2.6. The standard FEM solution (a) and the CutFEM solution (b) of the interface problem. The interface is highlighted by the black curve in (b).
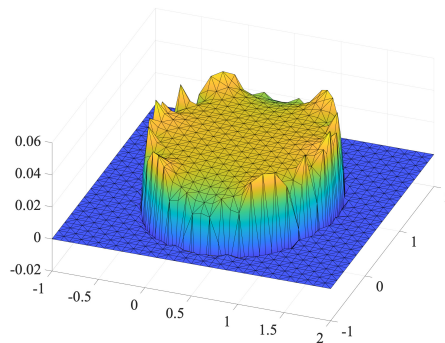

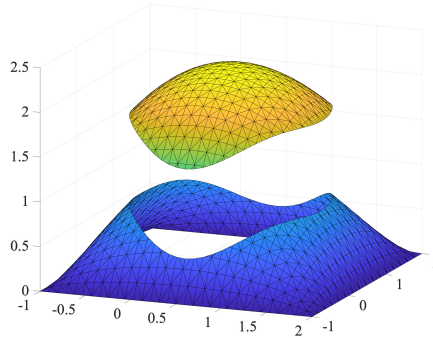Figure 2.7. The difference between the standard FEM and CutFEM solutions.

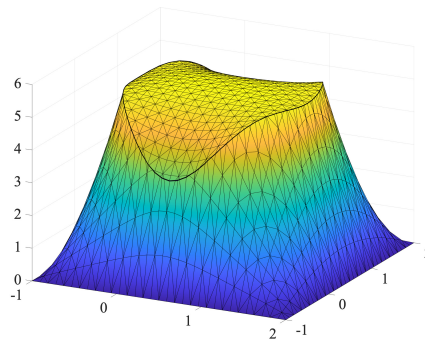Figure 2.8. The CutFEM solution of the interface problem with $g_0 \neq 0$.

Figure 2.9. The CutFEM solution of the interface problem with $f_0 \neq 0$.

We compare the standard continuous FEM with CutFEM on the same mesh when $\alpha_1 = 10$, $\alpha_2 = 1$ and $f_0 = g_0 = 0$. The mesh is not aligned with the interface, which is represented by a piecewise linear approximation. Exact integration, accounting for the interface position, is performed in both methods. In Figure 2.6 we show the two solutions, and in Figure 2.7 we show the difference between the CutFEM solution and the standard continuous FEM solution. Note that in this example there is a discontinuity in the normal derivative of the solution and the error between the CutFEM solution, and the standard continuous FEM solution is not limited to the vicinity of the interface. Instead, it affects the solution globally in Ω_2.

In Figure 2.8 we show the CutFEM solution when $\alpha_1 = \alpha_2 = 1$, $f_0 = 0$ and $g_0 = 1$, and in Figure 2.9 we show the result when $\alpha_1 = \alpha_2 = 1$, $f_0 = 10$ and $g_0 = 0$. The cut finite element approach is seen to handle discontinuities easily, both in the solution and in the gradient of the solution.

Finally, we consider the Stokes interface problem (2.71)–(2.75) and a static drop, represented as a circle with radius $r = 0.5$. The viscosities of both fluids are set to one, $\boldsymbol{f}_i = 0$, and we choose $\sigma = 1$. Thus the exact velocity is zero, and due to the surface tension force, there is a jump in the exact pressure across the interface,
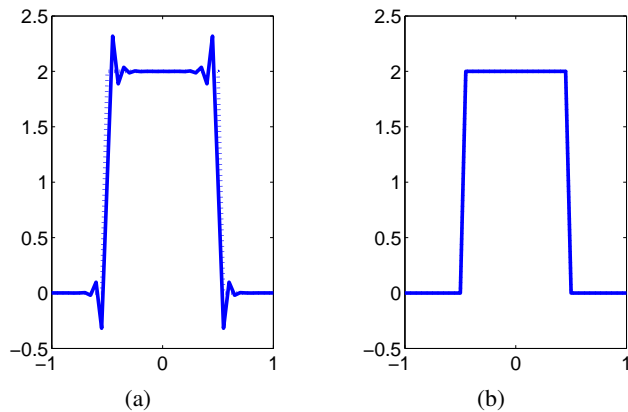
Figure 2.10. The approximate pressure for the Stokes interface problem: the standard FEM solution (a) and the CutFEM solution (b). The exact pressure is represented by the dotted line in (a).

equal to the magnitude of the curvature. We compare the standard continuous FEM with CutFEM on the same mesh using P1 iso P2 elements (linear elements both for the velocity and pressure, but on different meshes). In Figure 2.10 we show the cross-section of the pressure approximation from both CutFEM and the standard continuous FEM. We observe that the pressure solution using CutFEM is accurate, and in this case the exact pressure is obtained. However, since the mesh is not fitted to the interface where the pressure discontinuity occurs, the approximate pressure solution obtained using the standard FEM with globally continuous elements exhibits oscillations around the interface. The approximation of the velocity field is exact to machine precision using CutFEM, whereas with the standard FEM we observe spurious currents (unphysical velocities) around the interface. The CutFEM results hold for both $S_b = s_{h,p}(p, q)$ and $S_b = s_{h,p}(\text{div}\,\boldsymbol{u}_h, q)$. The standard FEM solution is based on the discretization of the weak form (2.79)–(2.80).

3. Fundamental analysis of CutFEM

In this section we present the fundamental analysis of CutFEM for second-order symmetric problems. As discussed in the previous section, cut finite element methods impose boundary or interface conditions weakly on unfitted meshes using a consistent penalty method (such as Nitsche's method) or via Lagrange multipliers. The analysis of cut finite element discretizations using Lagrange multipliers is addressed in Section 7.

3.1. Abstract formulation

Consider the following abstract problems.

1. *The continuous problem.* Find $u \in W$ such that

$$a(u, v) = l(v) \quad \text{for all } v \in W, \tag{3.1}$$

where $a(u, v)$ is a bilinear form and $l(v)$ is a linear functional corresponding to the weak formulation of a second-order symmetric boundary value problem. The boundary conditions are incorporated in the function space W, with homogeneous Dirichlet boundary conditions assumed for simplicity. In the case of non-homogeneous Dirichlet boundary conditions, the trial and the test space will differ (see the boundary value problem in Section 2.1).

2. *The cut finite element method (CutFEM).* Find $u_h \in W_h$ such that

$$A_h(u_h, v) = l_h(v) \quad \text{for all } v \in W_h, \tag{3.2}$$

where A_h is a bilinear form given by

$$A_h(v, w) = a_h(v, w) + s_h(v, w). \tag{3.3}$$

Here a_h and l_h represent the discretized bilinear form and linear functional, respectively. These forms may coincide with the continuous counterparts a and l, or, in the case of CutFEM based on Nitsche's method, they may differ slightly due to the weak imposition of boundary or interface conditions (for examples, see Section 2). The term s_h represents the stabilization form. This section states abstract assumptions on the stabilization form that ensure stability and well-conditioned discretized systems, independent of the cuts in the unfitted mesh. Then, in Section 4, we provide several concrete examples of such stabilization operators. In the abstract setting, we do not explicitly account for the dependences of the coefficients in the forms. However, we will consider several examples below where we include the dependences of the problem parameters.

To derive *a priori* error estimates, we make the following assumptions.

A1. *Consistency.* The exact solution $u \in \widetilde{W}$ also satisfies

$$a_h(u, v) = l_h(v) \quad \text{for all } v \in W_h, \tag{3.4}$$

where $\widetilde{W} \subset W$.

A2. *Continuity.* There is a norm $\||\cdot\||_h$ such that

$$a_h(v, w) \lesssim \||v\||_h \||w\||_h \quad \text{for all } v, w \in \widetilde{W} + W_h, \tag{3.5}$$

and $\||w\||_h$ is well-defined for all $w \in \widetilde{W} + W_h$. Furthermore, the stabilization form is an inner product on W_h, induces a norm $\|v\|_{s_h}^2 = s_h(v, v)$, and by the Cauchy–Schwarz inequality we have

$$s_h(v, w) \lesssim \|v\|_{s_h} \|w\|_{s_h} \quad \text{for all } v, w \in W_h. \tag{3.6}$$

A3. *Stability.* On W_h we have

$$\||v\||_{h,\star} \lesssim \sup_{w \in W_h \setminus \{0\}} \frac{A_h(v, w)}{\||w\||_{h,\star}} \quad \text{for all } v \in W_h \tag{3.7}$$

uniformly, where

$$\||v\||_{h,\star}^2 = \||v\||_h^2 + \|v\|_{s_h}^2. \tag{3.8}$$

A4. *Approximation.* There is an interpolation operator $\pi_h \colon H^s(\mathcal{O}) \to W_h$, $s \geq 1$, such that for $v \in H^s(\mathcal{O})$

$$\||v - \pi_h v\||_h \lesssim h^{s-1}\|v\|_{H^s(\mathcal{O})}, \quad 1 \leq s \leq p+1. \tag{3.9}$$

Furthermore, the stabilization form s_h satisfies the weak consistency

$$\|\pi_h v\|_{s_h} \lesssim h^{s-1}\|v\|_{H^s(\mathcal{O})}, \quad 1 \leq s \leq p+1. \tag{3.10}$$

Note that in assumption A1 we introduce a new space $\widetilde{W}$ because we typically need to assume that the weak solution to (3.1) is regular enough for (3.4) to hold, due to the bilinear forms a and a_h. Compare the bilinear forms a and a_h in Section 2, where the form a_h arises from applying Nitsche's method. The norm $\|| \cdot \||_h$ is typically associated with a_h. The domain $\mathcal{O}$ refers to the physical domain. In the context of the boundary value problem in Section 2.1, $\mathcal{O}$ corresponds to Ω, while for the interface problem in Section 2.2, it represents the disjoint union of the different subdomains, $\mathcal{O} = \bigsqcup_i \Omega_i$. The norm $\|v\|_{H^s(\mathcal{O})}^2$ is then defined as the sum of the norms over each subdomain,

$$\|v\|_{H^s(\mathcal{O})}^2 = \sum_i \|v_i\|_{H^s(\Omega_i)}^2 \quad \text{and} \quad \|v\|_{s_h}^2 = \sum_i \|v_i\|_{s_{h,i}}^2. \tag{3.11}$$

Next we will establish optimal order *a priori* estimates provided assumptions A1–A4 are satisfied. We will then construct interpolation operators π_h satisfying assumption A4. Finally, we will verify that assumptions A1–A3 hold for the cut finite element methods introduced in Section 2 for the boundary value problem, the interface problem and the coupled bulk–surface problem. We will see that assumption A3 (stability), depending on a_h, may impose an additional design criterion for the stabilization form s_h.

3.2. Error estimate

Theorem 3.1. For $u \in \widetilde{W} \cap H^{p+1}(\mathcal{O})$, and provided A1–A4 hold, there exists a constant such that

$$\||u - u_h\||_h \lesssim h^p \|u\|_{H^{p+1}(\mathcal{O})}. \tag{3.12}$$

Proof. We begin by splitting the error into two parts using the interpolation operator

$$\||u - u_h\||_h \lesssim \||u - \pi_h u\||_h + \||\pi_h u - u_h\||_h. \tag{3.13}$$

For the first term in (3.13), we directly conclude, using the interpolation estimate (3.9) (assumption A4), that

$$\||u - \pi_h u\||_h \lesssim h^p \|u\|_{H^{p+1}(\mathcal{O})}. \tag{3.14}$$

For the second term in (3.13) we use the definition of $||| \cdot |||_{h,\star}$ (equation (3.8)) and apply assumption A3 (stability) to conclude that

$$|||\pi_h u - u_h|||_h \leq |||\pi_h u - u_h|||_{h,\star} \lesssim \sup_{w \in W_h \setminus \{0\}} \frac{A_h(\pi_h u - u_h, w)}{|||w|||_{h,\star}}. \qquad (3.15)$$

We estimate the numerator in (3.15) by using the fact that (3.2), assumption A1 (consistency), A2 (continuity) and assumption A4 (approximation) all hold. This leads to

$$\begin{aligned}
A_h(\pi_h u - u_h, w) &= A_h(\pi_h u, w) - l_h(w) \\
&= a_h(\pi_h u, w) - l_h(w) + s_h(\pi_h u, w) \\
&= a_h(\pi_h u - u, w) + s_h(\pi_h u, w) \\
&\lesssim |||\pi_h u - u|||_h |||w|||_h + \|\pi_h u\|_{s_h} \|w\|_{s_h} \\
&\lesssim \left(|||\pi_h u - u|||_h^2 + \|\pi_h u\|_{s_h}^2 \right)^{1/2} |||w|||_{h,\star} \\
&\lesssim h^p \|u\|_{H^{p+1}(\mathcal{O})} |||w|||_{h,\star}.
\end{aligned} \qquad (3.16)$$

Combining (3.15) with (3.16), we get

$$|||\pi_h u - u_h|||_{h,\star} \lesssim h^p \|u\|_{H^{p+1}(\mathcal{O})}. \qquad (3.17)$$

Finally, the result follows from (3.13), (3.14), (3.15) and (3.17). $\qquad \square$

Next we shall derive an L^2-error estimate. To that end, let $\phi \in W$ be the solution to the dual problem

$$a(v, \phi) = (\psi, v) \quad \text{for all } v \in W, \qquad (3.18)$$

with $\psi \in L^2(\mathcal{O})$, and assume that we have the elliptic regularity

$$\|\phi\|_{H^2(\mathcal{O})} \lesssim \|\psi\|_{L^2(\mathcal{O})}. \qquad (3.19)$$

Furthermore, we assume that $\phi \in \widetilde{W} \cap H^2(\mathcal{O})$ and the discrete form a_h is adjoint consistent,

$$a_h(v, \phi) = (v, \psi) \quad \text{for all } v \in W_h + \widetilde{W}. \qquad (3.20)$$

Theorem 3.2. For $u \in \widetilde{W} \cap H^{p+1}(\mathcal{O})$, and provided A1–A4, the elliptic regularity (3.19), and the adjoint consistency (3.20) all hold, there exists a constant such that

$$\|u - u_h\|_{L^2(\mathcal{O})} \lesssim h^{p+1} \|u\|_{H^{p+1}(\mathcal{O})}. \qquad (3.21)$$

Setting $v = u - u_h$ in (3.20), we get

$$\begin{aligned}
(\psi, u - u_h)_{\mathcal{O}} &= a_h(u - u_h, \phi) \\
&= a_h(u - u_h, \phi - \pi_h \phi) + a_h(u - u_h, \pi_h \phi) \\
&= a_h(u - u_h, \phi - \pi_h \phi) + \underbrace{l_h(\pi_h \phi) - a_h(u_h, \pi_h \phi)}_{= s_h(u_h, \pi_h \phi)}
\end{aligned}$$

$$
\begin{aligned}
&= a_h(u - u_h, \phi - \pi_h \phi) + s_h(u_h, \pi_h \phi) \\
&\lesssim \|\|u - u_h\|\|_h \|\|\phi - \pi_h \phi\|\|_h + \|u_h\|_{s_h} \|\pi_h \phi\|_{s_h} \\
&\lesssim \|\|u - u_h\|\|_h \|\|\phi - \pi_h \phi\|\|_h \\
&\quad + (\|u_h - \pi_h u\|_{s_h} + \|\pi_h u\|_{s_h}) \|\pi_h \phi\|_{s_h} \\
&\lesssim h^{p+1} \|u\|_{H^{p+1}(\mathcal{O})} \|\phi\|_{H^2(\mathcal{O})} \\
&\lesssim h^{p+1} \|u\|_{H^{p+1}(\mathcal{O})} \|\psi\|_{L^2(\mathcal{O})},
\end{aligned}
\tag{3.22}
$$

where we used the energy error estimate (3.12) and estimate (3.17), assumption (3.10) on s_h, interpolation error estimates, and finally the elliptic regularity (3.19). Taking $\psi = u - u_h$ concludes the proof.

3.3. Useful inequalities

Here we recall some inequalities that will be used in the forthcoming analysis. For $T \in \mathcal{T}_h$, we have the standard trace inequality (see e.g. Brenner and Scott 2008)

$$
\|v\|_{\partial T}^2 \lesssim h^{-1} \|v\|_T^2 + h \|\nabla v\|_T^2, \quad v \in H^1(T),
\tag{3.23}
$$

and a trace inequality for cut elements, which is frequently used in CutFEM (see Wu and Xiao 2019),

$$
\|v\|_{T \cap \Omega_0}^2 \lesssim h^{-1} \|v\|_T^2 + h \|\nabla v\|_T^2, \quad v \in H^1(T),
\tag{3.24}
$$

where the constant is independent of how Ω_0 intersects T and of h. We also frequently use the standard inverse inequality (see Brenner and Scott 2008)

$$
|v|_{H^j(T)}^2 \lesssim h^{-2(j-s)} \|v\|_{H^s(T)}^2, \quad 0 \le s \le j, \ v \in W_h,
\tag{3.25}
$$

which, when combined with (3.24), yields the following for $v \in W_h$:

$$
\|v\|_{T \cap \Omega_0}^2 \lesssim h^{-1} \|v\|_T^2, \quad v \in W_h.
\tag{3.26}
$$

3.4. Approximation properties

Here we construct interpolation operators for bulk domains and embedded surfaces. To simplify the description, we consider the case when there is one bulk domain $\mathcal{O} = \Omega$ or one surface $\mathcal{O} = \Omega_0$. For interface problems with several subdomains Ω_i, interpolation operators have to be constructed in the same way, but for each subdomain and finite element space $V_{h,i}$.

The main idea when constructing interpolation operators for CutFEM is to first extend the function that we shall approximate using a stable extension operator, and then to interpolate the extended function using a stable interpolation operator.

Bulk domain. Let $E_B \colon H^s(\Omega) \to H^s(\mathbb{R}^d)$ be an extension operator with $s \ge 1$, such that $E_B v|_\Omega = v$ and

$$
\|E_B v\|_{H^s(\mathbb{R}^d)} \lesssim \|v\|_{H^s(\Omega)} \quad \text{for all } v \in H^s(\Omega),
\tag{3.27}
$$

where we refer to Stein (1970) for details. Recall from Section 2.1 that the domain Ω is embedded in a computational domain $\widetilde{\Omega}$, and recall the definition of the active domain Ω_h, as given in equation (2.5), and also that V_h denotes the finite element space defined on this active domain.

Let $\pi_{h,C} \colon L^2(\widetilde{\Omega}) \to V_h$ denote the Clément interpolation operator. For each element $T \in \mathcal{T}_h$ we have the following interpolation error estimate:

$$\|w - \pi_{h,C}w\|_{H^m(T)} \le Ch^{p+1-m}\|w\|_{H^{p+1}(N_h(T))}, \quad 0 \le m \le p+1, \qquad (3.28)$$

where $N_h(T) \subset \Omega_h$ is the union of the neighbouring elements of T. We now define the interpolation operator $\pi_h \colon L^2(\Omega) \to V_h$ by

$$\pi_h v = \pi_{h,C} E_B v. \qquad (3.29)$$

Using the interpolation error estimate in (3.28) and the stability of the extension operator (3.27), we obtain

$$\begin{aligned}
\|v - \pi_h v\|_{H^m(\Omega)} &\le \|E_B v - \pi_{h,C} E_B v\|_{H^m(\Omega_h)} \\
&\lesssim h^{p+1-m}\|E_B v\|_{H^{p+1}(\Omega_h)} \\
&\lesssim h^{p+1-m}\|v\|_{H^{p+1}(\Omega)}.
\end{aligned} \qquad (3.30)$$

Surfaces. Let $\Omega_0 \subset \mathbb{R}^d$ be a smooth, embedded codimension-one hypersurface. Let $\mathrm{dist}(x, \Omega_0) = \inf_{y \in \Omega_0} \|x - y\|_{\mathbb{R}^d}$ be the distance function associated with Ω_0, and let

$$U_\delta(\Omega_0) = \{x \in \mathbb{R}^d \mid \mathrm{dist}(x, \Omega_0) \le \delta\} \qquad (3.31)$$

denote the tubular neighbourhood of Ω_0 with thickness $2\delta > 0$. Then, for $\delta_0 > 0$ small enough, the closest-point projection $p_{\Omega_0} \colon U_{\delta_0}(\Omega_0) \to \Omega_0$ is well-defined, and we can define an extension operator $E_S \colon H^s(\Omega_0) \to H^s(U_\delta(\Omega_0))$ such that $E_S v = v \circ p_{\Omega_0}$ and

$$\|E_S v\|_{H^s(U_\delta(\Omega_0))} \lesssim \delta^{1/2}\|v\|_{H^s(\Omega_0)}, \quad v \in H^s(\Omega_0), \qquad (3.32)$$

for any $0 < \delta \le \delta_0$. In the same way as for the bulk domain, we define the interpolation operator $\pi_h \colon H^s(\Omega_0) \to V_{h,0}$ by

$$\pi_h v = \pi_{h,C} E_S v. \qquad (3.33)$$

Recall from Section 2.3 the definition of the active domain $\Omega_{h,0}$ (see equation (2.65)) and the finite element space $V_{h,0}$, defined on this domain. From equation (3.28) we obtain

$$\begin{aligned}
\|E_S v - \pi_{h,C} E_S v\|_{H^m(\Omega_{h,0})} &\lesssim h^{p+1-m}\|E_S v\|_{H^{p+1}(\Omega_{h,0})} \\
&\lesssim h^{p+1-m}h^{1/2}\|v\|_{H^{p+1}(\Omega_0)},
\end{aligned} \qquad (3.34)$$

for $h \in (0, h_0]$, with h_0 small enough to guarantee that $\Omega_{h,0} \subset U_{\delta_0}(\Omega_0)$ and $\Omega_{h,0} \subset U_\delta(\Omega_0)$ with $\delta \lesssim h$. Note that the patch $N_h(T)$ for $T \in \mathcal{T}_h$ (see equation (3.28)) can always be adjusted so that $N_h(T) \subset \Omega_{h,0}$.

To bound the interpolation error on the surface, we use the elementwise trace inequality (3.24) and combine it with equation (3.34) to obtain

$$
\begin{aligned}
\|\nabla_0^m(v - \pi_h v)\|_{\Omega_0}^2 &\lesssim h^{-1}\|\nabla^m(E_S v - \pi_{h,C}E_S v)\|_{\Omega_{h,0}}^2 \\
&\quad + h\|\nabla^{m+1}(E_S v - \pi_{h,C}E_S v)\|_{\Omega_{h,0}}^2 \\
&\lesssim h^{2(p+1-m)}\|v\|_{H^{p+1}(\Omega_0)}^2.
\end{aligned}
\tag{3.35}
$$

3.5. Condition number estimate

Next we prove a bound of the condition number of the stiffness matrix associated with the cut finite element method defined by (3.2). The stiffness matrix $\widehat{A}_h$ is defined by

$$
(\widehat{A}_h\widehat{v}, \widehat{w})_{\mathbb{R}^N} = A_h(v, w), \quad v, w \in W_h.
\tag{3.36}
$$

The operator $W_h \ni v \mapsto \widehat{v} \in \mathbb{R}^N$ is the coefficient extraction operator, which maps the function v to the vector of coefficients $\widehat{v} = (\widehat{v}_1, \widehat{v}_2, \ldots, \widehat{v}_N)$ with respect to a standard finite element basis $\{\varphi_i\}_{i=1}^N$ in W_h, and the expansion

$$
v = \sum_{i=1}^N \widehat{v}_i\varphi_i.
\tag{3.37}
$$

Recall that for a symmetric positive semidefinite problem, the spectral condition number is defined as

$$
\text{cond}(\widehat{A}_h) = \frac{\lambda_{\max}}{\lambda_{\min}},
\tag{3.38}
$$

where $\lambda_{\max}$ and $\lambda_{\min}$ are the maximum and minimum eigenvalues, respectively, of the eigenvalue problem

$$
\widehat{A}_h\widehat{v} = \lambda\widehat{v}.
\tag{3.39}
$$

Recall that the domain $\mathcal{O}$ refers to the physical domain, and let $\mathcal{O}_h$ denote the active domain associated with $\mathcal{O}$, as described in Section 2. In the context of the boundary value problem in Section 2.1, $\mathcal{O}_h$ corresponds to Ω_h, while for the interface problem in Section 2.2, it represents the disjoint union of the different active subdomains, $\mathcal{O}_h = \bigsqcup_i \Omega_{h,i}$. Let the norm $\|v\|_{\mathcal{O}_h}$ of a function $v = (v_1, v_2) \in W_h$ be defined as

$$
\|v\|_{\mathcal{O}_h}^2 = \sum_i \|v_i\|_{\Omega_{h,i}}^2.
\tag{3.40}
$$

Here we focus on bulk problems. For coupled bulk–surface problems, we need to precondition the problem by setting $v_0 = h^{1/2}\tilde{v}_0$ and solving for $\tilde{v}_0$. For further details, see Section 3.8 and Burman, Hansbo, Larson and Zahedi (2016a).

To derive an estimate of the condition number, we will need the following assumptions.

A5. *Inverse bound.* There exists a constant such that

$$\||v\||_{h,\star} \lesssim h^{-1}\|v\|_{\mathcal{O}_h}, \quad v \in W_h. \tag{3.41}$$

This inverse bound usually follows by the trace inequality and from standard inverse inequalities for standard finite element spaces on quasi-uniform meshes; see Section 3.3.

A6. *Poincaré inequality.* There exists a constant such that

$$\|v\|_{\mathcal{O}_h} \lesssim \||v\||_{h,\star}, \quad v \in W_h. \tag{3.42}$$

This Poincaré inequality requires stabilization to control the finite element functions in W_h on $\mathcal{O}_h$.

A7. *Norm equivalence.* There exist constants such that

$$h^d\|\widehat{v}\|_{\mathbb{R}^N}^2 \sim \|v\|_{\mathcal{O}_h}^2, \quad v \in W_h. \tag{3.43}$$

This standard estimate follows from the quasi-uniformity of the mesh and the use of a nodal basis (Ern and Guermond 2006).

Next we will show that a similar bound on the spectral condition number, which is satisfied by standard finite element methods, also holds for CutFEM, provided assumptions A2–A3 and A5–A7 are satisfied. We will verify assumption A6 in Section 4.

Theorem 3.3. Provided A2–A3 and A5–A7 hold, there exists a constant such that

$$\operatorname{cond}(\widehat{A}_h) \lesssim h^{-2}. \tag{3.44}$$

Proof. The eigenvalues are characterized by the Rayleigh quotient

$$\frac{(\widehat{A}_h\widehat{v}, \widehat{v})_{\mathbb{R}^N}}{\|\widehat{v}\|_{\mathbb{R}^N}^2} = \frac{A_h(v,v)}{\|\widehat{v}\|_{\mathbb{R}^N}^2}. \tag{3.45}$$

To bound $A_h(v,v)$ from above, we use assumption A2 (continuity (3.5)–(3.6)), A5 (inverse bound (3.41)), followed by A7 (norm equivalence (3.43)). This gives the estimate

$$A_h(v,v) \lesssim \||v\||_h^2 \lesssim h^{-2}\|v\|_{\mathcal{O}_h}^2 \lesssim h^{d-2}\|\widehat{v}\|_{\mathbb{R}^N}^2. \tag{3.46}$$

Therefore we have

$$\lambda_{\max} = \max_{v \in W_h} \frac{A_h(v,v)}{\|\widehat{v}\|_{\mathbb{R}^N}} \lesssim h^{d-2}. \tag{3.47}$$

To derive a bound from below, we use assumption A3 (stability (3.7)), A7 (norm equivalence (3.43)) and A6 (Poincaré inequality (3.42)), and proceed as follows:

$$h^d\|\widehat{v}\|_{\mathbb{R}^N}^2 \lesssim \|v\|_{\mathcal{O}_h}^2 \lesssim \||v\||_{h,\star}^2 \lesssim A_h(v,v). \tag{3.48}$$

From this we conclude that

$$\lambda_{\min} = \min_{v \in W_h} \frac{A_h(v,v)}{\|\widehat{v}\|_{\mathbb{R}^N}} \gtrsim h^d. \tag{3.49}$$

Combining the bounds for $\lambda_{\max}$ and $\lambda_{\min}$ completes the proof. $\qquad\square$

In the following subsections we verify some of the assumptions for the boundary value problem, the interface problem and the coupled bulk–surface problem, presented in Section 2.

3.6. Nitsche's method for a boundary value problem

Recall the boundary value problem presented in Section 2.1. The continuous problem is as follows: find $u \in V_g$ such that

$$a(u,v) = l(v) \quad \text{for all } v \in V_0, \tag{3.50}$$

where

$$a(v,w) = (\alpha \nabla v, \nabla w)_\Omega, \quad l(v) = (f,v)_\Omega, \tag{3.51}$$

and

$$V_g = \{v \in H^1(\Omega) \mid v = g \text{ on } \partial\Omega\}. \tag{3.52}$$

For the cut finite element method based on Nitsche's method, we seek $u_h \in V_h$ such that

$$A_h(u_h, v) = l_h(v) \quad \text{for all } v \in V_h, \tag{3.53}$$

where the forms are defined as follows:

$$A_h(v,w) = a_h(v,w) + \tau s_h(v,w), \tag{3.54}$$

$$a_h(v,w) = (\alpha \nabla v, \nabla w)_\Omega - (n \cdot \alpha \nabla v, w)_{\partial\Omega}$$
$$\qquad\qquad - (v, n \cdot \alpha \nabla w)_{\partial\Omega} + \beta h^{-1}(v,w)_{\partial\Omega}, \tag{3.55}$$

$$l_h(w) = (f,w)_\Omega - (g, n \cdot \alpha \nabla w)_{\partial\Omega} + \beta h^{-1}(g,w)_{\partial\Omega}. \tag{3.56}$$

By assuming that the weak solution to (3.50) belongs to $\widetilde{W} = V_g \cap H^{3/2+\varepsilon}(\Omega)$, applying partial integration, and using the boundary condition, we obtain

$$a_h(u,v) - l_h(v) = (\alpha \nabla u, \nabla v)_\Omega - (n \cdot \alpha \nabla u, v)_{\partial\Omega} - (f,v)_\Omega$$
$$= (-\nabla \cdot \alpha \nabla u, v)_\Omega - (f,v)_\Omega = 0. \tag{3.57}$$

Thus the method is consistent, and assumption A1 holds.

Next, we define the norm

$$\|\|v\|\|_h^2 = \|\alpha^{1/2}\nabla v\|_\Omega^2 + h\|\alpha^{1/2}\nabla v\|_{\partial\Omega}^2 + h^{-1}\|\alpha^{1/2}v\|_{\partial\Omega}^2, \tag{3.58}$$

and we note that the following continuity result holds:

$$a_h(v,w) \le \max\left(1, \frac{\beta}{\alpha}\right) \|\|v\|\|_h \|\|w\|\|_h. \tag{3.59}$$

To prove assumption A3 (stability) we begin by

$$a_h(v,v) \geq \|\alpha^{1/2}\nabla v\|_\Omega^2 - 2|(n \cdot \alpha\nabla v, v)_{\partial\Omega}| + \beta h^{-1}\|v\|_{\partial\Omega}^2. \qquad (3.60)$$

Next, we estimate the negative term using the stabilization form s_h. Assuming that s_h provides the estimate

$$h\|\alpha^{1/2}\nabla v\|_{\partial\Omega}^2 \lesssim \|\alpha^{1/2}\nabla v\|_\Omega^2 + \|\alpha^{1/2}v\|_{s_h}^2, \qquad (3.61)$$

we can bound the boundary term as follows:

$$\begin{aligned}
2|(n \cdot \alpha\nabla v, v)_{\partial\Omega}| &\leq 2\|\alpha^{1/2}\nabla v\|_{\partial\Omega}\|\alpha^{1/2}v\|_{\partial\Omega} \\
&\leq \delta_1 h\|\alpha^{1/2}\nabla v\|_{\partial\Omega}^2 + \delta_1^{-1}h^{-1}\|\alpha^{1/2}v\|_{\partial\Omega}^2 \\
&\leq \delta_1 C(\|\alpha^{1/2}\nabla v\|_\Omega^2 + \|\alpha^{1/2}v\|_{s_h}^2) + \delta_1^{-1}h^{-1}\|\alpha^{1/2}v\|_{\partial\Omega}^2, \quad (3.62)
\end{aligned}$$

with $\delta_1 > 0$. Hence

$$\begin{aligned}
A_h(v,v) = a_h(v,v) + \tau s_h(v,v) &\geq (1 - \delta_1 C)\|\alpha^{1/2}\nabla v\|_\Omega^2 \\
&+ (\beta - \delta_1^{-1})h^{-1}\|\alpha^{1/2}v\|_{\partial\Omega}^2 + (\tau - \delta_1 C\alpha)\|v\|_{s_h}^2. \qquad (3.63)
\end{aligned}$$

To finalize the stability estimate, we add and subtract the term $\delta_0 h\|\alpha^{1/2}\nabla v\|_{\partial\Omega}^2$, and then use the estimate (3.61) again to bound the negative term. This gives

$$\begin{aligned}
A_h(v,v) = a_h(v,v) + \tau s_h(v,v) &\\
\geq (1 - \delta C)\|\alpha^{1/2}\nabla v\|_\Omega^2 &+ \delta_0 h\|\alpha^{1/2}\nabla v\|_{\partial\Omega}^2 \\
+ (\beta - \delta_1^{-1})h^{-1}\|\alpha^{1/2}v\|_{\partial\Omega}^2 &+ (\tau - \delta C\alpha)\|v\|_{s_h}^2. \qquad (3.64)
\end{aligned}$$

Choosing small enough constants $\delta_i > 0$ with $\delta = \delta_1 + \delta_0$, a sufficiently large Nitsche penalty parameter β and stabilization constant τ (proportional to α), we obtain the desired stability estimate.

For the condition number, assumption A5 (inverse bound) follows from applying the trace inequality (3.24) and standard inverse inequalities on elements (see Section 3.3). We obtain for $v \in V_h$

$$\begin{aligned}
\|\|v\|\|_{h,\star}^2 &= \|\|v\|\|_h^2 + \alpha\|v\|_{s_h}^2 \\
&= \|\alpha^{1/2}\nabla v\|_\Omega^2 + h\|\alpha^{1/2}\nabla v\|_{\partial\Omega}^2 + h^{-1}\|\alpha^{1/2}v\|_{\partial\Omega}^2 + \alpha\|v\|_{s_h}^2 \\
&\lesssim h^{-2}\|\alpha^{1/2}v\|_{\Omega_h}^2 + \alpha\|v\|_{s_h}^2. \qquad (3.65)
\end{aligned}$$

Thus, for assumption A5 to hold, we require the following inequality:

$$\|v\|_{s_h}^2 \lesssim h^{-2}\|v\|_{\Omega_h}^2. \qquad (3.66)$$

Using, for example, the ghost penalty stabilization form discussed in Section 2.1, it is straightforward to verify that this inequality holds. For assumption A6, we need the bound

$$\alpha\|v\|_{\Omega_h}^2 \lesssim \|\|v\|\|_h^2 + \alpha\|v\|_{s_h}^2, \qquad (3.67)$$

which, together with (3.61) and (3.66), provides design criteria for the stabilization form s_h. In Section 4 we will present stabilization forms that satisfy these conditions. Finally, assumption A7 (norm equivalence) holds, as shown in Ern and Guermond (2006) using a nodal basis.

3.7. The interface problem

We now consider the interface problem in Section 2.2. We focus on verifying assumption A3 (stability) and, in particular, explore how the weights η_i can be used to minimize the penalty parameter, both with and without the presence of the stabilization form.

Recall the definition of the bilinear form A_h, as given in equations (2.41)–(2.43). For $v \in W_h$ we have

$$A_h(v, v) = \sum_{i=1}^{2} \alpha_i \|\nabla v_i\|_{\Omega_i}^2 + \tau_i \|v_i\|_{s_{h,i}}^2 - 2(\langle n \cdot \alpha \nabla v \rangle, [v])_{\Omega_0} + \beta h^{-1} \|[v]\|_{\Omega_0}^2.$$

$$(3.68)$$

We will carry out the analysis in the following norm:

$$\|\|v\|\|_h^2 = \sum_{i=1}^{2} \|\alpha_i^{1/2} \nabla v_i\|_{\Omega_i}^2 + h \sum_{i=1}^{2} \eta_i \|\alpha_i^{1/2} \nabla v_i\|_{\Omega_0}^2 + h^{-1} \frac{\alpha_1 \alpha_2}{\alpha_1 + \alpha_2} \|[v]\|_{\Omega_0}^2. \quad (3.69)$$

Next, assuming that the stabilization ensures the inverse estimate

$$h\|\alpha_i^{1/2} \nabla v_i\|_{\Omega_0}^2 \lesssim \|\alpha_i^{1/2} \nabla v_i\|_{\Omega_i}^2 + \|\alpha_i^{1/2} v_i\|_{s_{h,i}}^2, \quad (3.70)$$

and using the definition of the weighted average

$$\langle n \cdot \alpha \nabla v \rangle = \eta_1 n_1 \cdot \alpha_1 \nabla v_1 - \eta_2 n_2 \cdot \alpha_2 \nabla v_2$$
$$= \eta_1 n_1 \cdot \alpha_1 \nabla v_1 + \eta_2 n_1 \cdot \alpha_2 \nabla v_2, \quad (3.71)$$

we obtain

$$2(\langle n \cdot \alpha \nabla v \rangle, [v])_{\Omega_0}$$

$$= \sum_{i=1}^{2} 2(\eta_i n_1 \cdot \alpha_i \nabla v_i, [v])_{\Omega_0}$$

$$\leq \sum_{i=1}^{2} \delta_i h \|\alpha_i^{1/2} \nabla v_i\|_{\Omega_0}^2 + \delta_i^{-1} h^{-1} \eta_i^2 \alpha_i \|[v]\|_{\Omega_0}^2$$

$$\leq \sum_{i=1}^{2} \delta_i C_i \big(\|\alpha_i^{1/2} \nabla v_i\|_{\Omega_i}^2 + \|\alpha_i^{1/2} v_i\|_{s_{h,i}}^2 \big) + \delta_i^{-1} \eta_i^2 \alpha_i h^{-1} \|[v]\|_{\Omega_0}^2, \quad (3.72)$$

for $\delta_i > 0$, with C_i being the constant in the estimate (3.70). Hence

$$A_h(v, v) \geq \sum_{i=1}^{2}(1 - \delta_i C_i)\|\alpha_i^{1/2}\nabla v_i\|_{\Omega_i}^2$$
$$+ \left(\beta - \sum_{i=1}^{2}\delta_i^{-1}\eta_i^2\alpha_i\right)h^{-1}\|[v]\|_{\Omega_0}^2 + \sum_{i=1}^{2}(\tau_i - \delta_i C_i \alpha_i)\|v_i\|_{s_{h,i}}^2. \quad (3.73)$$

To finalize the stability estimate, we add and subtract the term $\delta_0\eta_i h\|\alpha_i^{1/2}\nabla v_i\|_{\Omega_0}^2$, for $i = 1, 2$, where $0 \leq \eta_i \leq 1$, and then use the estimate (3.70) again to bound the negative term. This gives

$$A_h(v, v) \geq \sum_{i=1}^{2}(1 - \widetilde{\delta_i} C_i)\|\alpha_i^{1/2}\nabla v_i\|_{\Omega_i}^2 + \delta_0 h \sum_{i=1}^{2}\eta_i\|\alpha_i^{1/2}\nabla v_i\|_{\Omega_0}^2$$
$$+ \left(\beta - \max_{i=1,2}(\delta_i^{-1})\sum_{i=1}^{2}\eta_i^2\alpha_i\right)h^{-1}\|[v]\|_{\Omega_0}^2$$
$$+ \sum_{i=1}^{2}(\tau_i - \widetilde{\delta_i} C_i \alpha_i)\|v_i\|_{s_{h,i}}^2. \quad (3.74)$$

By choosing sufficiently small constants $\delta_i > 0$ and $\widetilde{\delta_i} = \delta_i + \delta_0\eta_i$, and selecting a sufficiently large Nitsche penalty parameter β such that

$$\beta > \max_{i=1,2}(\delta_i^{-1})\sum_{i=1}^{2}\eta_i^2\alpha_i \gtrsim \frac{\alpha_1\alpha_2}{(\alpha_1 + \alpha_2)}, \quad (3.75)$$

along with sufficiently large stabilization constants τ_i (proportional to α_i), we can obtain the desired stability estimate.

Choosing the weights to minimize the Nitsche penalty parameter. We note that the Nitsche penalty parameter β depends on the choice of weights η_i. By selecting these weights appropriately, we can minimize the required penalty parameter. Specifically, we observe from (3.74) that we want to select η_1 such that the expression $\sum_{i=1}^{2}\eta_i^2\alpha_i = \eta_1^2\alpha_1 + (1 - \eta_1)^2\alpha_2$ is minimized.

Taking the derivative of this expression with respect to η_1, we find that the optimal weights correspond to the harmonic mean of the coefficients α_1 and α_2 given by

$$\eta_1 = \frac{\alpha_2}{\alpha_1 + \alpha_2}, \quad \eta_2 = \frac{\alpha_1}{\alpha_1 + \alpha_2}. \quad (3.76)$$

With these weights, we have

$$\sum_{i=1}^{2}\eta_i^2\alpha_i = \frac{\alpha_1\alpha_2}{(\alpha_1 + \alpha_2)}, \quad (3.77)$$

and β can be chosen as

$$\beta = \beta_0 \frac{\alpha_1 \alpha_2}{(\alpha_1 + \alpha_2)}, \tag{3.78}$$

where β_0 is a constant. It is also important to understand how the method behaves when α_2 tends to zero or infinity, while α_1 and the right-hand side remain fixed. We find the following.

- When $\alpha_2 \to 0$, we have $\eta_1 = 0$ and $\eta_2 = 1$, and the problem reduces to a homogeneous Neumann condition for u_1 on Ω_0.

- When $\alpha_2 \to \infty$, we have $\eta_1 = 1$ and $\eta_2 = 0$, the solution becomes constant in Ω_2, and we obtain a Dirichlet boundary condition for u_1 on Ω_0. However, the constant value in Ω_2 remains unknown and must be determined as part of the solution.

Choosing the weights to handle stability without stabilization. Alternatively, we can define weights based on how the interface cuts the element. By selecting appropriate weights, we can prove stability with respect to the unstabilized norm $\|| \cdot \||_h$. Let us consider piecewise linear elements. In this case, the gradient is constant within each element, and we have the identity

$$h_{T,i} \|\alpha_i^{1/2} \nabla v_i\|_{\Omega_0 \cap T}^2 = \frac{|\Omega_i \cap T|}{|\Omega_0 \cap T|} \|\alpha_i^{1/2} \nabla v_i\|_{\Omega_0 \cap T}^2 = \|\alpha_i^{1/2} \nabla v_i\|_{\Omega_i \cap T}^2 \tag{3.79}$$

for any element $T \in \mathcal{T}_{h,i}$ that intersects the interface Ω_0, where we define

$$h_{T,i} = \frac{|\Omega_i \cap T|}{|\Omega_0 \cap T|}. \tag{3.80}$$

Using this, we obtain the estimate

$$2(\langle n \cdot \alpha \nabla v \rangle, [v])_{\Omega_0}$$

$$= \sum_{i=1}^{2} 2(\eta_i n_1 \cdot \alpha_i \nabla v_i, [v])_{\Omega_0}$$

$$\leq \sum_{i=1}^{2} \delta_i h_{T,i} \|\alpha_i^{1/2} \nabla v_i\|_{\Omega_0}^2 + \delta_i^{-1} h_{T,i}^{-1} \eta_i^2 \alpha_i \|[v]\|_{\Omega_0}^2$$

$$\leq \sum_{i=1}^{2} \delta_i \|\alpha_i^{1/2} \nabla v_i\|_{\Omega_{h,i}}^2 + \left(\sum_{i=1}^{2} \delta_i^{-1} \eta_i^2 h_{T,i}^{-1} \alpha_i \right) h h^{-1} \|[v]\|_{\Omega_0}^2. \tag{3.81}$$

Next, we add and subtract $\delta_0 h_{T,i} \|\alpha_i^{1/2} \nabla v_i\|_{\Omega_0}^2$, and use the identity in (3.79) to estimate the negative term. We obtain the following estimate:

$$a_h(v,v) \geq \sum_{i=1}^{2} (1 - \widetilde{\delta}_i) \|\alpha_i^{1/2} \nabla v_i\|_{\Omega_i}^2 + \delta_0 h \sum_{i=1}^{2} (h \eta_i h_{T,i}^{-1})^{-1} \eta_i \|\alpha_i^{1/2} \nabla v_i\|_{\Omega_0}^2$$

$$+ \left(\beta - \max_{i=1,2}(\delta_i^{-1}) h \sum_{i=1}^{2} \eta_i^2 h_{T,i}^{-1} \alpha_i \right) h^{-1} \|[v]\|_{\Omega_0}^2. \tag{3.82}$$

Here $\delta_i > 0$ must be chosen small enough with $\widetilde{\delta}_i = \delta_i + \delta_0$, and the Nitsche penalty parameter β must satisfy

$$\beta > \max_{i=1,2}(\delta_i^{-1}) h \sum_{i=1}^{2} \eta_i^2 h_{T,i}^{-1} \alpha_i. \tag{3.83}$$

By choosing the weights η_i so that $\sum_{i=1}^{2} \eta_i^2 h_{T,i}^{-1} \alpha_i$ is minimized, we obtain the weights corresponding to the harmonic average:

$$\eta_1 = \frac{h_{T,2}^{-1} \alpha_2}{h_{T,1}^{-1} \alpha_1 + h_{T,2}^{-1} \alpha_2} = \frac{h_{T,1} \alpha_2}{h_{T,2} \alpha_1 + h_{T,1} \alpha_2}, \tag{3.84}$$

$$\eta_2 = \frac{h_{T,1}^{-1} \alpha_1}{h_{T,1}^{-1} \alpha_1 + h_{T,2}^{-1} \alpha_2} = \frac{h_{T,2} \alpha_1}{h_{T,2} \alpha_1 + h_{T,1} \alpha_2}. \tag{3.85}$$

We now show that the constants in (3.82) remain bounded independently of the cut configuration, i.e. the values of $h_{T,1}$ and $h_{T,2}$. This will demonstrate coercivity (stability),

$$\|\|v\|\|_h^2 \lesssim a_h(v,v), \tag{3.86}$$

without the need for stabilization. More precisely, we will show that there exists a constant $C > 0$, independent of how the interface cuts the mesh, such that

$$h \eta_i h_{T,i}^{-1} \leq C, \tag{3.87}$$

if the following conditions hold:

$$|\Omega_0 \cap T| \lesssim h^{d-1} \tag{3.88}$$

and

$$\alpha_i \sim 1. \tag{3.89}$$

The first assumption means that the complexity of the interface is limited, and the second condition is satisfied for each fixed bounded constant coefficient pair α_1 and α_2. Note that using $0 \leq \eta_i \leq 1$ and $\alpha_i \sim 1$, we have

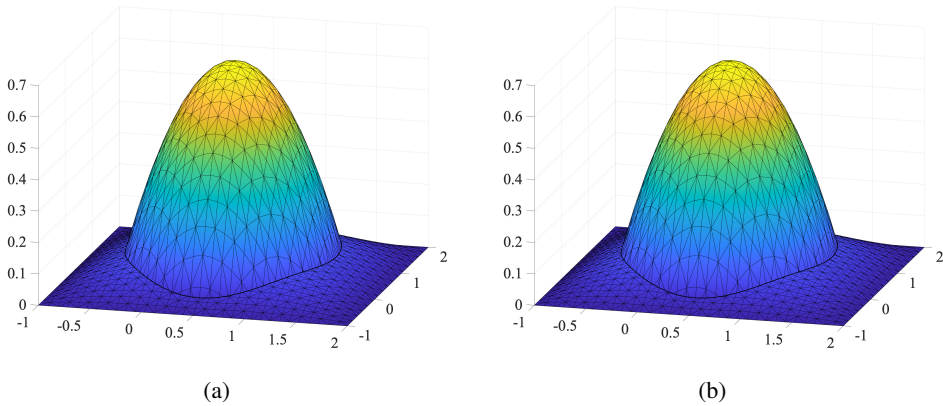$$h \eta_i^2 h_{T,i}^{-1} \alpha_i \leq h \eta_i h_{T,i}^{-1}. \tag{3.90}$$

Figure 3.1. The solution with $\tau_i = 0.1$ (a) and $\tau_i = 0$ (b).

Now,

$$h\eta_i h_{T,i}^{-1} = hh_{T,i}^{-1} \frac{h_{T,i}\alpha_j}{h_{T,2}\alpha_1 + h_{T,1}\alpha_2} = \frac{h\alpha_j}{h_{T,2}\alpha_1 + h_{T,1}\alpha_2} \sim \frac{h}{h_{T,1} + h_{T,2}}. \quad (3.91)$$

By observing that

$$h_{T,1} + h_{T,2} = \frac{|\Omega_1 \cap T|}{|\Omega_0 \cap T|} + \frac{|\Omega_2 \cap T|}{|\Omega_0 \cap T|} = \frac{|\Omega_1 \cap T| + |\Omega_2 \cap T|}{|\Omega_0 \cap T|} = \frac{|T|}{|\Omega_0 \cap T|}, \quad (3.92)$$

we conclude that

$$h\eta_i h_{T,i}^{-1} \sim \frac{h|\Omega_0 \cap T|}{|T|} \le C, \quad (3.93)$$

where we finally used (3.88). Thus we have shown that stability holds.

Note that to ensure that the condition number remains well-behaved, we need to add a stabilization form such that the following Poincaré inequality holds:

$$\sum_{i=1}^{2} \alpha_i \|v_i\|_{\Omega_{h,i}}^2 \lesssim \||v\||_h^2 + \sum_{i=1}^{2} \alpha_i \|v_i\|_{s_{h,i}}^2. \quad (3.94)$$

This demonstrates that while coercivity with respect to an unstabilized norm is achievable, at least for linear elements and each fixed and bounded pair of coefficients α_1 and α_2, stabilization is required to guarantee that the stiffness matrix remains well-conditioned.

Numerical illustration. We first show the cut finite element solution to the problem in Section 2.5 with $\tau_i = 0$ and compare it with the case where $\tau_i = 0.1$ (see Figure 3.1). The weights are chosen according to equations (3.84)–(3.85), ensuring stability also without stabilization.
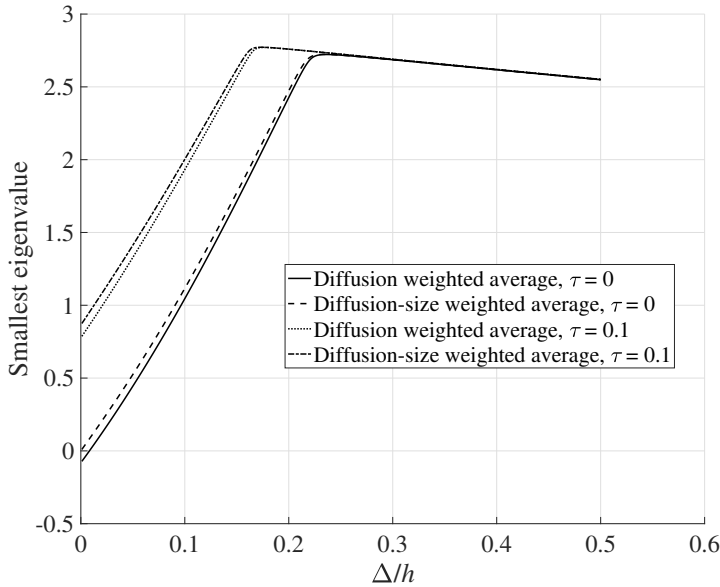
Figure 3.2. Smallest eigenvalue of the system matrix for different choices of weights, with and without stabilization. Δ denotes the distance from the interface to the node at $x = 0.5$.

To investigate the effect of the interface position on the eigenvalues and the conditioning of the discrete problem, we consider a one-dimensional interface problem defined on $x \in (0, 1)$ with diffusion parameters $\alpha_1 = 1$ (to the left of the cut) and $\alpha_2 = 10$ (to the right of the cut). We set $g_0 = f_0 = 0$, $f_i = 1$, and impose zero boundary conditions at $x = \{0, 1\}$. The domain is discretized with ten linear elements of equal size, and the position of the interface is varied, moving it from $x = 0.55$ towards the node at $x = 0.5$.

Figure 3.2 shows the effect on the smallest eigenvalue. We compare the diffusion-weighted average (3.76) with the diffusion–size average (3.84)–(3.85), both with and without stabilization. We observe that the diffusion-weighted average (3.76) eventually leads to a singular system matrix when stabilization is not applied, whereas the diffusion–size average does not. In Figure 3.3 we illustrate the effect of stabilization on the condition number of the system matrix. While the diffusion–size average remains stable, it still leads to severe ill-conditioning for a small cut. Stabilization effectively remedies this problem.

3.8. Coupled bulk–surface problem

Recalling Section 2.3, we have

$$A_h(v, w) = a(v, w) + s_h(v, w), \tag{3.95}$$
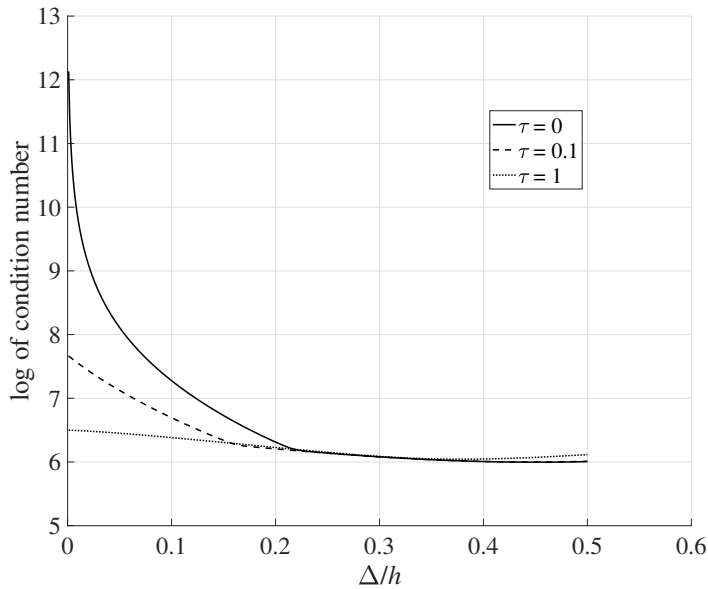
Figure 3.3. Condition number with and without stabilization, Here we use the diffusion–size weighted average.

with

$$a(v, w) = b_0(\alpha_0 \nabla_0 v_0, \nabla_0 w_0)_{\Omega_0}$$

$$+ \sum_{i=1}^{2} (b_i(\alpha_i \nabla v_i, \nabla w_i)_{\Omega_i} + ([bv]_i, [bw]_i)_{\Omega_0}), \qquad (3.96)$$

and thus in this case $a_h(v, w) = a(v, w)$. The energy norm is defined by

$$\|\|v\|\|_h^2 = a(v, v). \qquad (3.97)$$

As a result, we obtain consistency, continuity and stability (assumptions A1–A3), and thus we directly obtain error estimates.

To derive a condition number estimate, we first precondition the problem by using the substitution

$$v_0 = h^{1/2} \tilde{v}_0, \qquad (3.98)$$

and then we solve for $(\tilde{v}_0, v_1, v_2)$. Note that the same substitution is done for the test function.

We will need to verify the inverse bound (assumption A5) and the Poincaré inequality (assumption A6). For the preconditioned problem, the Poincaré inequality

takes the form

$$b_0\|\tilde{v}_0\|^2_{\Omega_{h,0}} + \sum_{i=1}^2 b_i\|v_i\|^2_{\Omega_{h,i}} \lesssim b_0 h\|\alpha_0^{1/2}\nabla_0\tilde{v}_0\|^2_{\Omega_0} + b_0 h\|\tilde{v}_0\|^2_{s_{h,0}}$$

$$+ \sum_{i=1}^2 b_i\|\alpha_i^{1/2}\nabla v_i\|^2_{\Omega_i} + \|[bv]_i\|^2_{\Omega_0} + b_i\|v_i\|^2_{s_{h,i}}. \tag{3.99}$$

To establish this inequality, we assume that the stabilization forms $s_{h,i}$ are such that

$$\|v_i - \lambda_i(v_i)\|^2_{\Omega_{h,i}} \lesssim \|\alpha_i^{1/2}\nabla v_i\|^2_{\Omega_i} + \|v_i\|^2_{s_{h,i}}, \quad i = 1,2, \tag{3.100}$$

For $i = 0$, we assume that we have

$$\|\tilde{v}_0 - \lambda_i(\tilde{v}_0)\|^2_{\Omega_{h,i}} \lesssim h\|\alpha_0^{1/2}\nabla\tilde{v}_0\|^2_{\Omega_i} + h\|\tilde{v}_0\|^2_{s_{h,0}}, \tag{3.101}$$

where we note that we have an additional h factor multiplying the first term that compensates for the difference in the dimension of Ω_0 and $\Omega_{h,0}$. Here $\lambda_i : V_{h,i} \to P_0(\Omega_{h,i})$ is a map that takes $v \in V_{h,i}$ to a constant function such that λ_i is the identity map on constant functions v_i. Here $P_0(\omega)$ is the space of constant functions on ω. We also note that in the preconditioned form we have control over the right-hand sides (3.100) and (3.101).

Choosing λ_i such that

$$(b_i(v_i - \lambda_i(v_i)), w)_{\Omega_0} = 0 \quad \text{for all } w \in P_0(\Omega_0), \tag{3.102}$$

which is the L^2-projection onto constant functions on Ω_0, we obtain

$$([b(v - \lambda(v))]_i, w)_{\Omega_0} = 0 \quad \text{for all } w \in P_0(\Omega_0) \tag{3.103}$$

and

$$\|[bv]_i\|^2_{\Omega_0} = \|[b(v - \lambda(v))]_i\|^2_{\Omega_0} + \|[b\lambda(v)]_i\|^2_{\Omega_0}. \tag{3.104}$$

Using (3.100), we proceed as follows:

$$b_0\|\tilde{v}_0\|^2_{\Omega_{h,0}} + \sum_{i=1}^2 b_i\|v_i\|^2_{\Omega_{h,i}}$$

$$\lesssim b_0\|\tilde{v}_0 - \lambda_0(\tilde{v}_0)\|^2_{\Omega_{h,0}} + b_0\|\lambda_0(\tilde{v}_0)\|^2_{\Omega_{h,0}}$$

$$+ \sum_{i=1}^2 b_i\|v_i - \lambda_i(v_i)\|^2_{\Omega_{h,i}} + b_i\|\lambda_i(v_i)\|^2_{\Omega_{h,i}}$$

$$\lesssim b_0 h\|\nabla_0\tilde{v}_0\|^2_{\Omega_{h,0}} + b_0\|\tilde{v}_0\|^2_{s_{h,0}} + b_0\|\lambda_0(\tilde{v}_0)\|^2_{\Omega_{h,0}}$$

$$+ \sum_{i=1}^2 b_i\|\alpha_i^{1/2}\nabla v_i\|^2_{\Omega_i} + b_i\|v_i\|^2_{s_{h,i}} + b_i\|\lambda_i(v_i)\|^2_{\Omega_{h,i}}. \tag{3.105}$$

Here we used the fact that $\lambda_i(v_i)$ is a constant function and the definition (3.102). It remains to bound

$$b_0\|\lambda_0(\tilde{v}_0)\|_{\Omega_{h,0}}^2 + \sum_{i=1}^2 b_i\|\lambda_i(v_i)\|_{\Omega_{h,0}}^2$$

$$\lesssim \underbrace{b_0 h\|\lambda_0(\tilde{v}_0)\|_{\Omega_0}^2}_{=b_0\|\lambda_0(v_0)\|_{\Omega_0}^2} + \sum_{i=1}^2 b_i\|\lambda_i(v_i)\|_{\Omega_0}^2 = \bigstar, \qquad (3.106)$$

where we used the fact that we have constant functions on domains with measures such that $|\Omega_{h,0}| \lesssim h|\Omega_0|$ and $|\Omega_{h,i}| \lesssim |\Omega_i| \lesssim |\Omega_0|$ for $i = 1, 2$, and finally for the first term the definition $v_0 = h^{1/2}\tilde{v}_0$.

First, using a trace inequality on Ω_1 (which holds since we have the homogeneous boundary condition on the outer boundary), we get

$$\|\lambda_1(v_1)\|_{\Omega_0}^2 \lesssim \|v_1\|_{\Omega_0}^2 \lesssim \|\alpha_1^{1/2}\nabla v_1\|_{\Omega_1}^2. \qquad (3.107)$$

Next we use this to bound the term involving $\lambda_0(v_0)$:

$$\|b_0\lambda_0(v_0)\|_{\Omega_0}^2 \lesssim \|b_0\lambda_0(v_0) - b_1\lambda_1(v_1)\|_{\Omega_0}^2 + b_1\|\lambda_1(v_1)\|_{\Omega_0}^2$$

$$\lesssim \|[b\lambda(v)]_1\|_{\Omega_0}^2 + b_1\|\alpha_1^{1/2}\nabla v_1\|_{\Omega_1}^2. \qquad (3.108)$$

Proceeding in the same way, we get

$$b_2\|\lambda_2(v_2)\|_{\Omega_0}^2 \lesssim \sum_{i=1}^2 \|[b\lambda(v)]_i\|_{\Omega_0}^2 + b_1\|\alpha_1^{1/2}\nabla v_1\|_{\Omega_1}^2, \qquad (3.109)$$

and we conclude that

$$\bigstar \lesssim \sum_{i=1}^2 \|[b\lambda(v)]_i\|_{\Omega_0}^2 + b_1\|\alpha_1^{1/2}\nabla v_1\|_{\Omega_1}^2$$

$$\lesssim \sum_{i=1}^2 \|[bv]_i\|_{\Omega_0}^2 + b_1\|\alpha_1^{1/2}\nabla v_1\|_{\Omega_1}^2, \qquad (3.110)$$

where we used (3.104). Finally, by combining this bound with (3.105), we arrive at the desired estimate (3.99).

Finally, we comment on assumption A5. For the bulk terms we have

$$b_i\|\nabla v_i\|_{\Omega_i}^2 \lesssim b_i\|\nabla v_i\|_{\Omega_{h,i}}^2 \lesssim b_i h^{-2}\|v_i\|_{\Omega_{h,i}}^2, \qquad (3.111)$$

and for the surface term

$$b_0 h\|\nabla_0\tilde{v}_0\|_{\Omega_0}^2 \lesssim b_0\|\nabla_0\tilde{v}_0\|_{\Omega_{h,0}}^2 \lesssim b_0 h^{-2}\|\tilde{v}_0\|_{\Omega_{h,0}}^2. \qquad (3.112)$$

The coupling terms can be estimated in a similar way, which completes the verification of the inverse inequality.

4. Weak stabilization

This section introduces weak stabilization forms for cut finite element methods in bulk domains. These forms are added to the weak formulation to improve control over the solution in the active mesh, beyond the physical domain. When the solution is not adequately controlled across the entire active mesh, problems such as ill-conditioned linear systems, loss of accuracy and severe time-step restrictions in time-dependent problems can arise, depending on the position of the boundary or the interface relative to the computational mesh. The fundamental idea behind the weak stabilization technique is to control the variation of the discrete functions between neighbouring elements. A standard approach for achieving this is by controlling the jump in normal derivatives across element faces, typically by adding appropriately scaled stiffness proportional to these jumps. However, we will also explore how this technique can be generalized in several directions.

In this section we assume that the physical domain is denoted by Ω and the active domain by Ω_h (for notation, refer to Section 2). In problems involving multiple bulk domains Ω_i separated by interfaces, stabilization must be applied in each active mesh $\Omega_{h,i}$ corresponding to each subdomain Ω_i individually. Therefore, all results presented in this section apply to each subdomain separately.

4.1. Abstract properties

A weak stabilization form for a second-order problem is a positive semidefinite bilinear form $s_{h,m}$ acting on V_h that satisfies the following assumptions.

- There exists a constant such that

$$\|\nabla^m v\|_{\Omega_h}^2 \lesssim \|\nabla^m v\|_{\Omega}^2 + \|v\|_{s_{h,m}}^2, \quad v \in V_h, \tag{4.1}$$

  where we recall that $\Omega_h = \cup_{T \in \mathcal{T}_h} T$ and $\|v\|_{\Omega_h}^2 = \sum_{T \in \mathcal{T}_h} \|v\|_T^2$. Here $m = 0$ or $m = 1$.

- There exists a constant such that the weak consistency condition (3.10) holds,

$$\|\pi_h v\|_{s_{h,m}} \lesssim h^{s-m} \|v\|_{H^s(\Omega)}, \quad 1 \le s \le p+1, \tag{4.2}$$

  where $\pi_h \colon H^s(\Omega) \to V_h$ is the interpolation operator introduced in Section 3.4 for bulk domains.

In the previous sections we used $s_{h,i}$ to denote the stabilization associated with the domain Ω_i. When necessary for clarity, we may write $s_{h,i,m}$, where the index i indicates that the stabilization form is associated with the domain Ω_i. However, in this section we consider only one bulk domain, so we adopt the simplified notation $s_{h,m}$, where m represents the order of derivatives that we control.

4.2. Examples of stabilization forms

We classify the elements in the active mesh into small and large elements, where small elements have a limited intersection with the domain Ω and therefore require

stabilization. More precisely, an element is considered large, given a parameter $0 \le \gamma \le 1$, if

$$\gamma \le \frac{|T \cap \Omega|}{|T|}. \tag{4.3}$$

Otherwise, the element is considered small.

We decompose the active mesh $\mathcal{T}_h$ and the domain Ω_h as

$$\mathcal{T}_h = \mathcal{T}_h^L \cup \mathcal{T}_h^S, \quad \Omega_h = \Omega_h^L \cup \Omega_h^S, \tag{4.4}$$

where Ω_h^L and Ω_h^S represent the domains formed by the large and small elements of the active mesh, respectively.

Face-based stabilization forms. The most common stabilization term for cut elements is the face or ghost penalty (Burman 2010), defined as

$$s_{h,m}(v, w) = \sum_{F \in \mathcal{F}_h} \sum_{j=1}^{p} \tau_j h^{2(j-m)+1} ([\nabla_n^j v], [\nabla_n^j w])_F, \tag{4.5}$$

where $m = 0, 1$, τ_j are positive constants, and $\mathcal{F}_h$ is the set of all interior faces shared by an element in $\mathcal{T}_h(\partial\Omega) = \{T \in \mathcal{T}_h \mid T \cap \partial\Omega \ne \phi\}$. The term $[\nabla_n^j v]$ denotes the jump in the jth normal derivative across the face F shared by two elements T_1 and T_2, that is,

$$[\nabla_n^j v] = \nabla_n^j v_1 - \nabla_n^j v_2, \tag{4.6}$$

where v_i denotes the function v on element T_i, and n is the unit normal to the face F outward directed with respect to T_1.

For simplicity, let us consider the case of linear elements, i.e. $p = 1$. In this case, for elements T_1 and T_2 sharing a face F, there exist constants such that for all $v \in V_h$,

$$\|v\|_{T_1}^2 \lesssim \|v\|_{T_2}^2 + h^3 \|[\nabla_n v]\|_F^2, \quad \|\nabla v\|_{T_1}^2 \lesssim \|\nabla v\|_{T_2}^2 + h\|[\nabla_n v]\|_F^2, \tag{4.7}$$

which correspond to $m = 0$ and $m = 1$, respectively. To derive these estimates, let v_i denote the polynomial on T_i, for $i = 1, 2$, and extend its definition to $T_1 \cup T_2$. Taylor expansion around a point $x_F \in F$ yields

$$\begin{aligned} v_1(x) - v_2(x) &= v_1(x_F) - v_2(x_F) + (x - x_F) \cdot \nabla(v_1 - v_2) \\ &= n \cdot (x - x_F) n \cdot \nabla(v_1 - v_2), \end{aligned} \tag{4.8}$$

since $v_1 - v_2 = 0$ on F. For the first estimate in (4.7), we subtract and add v_2, use the triangle inequality, and then apply the Taylor expansion,

$$\begin{aligned} \|v_1\|_{T_1}^2 &\lesssim \|v_1 - v_2\|_{T_1}^2 + \|v_2\|_{T_1}^2 \lesssim \|(x - x_F) \cdot \nabla(v_1 - v_2)\|_{T_1}^2 + \|v_2\|_{T_2}^2 \\ &\lesssim h^3 \|\nabla_n(v_1 - v_2)\|_F^2 + \|v_2\|_{T_2}^2 = h^3 \|[\nabla_n v]\|_F^2 + \|v_2\|_{T_2}^2. \end{aligned} \tag{4.9}$$

Here we used the estimate $\|v_2\|_{T_1} \lesssim \|v_2\|_{T_2}$, which holds because v_2 is a polynomial. The second estimate in (4.7) follows in a similar manner. However, note that
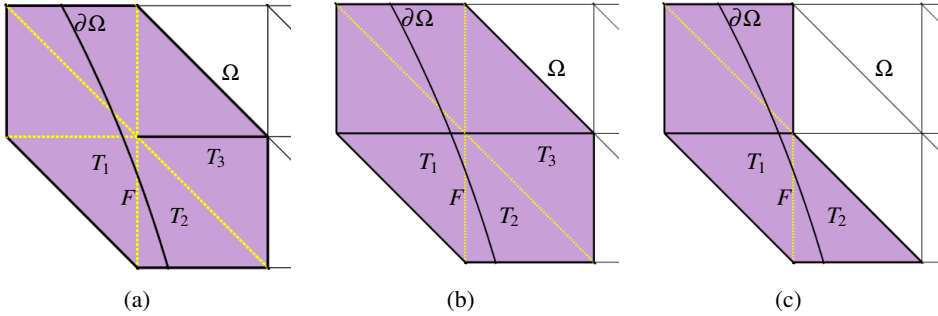
Figure 4.1. The idea behind stabilization. The dotted yellow edges and purple elements represent the edges and elements involved in the stabilization process. (a) Full stabilization. Stabilization is applied across all interior faces in the active mesh that are shared by an element in $\mathcal{T}_h(\partial\Omega) = \{T \in \mathcal{T}_h \mid T \cap \partial\Omega \neq \phi\}$. (b) Macro-element stabilization with $\gamma = 1$. In this case, all cut elements are considered small, and each small element is connected via stabilization to only one large element. The elements T_1 and T_2 belong to $\mathcal{T}_h^S$, but are connected to $T_3 \in \mathcal{T}_h^L$ via edges, on which stabilization is applied. (c) $\gamma = 0.3$. Here T_1 is small, while T_2 is classified as large and belongs to $\mathcal{T}_h^L$. Each small element is connected to one large element.

$\nabla v_1 - \nabla v_2 \neq 0$ on F, and the higher-order terms in the Taylor expansion vanish since the gradients are piecewise constant (for $p = 1$), leading to an h-scaling factor instead of the h^3-scaling factor.

Using the pairwise bounds, either directly or through a chain of neighbouring elements that share faces (see Figure 4.1), the degrees of freedom on small elements in $\mathcal{T}_h^S$ can be controlled by the degrees of freedom on large elements in $\mathcal{T}_h^L$, for which we have the robust inverse estimate

$$\|\nabla v\|_T^2 \lesssim \|\nabla v\|_{T\cap\Omega}^2, \quad T \in T_h^L, \tag{4.10}$$

and thus

$$\|\nabla v\|_{\Omega_h}^2 \lesssim \|\nabla v\|_\Omega^2 + \|v\|_{s_{h,1}}^2, \quad \|v\|_{\Omega_h}^2 \lesssim \|v\|_\Omega^2 + \|v\|_{s_{h,0}}^2. \tag{4.11}$$

Note that the constants in these estimates depend on the lengths of the paths connecting cut elements to interior elements, or, more generally, small elements to large elements. The length of these paths depends on both the properties and resolution of the boundary, as well as the mesh properties. It can be shown that the path length is uniformly bounded for smooth boundaries and locally quasi-uniform meshes with sufficiently small mesh sizes. For higher-order piecewise polynomial approximations ($p > 1$), the bound in equation (4.1) is derived in a similar manner to the $p = 1$ case, by simply including the higher-order terms in the Taylor expansion.

The stabilization term also satisfies the bound

$$\|v\|_{s_{h,m}} \lesssim \|\nabla^m v\|_{\Omega_h}, \quad v \in V_h, \tag{4.12}$$

for $m = 0, 1$. Recall the definition of $s_{h,m}$ in equation (4.5). The inequality in equation (4.12) follows from the triangle inequality, a standard trace inequality (see (3.23)) and standard inverse estimates (see (3.25)). These inequalities allow us to pass from the face F to the neighbouring elements T_1 and T_2, and removing the term ∇_n^{j-1} using the factor h^{j-1},

$$h^{2(j-m)+1}\|[\nabla_n^j v]\|_F^2 \lesssim \sum_{l=1}^2 h^{2(j-m)+1}\|\nabla_n^j v_l\|_F^2$$

$$\lesssim \sum_{l=1}^2 h^{2(j-m)}\|\nabla^j v_l\|_{T_l}^2 \lesssim \sum_{l=1}^2 \|\nabla^m v_l\|_{T_l}^2. \tag{4.13}$$

Thus we have the equivalence

$$\|\nabla^m v\|_\Omega^2 + \|v\|_{s_{h,m}}^2 \sim \|\nabla^m v\|_{\Omega_h}^2, \quad m = 0, 1. \tag{4.14}$$

Finally, stabilization can be applied more restrictively by connecting each small element in T_h^S to only one large element in T_h^S, and by choosing $\gamma < 1$ so that cut elements with a large intersection with the physical domain Ω are classified as large. In this case the set $\mathcal{F}_h$ in equation (4.5) will contain fewer faces compared to the full stabilization, where all interior faces shared by an element in $\mathcal{T}_h(\partial\Omega) = \{T \in \mathcal{T}_h \mid T \cap \partial\Omega \neq \phi\}$ are included in $\mathcal{F}_h$. An illustration can be found in Figure 4.1. We refer to Larson and Zahedi (2023) for further details of this so-called macro-element stabilization.

Element-based stabilization forms. An alternative implementation of the face penalty, which is particularly convenient for higher-order polynomials (as it avoids the need for higher-order derivatives), is given by (see Preuß 2018)

$$s_{h,m}(v, w) = \sum_{F \in \mathcal{F}_h} \tau h^{-2m}([v], [w])_{P(F)}, \tag{4.15}$$

or equivalently

$$s_{h,m}(v, w) = \sum_{F \in \mathcal{F}_h} \tau h^{2(1-m)}([\nabla v], [\nabla w])_{P(F)}, \tag{4.16}$$

where for each face $F \in \mathcal{F}_h$, $P(F)$ denotes the union of the two elements sharing the face F. Here the jump is defined as

$$[\nabla^l v] = \nabla^l v_1^e - \nabla^l v_2^e \quad \text{on } P(F) = T_1 \cup T_2, \quad l = 0, 1, \tag{4.17}$$

where v_i^e represents the polynomial v_i extended from T_i to $T_1 \cup T_2$ in the canonical way.

Projection-based stabilization forms. For this approach we consider stabilization on patches or macro-elements, where each small element is associated with a patch of neighbouring elements that contains a large element. We then penalize the difference between the finite element functions restricted to the patch and a global polynomial defined on the patch. More precisely, let $\{M_T : T \in \mathcal{T}_h^P\}$ be a set of patches, where $\mathcal{T}_h^P \subset \mathcal{T}_h^L$ is a subset of large elements that enumerate the patches, such that the patches cover all small elements, that is,

$$\Omega_h^S \subset \cup_{T \in \mathcal{T}_h^P} M_T. \tag{4.18}$$

We then define the stabilization form,

$$s_{h,m}(v, w) = \sum_{T \in \mathcal{T}_h^P} \tau h^{-2(1-m)} (\nabla^m(v - P_{k,m}v), \nabla^m(w - P_{k,m}w))_{M_T}, \tag{4.19}$$

for $m = 0, 1$, where $P_{k,m} : V_h|_{M_T} \to \mathbb{P}_k(M_T)$ is the L^2-projector for $m = 0$ and the Ritz projector for $m = 1$. The choice of the global polynomial is not critical; for instance, we may take the canonical extension of the polynomial on a large element in the patch.

Stabilized bilinear forms. We may alternatively take the viewpoint that we stabilize the inner products involved in the formulation, rather than adding a separate stabilization term. A typical formulation will involve $L^2(\Omega)$-inner products, and we can define the stabilized L^2-inner product on the space of discontinuous piecewise polynomials X_h as

$$(v, w)_{h,\Omega} = (v, w)_\Omega + s_h(v, w), \tag{4.20}$$

where, for example,

$$s_h(v, w) = \sum_{F \in \mathcal{F}_h} \sum_{j=0}^{p} \tau_j h^{2j+1} ([\nabla_n^j v], [\nabla_n^j w])_F. \tag{4.21}$$

Since the jump in the function itself is included in s_h, we can, as before (see (4.13)), show the following equivalences:

$$\|v\|_{h,\Omega} \sim \|v\|_{\Omega_h}, \quad \|\nabla v\|_{h,\Omega_h} \sim \|\nabla v\|_{\Omega_h}. \tag{4.22}$$

This approach is of particular interest when we have a finite element space that satisfies an inf-sup condition for standard elements:

$$m\|q\|_Q \leq \sup_{v \in V_h} \frac{b(v, q)}{\|v\|_V}, \tag{4.23}$$

where $b(v, q) = (Bv, q)_\Omega$ for some operator B, such as the divergence operator, and the finite element spaces are such that $BV_h = Q_h$. Then we stabilize the L^2-inner product, leading to

$$b_h(v, q) = (Bv, q)_\Omega + s_h(Bv, q). \tag{4.24}$$

Taking v such that $Bv = q$, we get

$$b_h(v, q) = (Bv, q)_\Omega + s_h(Bv, q) = (q, q)_\Omega + s_h(q, q) \gtrsim \|q\|^2_{\Omega_h}, \qquad (4.25)$$

which, together with the inequality $\|v\|_V \lesssim \|q\|_Q$, establishes the inf-sup condition. Specifically,

$$\|q\|_{\Omega_h} \lesssim \frac{b_h(v, q)}{\|q\|_Q} \lesssim \frac{b_h(v, q)}{\|v\|_V} \frac{\|v\|_V}{\|q\|_Q} \lesssim \frac{b_h(v, q)}{\|v\|_V}. \qquad (4.26)$$

On the other hand, if we take $q = Bv$, we obtain

$$b_h(v, Bv) = (Bv, Bv)_\Omega + s_h(Bv, Bv) \gtrsim \|Bv\|^2_{\Omega_h}. \qquad (4.27)$$

Thus both q and the constraint are controlled on the active mesh. This is a powerful tool whenever the two above choices of test functions are allowed. For instance, this is the case when approximating the Stokes equations or the Darcy equation, where the finite element space for the velocities has a divergence-free subspace with approximation properties. In such cases, both the pressure and the divergence can be controlled. See Frachon *et al.* (2024*a,b*) in the context where B is the divergence operator and the curl operator.

4.3. Generalized pairwise stabilization

We can generalize the construction of the stabilization form by assuming access to a mapping $S_h : \mathcal{T}_h^S \to \mathcal{T}_h^L$, which maps a small element T onto a large element $S_h(T)$ such that

$$\operatorname{diam}(S_h(T) \cup T) \lesssim h. \qquad (4.28)$$

Such a map exists for domains with Lipschitz boundaries and sufficiently small mesh sizes h; see Burman *et al.* (2022*c*). For each small element $T \in \mathcal{T}_h^S$, we define the jump as

$$[v]_T = v|_T - (v|_{S_h(T)})^e|_T, \qquad (4.29)$$

where $(v|_{S_h(T)})^e$ denotes the canonical extension of the polynomial on the large element $S_h(T)$.

A generalized stabilization form is then defined by

$$s_{h,m}(v, w) = \sum_{T \in \mathcal{T}_h^S} \tau h^{\alpha_m} b_T([v]_T, [w]_T), \qquad (4.30)$$

where b_T is a positive semidefinite form, and α_m is chosen so that $s_{h,m}$ stabilizes the H^m-norm:

$$\|v\|^2_{H^m(\Omega_h)} \lesssim \|v\|^2_{H^m(\Omega)} + \|v\|^2_{s_{h,m}}. \qquad (4.31)$$

Further, the following weak consistency holds:

$$\|\pi_h v\|_{s_{h,m}} \lesssim h^{s-m} \|v\|_{H^s(\Omega)}, \quad m \le s \le p + 1. \qquad (4.32)$$

We now provide examples of generalized pairwise stabilization forms.

H^m stabilization. Let

$$b_T([v]_T, [w]_T) = ([v]_T, [w]_T)_{H^m(T)} \tag{4.33}$$

and $\alpha_m = 0$ in equation (4.30). This gives

$$s_{h,m}(v, w) = \sum_{T \in \mathcal{T}_h^S} \tau([v]_T, [w]_T)_{H^m(T)}, \tag{4.34}$$

with $[v]_T$ as in equation (4.29). We then have, for $v \in V_h$ and $T \in \mathcal{T}_h^S$,

$$\begin{aligned}
\|v\|_{H^m(T)}^2 &\lesssim \|v - (v|_{S_h(T)})^e\|_{H^m(T)}^2 + \|(v|_{S_h(T)})^e\|_{H^m(T)}^2 \\
&\lesssim \|[v]_T\|_{H^m(T)}^2 + \|v\|_{H^m(S_h(T))}^2.
\end{aligned} \tag{4.35}$$

This gives the global bound

$$\begin{aligned}
\|v\|_{H^m(\Omega_h)}^2 &= \|v\|_{H^m(\Omega_h^L)}^2 + \sum_{T \in \mathcal{T}_h^S} \|v\|_{H^m(T)}^2 \\
&\lesssim \|v\|_{H^m(\Omega_h^L)}^2 + \sum_{T \in \mathcal{T}_h^s} \|[v]_T\|_{H^m(T)}^2 + \|v\|_{H^m(S_h(T))}^2 \\
&\lesssim \|v\|_{H^m(\Omega_h^L)}^2 + \|v\|_{s_{h,m}}^2,
\end{aligned} \tag{4.36}$$

where we used that S_h maps T to a large element in $\mathcal{T}_h^L$. Thus we directly get stabilization of the H^m-norm.

Normal gradient and L^2 control. We now present a stabilization form specifically designed to address the inverse inequality for the normal gradient, which is essential for proving coercivity in Nitsche's method, as well as the L^2 control needed to bound the condition number. Let

$$s_h(v, w) = \sum_{T \in \mathcal{T}_h^S(\partial\Omega)} \tau_1 h(\nabla_n [v]_T, \nabla_n [w]_T)_{T \cap \partial\Omega} + \tau([v], [w])_T. \tag{4.37}$$

The first term gives precisely the inverse inequality

$$h\|\nabla_n v\|_{\partial\Omega}^2 \lesssim \|\nabla v\|_{\Omega}^2 + \|v\|_{s_h}^2, \tag{4.38}$$

while the second term ensures the L^2 control

$$\|v\|_{\Omega_h}^2 \lesssim \|v\|_{\Omega}^2 + \|v\|_{s_h}^2. \tag{4.39}$$

5. Weak stabilization on surfaces

As with bulk problems, we ensure adequate control of the approximate solution to surface PDEs across the entire active mesh by incorporating stabilization terms into the weak formulation of CutFEM. These stabilization forms are necessary to obtain a uniform bound on the condition number, and, in certain cases (e.g. for Lagrange multipliers), they are also required for stability, as discussed in Section 7.

5.1. Abstract properties

Let Ω_0 be $(d-1)$-dimensional surface embedded in $\mathbb{R}^d$, with $d = 2$ or 3. Consider an active mesh $\mathcal{T}_{h,0}$ of d-dimensional elements that cover Ω_0. The union of the elements in $\mathcal{T}_{h,0}$ forms the domain $\Omega_{h,0}$, and we have a finite element space $V_{h,0}$ defined on this active mesh, as described in Section 2.

A weak stabilization form is a positive semidefinite bilinear form $s_{h,m}$ acting on $V_{h,0}$, which satisfies the following conditions.

- There exists a constant such that

$$\|\nabla^m v\|^2_{\Omega_{h,0}} \lesssim h\|\nabla_0^m v\|^2_{\Omega_0} + \|v\|^2_{s_{h,m}}, \quad v \in V_{h,0}, \quad m = 0, 1, \qquad (5.1)$$

  where ∇_0 denotes the tangential gradient on Ω_0, and the factor h compensates for the difference in dimensions.

- There exists a constant such that weak consistency holds:

$$\|\pi_h v\|_{s_{h,m}} \lesssim h^{s-m}\|v\|_{H^s(\Omega_0)}, \quad 1 \le s \le p+1, \quad m = 0, 1, \qquad (5.2)$$

  where $\pi_h \colon H^s(\Omega_0) \to V_{h,0}$ is the interpolation operator defined in Section 3.4 for surfaces.

When necessary for clarity, we may write $s_{h,0,m}$, where the additional index 0 indicates that the stabilization form is associated with a surface Ω_0. In this section we only consider surfaces, and therefore we use the simplified notation $s_{h,m}$, where m indicates the order of derivatives that we control.

Depending on the problem, stronger control than that stated in equation (5.1) may be required. In such cases, the stabilization form $s_{h,m}$ may scale differently, satisfying a modified version of (5.1). For instance, both sides of (5.1) could be multiplied by h^{-1}, and the stabilization form may then satisfy that estimate instead. However, the stabilization must still scale in such a way that weak consistency (5.2) is satisfied.

As an example, in Section 2 we presented a ghost penalty stabilization form in equation (2.70) (for $i = 0$) for continuous linear elements and $m = 1$. This was the first stabilization form introduced for cut finite element discretizations of surface PDEs; see Burman *et al.* (2015c). Later, Zahedi (2017) and Larson and Zahedi (2019) incorporated normal derivatives at the interface, which, together with the ghost penalty, could achieve a uniform bound on the condition number, even for elements of higher order than linear. It was then demonstrated that a weaker ghost penalty term (with an h scaling) can be chosen when normal derivative control at the interface is included. Next we provide further details of how such stabilization forms can be constructed.

5.2. Construction of a surface stabilization form

On a surface, we say that an element $T \in \mathcal{T}_h$ is large if

$$\gamma \leq \frac{h|T \cap \Omega_0|}{|T|}, \tag{5.3}$$

where the factor h compensates for the fact that $T \cap \Omega_0$ is $(d-1)$-dimensional and T is d-dimensional. We divide the elements into large and small, i.e. $\mathcal{T}_h = \mathcal{T}_h^L \cup \mathcal{T}_h^S$. Let $\{M_T : T \in \mathcal{T}_h^P\}$ be a set of patches, where $\mathcal{T}_h^P \subset \mathcal{T}_h^L$ is a subset of the large elements that enumerate the patches, such that

$$\max_{T \in \mathcal{T}_h^P} \operatorname{diam}(M_T) \lesssim h, \tag{5.4}$$

and the patches cover all elements,

$$\Omega_{h,0} \subset \cup_{T \in \mathcal{T}_h^P} M_T, \quad m = 0, 1. \tag{5.5}$$

We define the stabilization form as

$$s_{h,m}(v, w) = \sum_{T \in \mathcal{T}_h^P} s_{h,m,M_T}(v, w), \quad m = 0, 1, \tag{5.6}$$

where $s_{h,m,M_T}(v, w)$ is a stabilization form for each patch, such that

$$\|\nabla^m v\|_{M_T}^2 \lesssim h \|\nabla_0^m v\|_{M_T \cap \Omega_0}^2 + \|v\|_{s_{h,m,M_T}}^2. \tag{5.7}$$

Thus we obtain the global bounds

$$\|\nabla^m v\|_{\Omega_{h,0}}^2 \lesssim h \|\nabla_0^m v\|_{\Omega_0}^2 + \|v\|_{s_{h,m}}^2, \quad m = 0, 1. \tag{5.8}$$

The term $\|\nabla_0^m v\|_{\Omega_0}^2$ is controlled by the form associated with the partial differential equation. For instance, for a second-order elliptic partial differential equation on Ω_0, we have

$$\|\nabla_0 v\|_{\Omega_0}^2 \lesssim a(v, v), \quad v \in H^1(\Omega_0), \tag{5.9}$$

and for $m = 0$, the operator may directly provide the L^2 control. If not, we work in $H^1(\Omega_0)/\mathbb{R}$ and use the Poincaré inequality

$$\|v\|_{\Omega_0} \lesssim \|\nabla_0 v\|_{\Omega_0}, \quad v \in H^1(\Omega_0)/\mathbb{R}. \tag{5.10}$$

The patch stabilization form $s_{h,m,M_T}(v, w)$ needs to control both the variation of the function on the patch and the variation in the direction normal to the surface. An example of such a stabilization form is given by (see Larson and Zahedi 2019, 2023)

$$s_{h,m,M_T}(v, w) = s_{h,m,M_T,\star}(v, w) + \sum_{j=1}^{p} \tau_{0,j} h^{2(j-m)+1} (\nabla_n^j v, \nabla_n^j w)_{\Omega_0}, \tag{5.11}$$

where $s_{h,m,M_T,\star}(v,w)$ is a form such that

$$\|\nabla^m(v-v_T)\|_{M_T} \lesssim \|v\|_{s_{h,m,M_T,\star}}, \tag{5.12}$$

with $v_T = (v|_T)^e$, the canonical extension of the polynomial on the large element $T \in \mathcal{T}_h^P$.

For simplicity we verify (5.1) for $p = 1$. Adding and subtracting v_T and using the triangle inequality, we obtain for $m = 0, 1$ the following estimate:

$$\begin{aligned}
\|\nabla^m v\|_{M_T}^2 &\leq \|\nabla^m(v-v_T)\|_{M_T}^2 + \|\nabla^m v_T\|_{M_T}^2 \\
&\lesssim \|v\|_{s_{h,m,M_T,\star}}^2 + h^{3-2m}\|\nabla_n v_T\|_{T\cap\Omega_0}^2 + h\|\nabla_0^m v_T\|_{T\cap\Omega_0}^2 \\
&\lesssim \|v\|_{s_{h,m,M_T,\star}}^2 + h^{3-2m}\|\nabla_n v\|_{M_T\cap\Omega_0}^2 + h\|\nabla_0^m v\|_{M_T\cap\Omega_0}^2.
\end{aligned} \tag{5.13}$$

Here we used the inverse inequality

$$\|\nabla^m w_T\|_{M_T}^2 \lesssim h^{3-2m}\|\nabla_n w_T\|_{T\cap\Omega_0}^2 + h\|\nabla_0^m w_T\|_{T\cap\Omega_0}^2, \quad m = 0, 1, \tag{5.14}$$

which holds since w_T is a polynomial and T is a large element. Furthermore, we assumed that the form $s_{h,m,M_T,\star}$ provides the control in (5.12).

To achieve this, we may use the ghost penalty form

$$s_{h,m,M_T,\star}(v,w) = \sum_{F\in\mathcal{F}_h(M_T)} \sum_{j=1}^p h^{2(j-m)+1}([\nabla^j v],[\nabla^j w])_F, \tag{5.15}$$

where $\mathcal{F}_h(M_T)$ is the set of internal faces in M_T. Alternatively, we could use the element-based stabilization in equation (4.15), or a patch stabilization form,

$$s_{h,m,M_T,\star}(v,w) = \sum_{T'\in\mathcal{T}_h^S, T'\subset M_T} (\nabla^m(v-v_T),\nabla^m(w-w_T))_{T'}, \tag{5.16}$$

where we control the difference between v and the extension v_T of v restricted to the large element. For the latter, we directly obtain the estimate in equation (5.12). For the face-based stabilization, we connect every element to the large element via a chain of elements and use the control of the variation across the faces; see (4.7).

Finally, we verify the weak consistency (5.2) for the patch stabilization form. We have

$$\|\pi_h u\|_{s_{h,m,M_T,\star}}^2 = \sum_{T'\in\mathcal{T}_h^S, T'\subset M_T} \|\nabla^m(\pi_h u - (\pi_h u)_T)\|_{T'}^2. \tag{5.17}$$

For any polynomial w on M_T, we know that $(\pi_h w)_T = w_T = w$, and therefore

$$\begin{aligned}
\|\nabla^m(\pi_h u - (\pi_h u)_T)\|_{T'} &= \|\nabla^m(\pi_h(u-w) - (\pi_h(u-w))_T)\|_{T'} \\
&\leq \|\nabla^m(\pi_h(u-w))\|_{T'} \leq h^{-m}\|u-w\|_{M_T} \\
&\lesssim h^{p+1-m}\|u\|_{\Omega_0},
\end{aligned} \tag{5.18}$$

where we used an inverse estimate to remove the gradient, the L^2-stability of the interpolation operator, and finally polynomial approximation.

It remains to verify the consistency for the normal stabilization term. We use the fact that $\nabla_n E_S u = 0$, where $E_S u = u \circ p_{\Omega_0}$ is the extension of u via the closest point mapping p_{Ω_0} associated with Ω_0. Using the definition of the interpolation operator and the interpolation estimate (3.35) (see Section 3.4), we obtain

$$
\begin{aligned}
h^{3-2m}\|\nabla_n \pi_h u\|^2_{T \cap \Omega_0} &= h^{3-2m}\|\nabla_n(\pi_h u - E_S u)\|^2_{T \cap \Omega_0} \\
&\lesssim h^{3-2m} h^{2P}\|u\|^2_{H^{P+1}(\Omega_0)}.
\end{aligned} \tag{5.19}
$$

This completes the verification. Note that the normal stabilization term could scale with weaker h-dependence and still satisfy the weak consistency in equation (5.2).

The stabilization forms presented here essentially follow the approach introduced by Larson and Zahedi (2023), who proposed patch-based stabilization forms involving both normal control on the surface and variation control on the patch. Alternatively, one can use normal stabilization on the elements, as proposed by Grande *et al.* (2018) and Burman *et al.* (2018c), and defined as

$$
s_{h,m}(v, w) = h^{2-2m}(\nabla_{n^e} v, \nabla_{n^e} w)_{\Omega_{h,0}}, \tag{5.20}
$$

where $n^e = n \circ p_{\Omega_0}$. The analysis with only this stabilization is more complicated, but if we add a stabilization form $s_{h,m,M_T,\star}$ satisfying (5.12), we can adopt the proof outlined above. For linear elements, one may opt for full gradient stabilization, as described in Burman *et al.* (2016b).

6. Strong stabilization

An alternative to weak stabilization is instead to strongly stabilize the finite element space by eliminating unstable degrees of freedom so that optimal approximation properties are preserved. The approach may also be viewed as constructing a discrete extension operator, which was introduced in Johansson and Larson (2013) for discontinuous finite element spaces and in Badia *et al.* (2018) for continuous finite element spaces. Burman *et al.* (2022c, 2023b) have developed an abstract general framework for constructing the extension operators, which we will follow here. The relation between stabilized formulations and formulations using extension was discussed in Burman, Hansbo and Larson (2022e).

6.1. Construction of a discrete extension operator

Recall that an element is considered large if

$$
\gamma|T| \leq |T \cap \Omega|, \tag{6.1}
$$

for a positive parameter γ; otherwise the element is classified as small. Consider a finite element space V_h with a standard locally supported basis $\mathcal{B} = \{\varphi_i\}_{i=1}^N$. We say that a basis function is small if its support does not contain any large element; otherwise the basis function is large. By decomposing the basis into the set of large and small basis functions $\mathcal{B} = \mathcal{B}^L \cup \mathcal{B}^S$, we may also decompose our finite element

space into two subspaces

$$V_h = V_h^L \oplus V_h^S = \mathrm{span}(\mathcal{B}^L) \oplus \mathrm{span}(\mathcal{B}^S), \tag{6.2}$$

where V_h^L is spanned by the large basis functions and V_h^S by the small basis functions.

For $v \in V_h$, we can write $v = v^S + v^L$, where the superscript S denotes the component in V_h^S and L the component in V_h^L. We also introduce the set of indices corresponding to large basis functions, which we denote by I^L.

The extension operator will essentially use information from V_h^L to construct an element in $V_h^L \oplus V_h^S$ with proper stability and approximation properties. With natural assumptions, the extension operator will also preserve V_h^L.

Recalling the mapping $S_h(T)$, which maps an element T onto a large element such that

$$\mathrm{diam}(S_h(T) \cup T) \lesssim h, \tag{6.3}$$

we introduce a preliminary extension operator B_h that extends V_h^L into a dG-space X_h that contains V_h defined by

$$(B_h v)|_T = \begin{cases} (v|_{S_h(T)})^e|_T, & T \text{ small}, \\ v|_T, & T \text{ large}. \end{cases} \tag{6.4}$$

Here v^e denotes the canonical extension of a polynomial v on T to a polynomial on $\mathbb{R}^d$. Next we use an interpolation operator π_h to map X_h onto V_h. By composing B_h with the interpolation operator π_h, we will obtain our extension operator. To that end, let $\pi_h \colon X_h \to V_h$ be an interpolation operator

$$\pi_h v = \sum_{i \in I} \psi_i(v) \varphi_i, \tag{6.5}$$

such that

$$\|\pi_h v\|_{H^1(\Omega_h)} \lesssim \|v\|_{H^1(\Omega_h)}, \quad v \in X_h. \tag{6.6}$$

Typical choices are operators of Clément type. Finally, we define the extension operator E_h as the composition of B_h and π_h:

$$E_h \colon V_h^L \ni v^L \mapsto \pi_h B_h v^L \in V_h^E \subset V_h, \tag{6.7}$$

where we define the extended finite element space by

$$V_h^E = E_h(V_h^L) \subset V_h. \tag{6.8}$$

6.2. Basic properties

The extension operator $E_h \colon V_h^L \to V_h$ is linear and injective. If the interpolation operator is such that

$$\pi_h v = v, \quad v \in V_h, \tag{6.9}$$

and the functionals ψ_i are chosen to preserve the finite element space and such that

$$\begin{cases} \psi_i \colon L^2(\text{supp}(\varphi_i) \cap \Omega_h^L) \to \mathbb{R} & \text{if } i \in I^L, \\ \psi_i \colon L^2(\text{supp}(\varphi_i)) \to \mathbb{R} & \text{otherwise,} \end{cases} \tag{6.10}$$

where Ω_h^L denotes the domain formed by the large elements (see (4.4)), then the extension operator has the following structure:

$$E_h v^L = (E_h v^L)^L + (E_h v^L)^S = v^L + (E_h v^L)^S. \tag{6.11}$$

To show that $(E_h v^L)^L = v^L$, we have the following identities:

$$(E_h v)^L = (\pi_h B_h v)^L = \sum_{i \in I^L} \psi_i(B_h v)\varphi_i = \sum_{i \in I^L} \psi_i(v)\varphi_i = v^L. \tag{6.12}$$

Here we used the identities $\psi_i(w) = \psi_i(w|_{\Omega_h^L})$ for $i \in I^L$ and $B_h v = v$ on Ω_h^L, which are consequences of (6.10) and (6.4), respectively. These identities together imply that E_h preserves V_h^L.

6.3. Matrix formulation

Here we summarize the basic steps in the matrix calculations involved in solving a problem using the discrete extension operator.

- Assemble the square linear system of equations for the original method

$$\widehat{A}\widehat{u}_h = \widehat{b}, \tag{6.13}$$

  where $\widehat{u} \in \mathbb{R}^{\dim(V_h)}$ are coefficients for the full approximation space V_h.

- Given $\gamma \geq 0$ and the small-to-large element association S_h, assemble the discrete extension matrix $\widehat{E}_h \in \mathbb{R}^{\dim(V_h) \times \dim(V_h^L)}$ such that

$$\widehat{v}^E = \widehat{E_h v^L} = \widehat{E}_h \widehat{v}^L, \tag{6.14}$$

  following the construction above. If $\gamma = 0$, this reduces to the identity matrix.

- Solve the reduced system

$$(\widehat{E}_h^\top \widehat{A} \widehat{E}_h)\widehat{u}_h^L = \widehat{E}_h^\top \widehat{b}, \tag{6.15}$$

  where $\widehat{u}_h^L \in \mathbb{R}^{\dim(V_h^L)}$ are coefficients for the extended space V_h^E.

- Expand in coefficients for V_h:

$$\widehat{u}_h^E = \widehat{E}_h \widehat{u}_h^L. \tag{6.16}$$

6.4. Theoretical results

We have the following theoretical results.

- *Stability.* For $v \in V_h^E \subset H^1(\Omega_h)$,

$$\|\nabla^m v\|_{\Omega_h} \lesssim \|\nabla^m v\|_\Omega, \quad m = 0, 1. \tag{6.17}$$

- *Approximation.* Let $\pi_h^E = E_h \tilde{\pi}_h$, where $\tilde{\pi}_h$ is an interpolation operator constructed as in Section 3.4. For $v \in H^{p+1}(\Omega)$,

$$\|v - \pi_h^E v\|_{H^m(\Omega_h)} \lesssim h^{p+1-m} \|v\|_{H^{p+1}(\Omega)}, \quad 0 \le m \le p+1. \qquad (6.18)$$

- *Equivalence to DoFs-norm:*

$$\|v\|_{\Omega}^2 \sim \|v\|_{\Omega_h}^2 \sim h^d \|\hat{v}\|_{\mathbb{R}^N}^2, \quad v \in V_h^E. \qquad (6.19)$$

We refer to Burman *et al.* (2022c, 2023b) for proofs of these results.

6.5. The relation between weak and strong stabilization

This section explores the relationship between the strong and weak stabilization approaches. More precisely, we show that there is a weak stabilization form such that the strong stabilization is obtained in the limit when we let the stabilization parameter tend to infinity.

For each small basis function, ϕ_i associates an element $T_i \subset \mathrm{supp}(\phi_i) \subset \Omega_h^S$, and we define

$$s_{h,m}(v, w) = \sum_{i \in I^S} h^{d-2m} \psi_i([v]_{T_i}) \psi_i([w]_{T_i}), \qquad (6.20)$$

where I^S is the index set for the small basis functions and $\psi_i \colon L^2(T_i) \to \mathbb{R}$ is a functional that provides the value of the degree of freedom such that

$$v = \sum_{i \in I} \psi_i(v) \varphi_i, \quad v \in V_h. \qquad (6.21)$$

For this stabilization form, we have the following stability estimate:

$$
\begin{aligned}
\|v\|_{H^m(\Omega_h)}^2 &\lesssim \|v - E_h v\|_{H^m(\Omega_h)}^2 + \|E_h v\|_{H^m(\Omega_h)}^2 \\
&\lesssim h^{-2m} \|v - E_h v\|_{\Omega_h}^2 + \|E_h v\|_{H^m(\Omega_h)}^2 \\
&\lesssim h^{-2m} \sum_{i \in I} h^d |\psi_i(v - E_h v)|^2 + \|E_h v\|_{H^m(\Omega_h)}^2 \\
&\lesssim \|v\|_{s_{h,m}}^2 + \|v\|_{H^m(\Omega)}^2.
\end{aligned}
\qquad (6.22)
$$

Note that we can change E_h to B_h.

Next, to investigate the relationship between the strong stabilization and the degree of freedom stabilization, we note that

$$\psi_i([v]_T) = \psi_i(v) - \psi_i(B_h v) = \psi_i(v) - \psi_i(E_h v^L) = \psi_i(v - E_h v^L), \qquad (6.23)$$

since

$$\psi_i(E_h v^L) = \psi_i \left(\sum_j \psi_j(B_h v^L) \varphi_j \right) = \sum_j \psi_j(B_h v^L) \underbrace{\psi_i(\varphi_j)}_{=\delta_{ij}} = \psi_i(B_h v^L). \quad (6.24)$$

We thus have

$$s_{h,m}(v, w) = \sum_{i \in I^S} h^{d-2m} \psi_i([v]_{T_i}) \psi_i([w]_{T_i})$$

$$= \sum_{i \in I^S} h^{d-2m} \psi_i(v - E_h v) \psi_i(w - E_h w). \qquad (6.25)$$

This means we control the distance between a function $v \in V_h$ and the stable extension $E_h v$.

It follows that when the stabilization parameter τ tends to infinity, the solution to the stabilized problem

$$a_h(u_{h,\tau}, v) + \tau s_{h,m}(u_{h,\tau}, v) = l_h(v) \quad \text{for all } v \in V_h \qquad (6.26)$$

will converge to the solution u_h^E of the strongly stabilized problem

$$a_h(u_h^E, v) = l_h(v) \quad \text{for all } v \in V_h^E, \qquad (6.27)$$

since

$$a_h(u_{h,\tau}, v) + \tau s_{h,m}(u_{h,\tau}, v) = l_h(v) = a_h(u_h^E, v), \qquad (6.28)$$

and thus we get

$$a_h(u_{h,\tau} - u_h^E, v) + \tau s_{h,m}(u_{h,\tau} - u_h^E, v) = 0 \quad \text{for all } v \in V_h. \qquad (6.29)$$

Let $\vertiii{\cdot}_h$ be an energy norm associated with a_h such that $a_h + \tau s_{h,m}$ is coercive and a_h is continuous with respect to $\vertiii{\cdot}_h$. Setting $w = u_{h,\tau} - u_h^E$ and using stability bounds for the finite element solutions, followed by the consistency (6.29), yields

$$\vertiii{w}_h^2 + \tau \|w\|_{s_{h,m}}^2 \lesssim a_h(w, w) + \tau s_{h,m}(w, w)$$

$$= a_h(w, u_h^E) + \tau s_{h,m}(w, u_h^E)$$

$$= a_h(w, u_h^E)$$

$$\lesssim \vertiii{w}_h \vertiii{u_h^E}_h. \qquad (6.30)$$

Here we used the identity $s_{h,m}(w, u_h^E) = 0$, which follows from the definition of $s_{h,m}$ in (6.25). We keep τ outside the norm $\|\cdot\|_{s_{h,m}}$ for clarity.

We conclude that

$$\tau \|u_{h,\tau} - u_h^E\|_{s_{h,m}} \lesssim \vertiii{u_h^E}_h \lesssim 1, \qquad (6.31)$$

and now keeping h fixed and letting $\tau \to \infty$, the result follows. Indeed, since $\lim_{\tau \to \infty} \|u_{h,\tau} - u_h^E\|_{s_{h,m}} = 0$, we conclude that $u_{h,\tau} \in V_h^E$ and hence $u_{h,\tau} = u_h^E$.

We remark that this result shows that there are no locking effects for large values of the stabilization parameter τ for weak stabilization as defined by (6.25). In contrast, a standard ghost penalty stabilization (without the use of macro-elements) forces the solution into the kernel of the stabilization form as the parameter τ tends

to infinity, which typically leads to locking for large values of the stabilization parameter. For instance, when ghost penalty stabilization penalizing derivative jumps is applied on all faces, the kernel of the stabilization form acting on the space of continuous piecewise polynomials of degree p is the space of global polynomials of degree p.

7. Lagrange multiplier methods

In the previous examples we considered Nitsche's method for the imposition of boundary and interface conditions. Another approach for weak imposition of interface constraints is to use Lagrange multipliers. The use of Lagrange multipliers for the imposition of constraints in finite element methods dates back to the seminal works of Babuška (1972/73) and Brezzi (1974). In the case of fictitious domain methods using finite element methods, they were introduced and analysed by Girault and Glowinski (1995), and on cut meshes, using stabilization, by Burman and Hansbo (2010*a*).

To design cut finite element methods with Lagrange multipliers, we add an additional variable on the interface that allows us to impose boundary or interface conditions as an additional equation. This has the disadvantage of adding additional degrees of freedom, and the linear system to solve is that of a saddle point problem, which is more demanding than the symmetric system from Nitsche's method. On the other hand, the multiplier gives an independent variable for the approximation of the flux variable, which can be advantageous in some cases. It can enhance conservation for fluid problems, and for problems with non-linear diffusion the interface terms of the formulation remain linear. For cut elements, the Lagrange multiplier approach has some advantageous stability properties, and indeed methods can be designed that do not require any stabilization for optimal accuracy. Nevertheless, stabilization can be useful to facilitate the satisfaction of the so-called inf-sup stability condition that appears due to the saddle point structure, and also to improve on the conditioning of the linear system. Using Lagrange multipliers can also allow for coupling methods that are much less invasive in the solvers of the coupled sub-problems, as we shall see in the next section.

In the context of the fictitious domain problem, below we will first discuss how to design cut finite element methods using Lagrange multipliers that are stable without stabilization, and then we will discuss some known stabilization techniques. In this section we only consider the fictitious domain problem. Interface problems discretized using Lagrange multipliers will be treated in the next section on hybridized methods.

7.1. Model problem

Let Ω be a domain in $\mathbb{R}^d$ with piecewise smooth Lipschitz-continuous boundary Ω_0 and exterior unit normal n. More precisely, let Ω_0 be defined by the union of

smooth manifolds $\Omega_{0,i}$, $i = 1, \ldots, N$, defined by a differentiable map $\hat{x}_i \colon \hat{\Omega}_{0,i} \subset \mathbb{R}^{d-1} \to \Omega_{0,i} \subset \mathbb{R}^d$. Collecting the $\hat{x}_i$, we define a map $\hat{x}_{\Omega_0}$ from $\{\hat{\Omega}_{0,i}\}_{i=1}^N$ to Ω_0. We consider the following problem: find $u \colon \Omega \to \mathbb{R}$ such that

$$-\alpha \Delta u = f \quad \text{in } \Omega, \tag{7.1}$$

$$u = g \quad \text{on } \Omega_0, \tag{7.2}$$

where $f \in L^2(\Omega)$, $g \in H^{1/2}(\Omega_0)$, are given functions.

7.2. Modelling using calculus of variations

In many applications the above model is obtained from an energy argument. Indeed, the solution sought is the one minimizing a certain energy, in our case the Dirichlet energy

$$\mathcal{J}(v) = \int_\Omega \left(\frac{\alpha}{2} |\nabla v|^2 - vf \right) \mathrm{d}x. \tag{7.3}$$

An equivalent formulation to the one above is obtained by minimizing (7.3) over the subset of functions in $H^1(\Omega)$ for which $u = g$ on Ω_0.

The idea of Lagrange multipliers is to instead minimize over $H^1(\Omega)$, i.e. relaxing the optimization to the whole space, but introduce the boundary condition as a constraint. To make this more precise, it is useful to introduce the corresponding Lagrangian functional:

$$\mathcal{L}(v, \mu) = \mathcal{J}(v) + (\mu, v - g)_{\Omega_0}. \tag{7.4}$$

Here μ is the Lagrange multiplier, and the second term on the right-hand side should be interpreted as the duality pairing between $H^{-1/2}(\Omega_0)$ and $H^{1/2}(\Omega_0)$. We recall that $g \in H^{1/2}(\Omega_0)$, and if $v \in H^1(\Omega)$, its trace on Ω_0, $\gamma v \in H^{1/2}(\Omega_0)$, so for $\mu \in H^{-1/2}(\Omega_0)$ the form is well-defined. The solution is now obtained as the saddle point of (7.4).

Formally deriving the Lagrangian results in the following Euler–Lagrange equations: find $u \in H^1(\Omega)$, $\lambda \in H^{-1/2}(\Omega_0)$ such that

$$a(u, v) + b(\lambda, v) = l(v) \qquad \text{for all } v \in H^1(\Omega), \tag{7.5}$$

$$b(\mu, u) = b(\mu, g) \quad \text{for all } \mu \in H^{-1/2}(\Omega_0), \tag{7.6}$$

where $a(u, v) = (\alpha \nabla u, \nabla v)_\Omega$, $b(\mu, v) = (\mu, v)_{\Omega_0}$ and $l(v) = (f, v)_\Omega$. This is the weak formulation for the constrained minimization problem. Observe that now the boundary condition is enforced through an additional equation and the additional unknown λ makes the number of equations and unknowns match. We introduce the norms $\| \cdot \|_\Lambda$ and $\| \cdot \|_V$ that for the model problem would be chosen as

$$\| \cdot \|_\Lambda = \alpha^{-1/2} \| \cdot \|_{H^{-1/2}(\Omega_0)} \quad \text{and} \quad \| \cdot \|_V = \alpha^{1/2} \| \cdot \|_{H^1(\Omega)}. \tag{7.7}$$

7.3. Existence and uniqueness of the weak solution

The forms a and b are bounded linear operators,

$$a(u, v) \leq M_a \|u\|_V \|v\|_V \quad \text{and} \quad b(\mu, v) \leq M_b \|\mu\|_\Lambda \|v\|_V, \tag{7.8}$$

with M_a and M_b positive constants. Continuity for b follows since by duality, followed by a trace inequality, for all $(v, \mu) \in H^1(\Omega) \times H^{-1/2}(\Omega_0)$

$$|b(\mu, v)| \leq \alpha^{-1/2} \|\mu\|_{H^{-1/2}(\Omega_0)} \alpha^{1/2} \|v\|_{H^{1/2}(\Omega_0)} \leq M_b \|\mu\|_\Lambda \|v\|_V, \tag{7.9}$$

where we applied a global trace inequality in the second step and we see that M_b coincides with the trace constant.

In this case we cannot apply the Lax–Milgram lemma immediately, since the form $b(\cdot, \cdot)$ does not enter the framework. However, if we rewrite the solution as $u = u_0 + u_g$, where $u_0 \in H_0^1(\Omega)$ and $u_g \in H^1(\Omega)$ is the harmonic extension of g, i.e. $\Delta u_g = 0$ in Ω and $\gamma u_g = g$, we obtain the following formulation: find $u_0 \in H_0^1(\Omega)$ such that

$$a(u_0, v) = l(v) - a(u_g, v) \quad \text{for all } v \in H_0^1(\Omega). \tag{7.10}$$

This weak formulation is well-posed by the Lax–Milgram lemma since a is coercive on $H_0^1(\Omega)$. The form $b(\cdot, \cdot)$ vanishes here since $b(\cdot, v) = 0$, for all $v \in H_0^1(\Omega)$, that is, a is coercive on the kernel of b. The existence and uniqueness of the Lagrange multiplier is a consequence of Brezzi's theorem (Brezzi 1974). The key condition is that the form $b(\cdot, \cdot)\colon H^{-1/2}(\Omega_0) \times H^1(\Omega) \to \mathbb{R}$ is a bounded linear operator and there exists $c_b > 0$ such that, for all $\mu \in H^{-1/2}(\Omega_0)$,

$$\|\mu\|_{H^{-1/2}(\Omega_0)} \lesssim \sup_{v \in H^1(\Omega) \setminus \{0\}} \frac{b(\mu, v)}{\|v\|_{H^1(\Omega)}}. \tag{7.11}$$

If this condition is satisfied, there exists a unique solution λ to (7.5). In our case $b(\cdot, \cdot)$ is simply the duality pairing between $H^{-1/2}(\Omega_0)$ and $H^{1/2}(\Omega_0)$, and since

$$\|\mu\|_{H^{-1/2}(\Omega_0)} = \sup_{v \in H^{1/2}(\Omega_0) \setminus \{0\}} \frac{(\mu, v)_{\Omega_0}}{\|v\|_{H^{1/2}(\Omega_0)}}, \tag{7.12}$$

the condition (7.11) holds, by harmonic extension. Hence there exists a unique $\lambda \in H^{-1/2}(\partial\Omega)$ such that

$$(\lambda, v)_{\Omega_0} = l(v) - a(u, v) \quad \text{for all } v \in H^1(\Omega). \tag{7.13}$$

The multiplier also satisfies the stability estimate

$$\begin{aligned}
\|\lambda\|_{H^{-1/2}(\Omega_0)} &= \sup_{v \in H^1(\Omega) \setminus \{0\}} \frac{(\lambda, v)_{\Omega_0}}{\|v\|_{H^{1/2}(\Omega_0)}} \\
&= \sup_{v \in H^1(\Omega) \setminus H_0^1(\Omega)} \frac{l(v) - a(u, v)}{\|v\|_{H^{1/2}(\Omega_0)}} \\
&\lesssim \|f\|_{H^1(\Omega)'} + \|g\|_{H^{1/2}(\Omega_0)}.
\end{aligned} \tag{7.14}$$

If we assume $f \in L^2(\Omega)$, apply the divergence theorem on the right-hand side of equation (7.13) and use that u satisfies $-\alpha\Delta u = f$, we obtain

$$(\lambda, v)_{\Omega_0} = (-n \cdot \alpha\nabla u, v)_{\Omega_0} \quad \text{for all } v \in H^1(\Omega). \tag{7.15}$$

It follows that if u is smooth enough that the trace of the normal gradient is well-defined in $H^{-1/2}(\Omega_0)$, then $\lambda = -n \cdot \alpha\nabla u$.

For sufficiently smooth interfaces, one may also show the following elliptic regularity estimate:

$$\|u\|_{H^{t+1}(\Omega)} + \|\lambda\|_{H^{t-1/2}(\Omega_0)} \lesssim \|f\|_{H^{t-1}(\Omega)} + \|g\|_{H^{t+1/2}(\Omega_0)}, \quad t \geq 1. \tag{7.16}$$

7.4. Cut finite element method using Lagrange multipliers

If we assume that u is discretized using the unfitted bulk finite element space, such that the restriction of the functions are in $H^1(\Omega)$, $V_h|_\Omega \subset H^1(\Omega_h)$ and λ is discretized using a finite-dimensional subspace of $H^{-1/2}(\partial\Omega)$, Λ_h, we may write the discretization of (7.5) as follows: find $(u_h, \lambda_h) \in V_h \times \Lambda_h$ such that

$$a(u_h, v) + b(\lambda_h, v) = l(v_h) \qquad \text{for all } v \in V_h, \tag{7.17}$$
$$b(\mu, u_h) - \tau_0 s_{h,0}(\lambda_h, \mu) = b(\mu, g) \quad \text{for all } \mu \in \Lambda_h. \tag{7.18}$$

Here $s_{h,0}$ is a symmetric positive semidefinite form introduced to stabilize the formulation and τ_0 is a non-negative constant. We assume that $s_{h,0}$ is weakly consistent; see Section 5. For $\tau_0 = 0$, this is a standard Lagrange multiplier formulation on the non-standard cut space V_h. As long as all elements have non-zero intersection with the physical domain, however small, the method can be designed so that it has optimal convergence without additional stabilizing terms. The caveat is that, as usual for Lagrange multiplier formulations, the stability of the formulation depends on the choice of the spaces V_h and Λ_h. Indeed, for the formulation to be uniformly stable, the spaces must satisfy a discrete equivalent to (7.11).

Satisfying the inf-sup condition on the discrete level is a bit more subtle than in the continuous case and will be discussed below. First let us consider the question of invertibility of the linear system associated with (7.17)–(7.18), on cut meshes. Let us assume that V_h is the cut finite element space introduced in Section 2, satisfying (3.30), and that we have a space for the multipliers Λ_h that satisfies the following condition with respect to V_h:

$$b(\lambda_h, v) = 0 \quad \text{for all } v \in V_h \quad \text{implies} \quad \lambda_h = 0. \tag{7.19}$$

This is the minimum condition needed for the linear system to be invertible. As we shall see later, a discrete version of (7.11) will be needed for the error analysis. If the active mesh is defined so that all elements have non-zero intersection with the physical domain, then the resulting linear system is invertible under minimal assumptions.

Lemma 7.1. Assume that $\|\nabla u_h\|_\Omega^2 \lesssim a(u_h, u_h)$ and that the condition (7.19) is satisfied. Then the linear system defined by (7.17)–(7.18) admits a unique solution.

Proof. Since (7.17)–(7.18) defines a square linear system, it is enough to show that the solution is unique. Consider the case $f = g = 0$ and take $v = u_h$, $\mu = \lambda_h$. Then $\|\nabla u_h\|_\Omega^2 + \tau_0 s_{h,0}(\lambda_h, \lambda_h) = 0$. Take $\mu = 1$ in (7.18) to see that

$$\int_{\Omega_0} u_h \, ds = 0. \tag{7.20}$$

It then follows by Poincaré's inequality that $u_h = 0$. It is immediate by (7.19) that $\lambda_h = 0$. $\qquad\square$

For simplicity we consider the case without ghost penalty for the bulk discretization below, and show that this leads to a method with optimal order of convergence. If control of the condition number of the system is required, ghost penalty stabilization can be added to the *a* form. The extension to that case is straightforward.

Several different choices of V_h and Λ_h are possible in the CutFEM framework. Observe that Λ_h and V_h do not have to be defined on the same meshes even if the subscript is the same. Below, V_h will always be chosen to be the unfitted finite element space defined on the active mesh. For Λ_h we will distinguish two situations that are both of interest for applications. The first case is when a surface mesh Σ_h is available on Ω_0. This is feasible if an explicit parametrization of the boundary is available. Then the discrete multiplier can be approximated in a boundary element space. The second situation is when the boundary is given implicitly. The meshing problem of the boundary can then be almost as complex as that of the bulk, and it may be attractive to define the discrete multiplier approximation using the bulk mesh in the unfitted fashion, as discussed in Section 2.3. Before discussing the different possible choices of spaces Λ_h, we consider the basic stability and error analysis for Lagrange multiplier methods of the form (7.17)–(7.18) on unfitted bulk meshes.

Stability and error estimates in an abstract setting. We will now adapt the framework of Section 3 to the case of Lagrange multipliers.

Define the triple norm

$$\||(v_h, \mu_h)\||_\tau^2 = \|v_h\|_V^2 + \|\mu_h\|_\Lambda^2 + \tau_0 \|\mu_h\|_{s_h}^2, \tag{7.21}$$

where the stabilization seminorm is defined by $\|\mu\|_{s_h} = s_{h,0}(\mu, \mu)^{1/2}$ for $\mu \in \Lambda_h$ and $\||(v_h, \mu_h)\||_0$ denotes the triple norm with $\tau_0 = 0$. When $\tau_0 > 0$, the norm is typically only well-defined on $V \times \Lambda_h$.

Consider the following compact formulation: find $(u_h, \lambda_h) \in V_h \times \Lambda_h$ such that

$$A[(u_h, \lambda_h), (v, \mu)] + \tau_0 s_{h,0}(\lambda_h, \mu) = L(v, \mu) \quad \text{for all } (v, \mu) \in V_h \times \Lambda_h, \tag{7.22}$$

where

$$A[(u_h, \lambda_h), (v, \mu)] = a(u_h, v) + b(\lambda_h, v) - b(\mu, u_h) \tag{7.23}$$

and

$$L(v, \mu) = l(v) + b(\mu, g). \tag{7.24}$$

For the analysis below, we require the following assumptions to be satisfied.

A1. *Consistency.* By construction, for $u_h \in V_h$ and $\lambda_h \in \Lambda_h$, we have

$$A[(u_h, \lambda_h), (v, \mu)] = A[(u, \lambda), (v, \mu)] - \tau_0 s_{h,0}(\lambda_h, \mu) \quad \text{for all } (v, \mu) \in V_h \times \Lambda_h. \tag{7.25}$$

A2. *Continuity.* Assume the bound (7.8). Then the following continuity holds for $v, y \in V$, $\mu, \eta \in \Lambda$:

$$A[(v, \mu), (y, \eta)] \lesssim |||(v, \mu)|||_0 |||(y, \eta)|||_0. \tag{7.26}$$

Below we will sometimes use the individual constants of continuity M_a and M_b for the forms a and b respectively, as introduced in (7.8). For $\mu_h, \zeta_h \in \Lambda_h$, assume that

$$s_{h,0}(\mu_h, \zeta_h) \leq \|\mu_h\|_{s_h} \|\zeta_h\|_{s_h}. \tag{7.27}$$

This condition holds by the Cauchy–Schwarz inequality for the symmetric stabilizations considered below.

A3. *Stability.* Assume that the following two stability conditions are satisfied for CutFEM using Lagrange multipliers.

- *Inf-sup stability of the form b.* For all $\mu_h \in \Lambda_h$,

$$\|\mu_h\|_\Lambda \lesssim \sup_{v \in V_h \setminus \{0\}} \frac{b(\mu_h, v)}{\|v\|_V} + \tau_0^{1/2} s_{h,0}(\mu_h, \mu_h)^{1/2} \tag{7.28}$$

  for some $\tau_0 \geq 0$.

- *Coercivity of the form a.* For the bulk variable, on the other hand, we assume that there exists $\alpha > 0$ such that, for all $v \in V_h$, there exists $\mu_v \in \Lambda_h$ such that

$$c_a^2 \|v\|_V^2 \leq a(v, v) + b(\mu_v, v), \tag{7.29}$$

  with $\|\mu_v\|_\Lambda \lesssim \|v\|_V$ and $\tau_0^{1/2} s_{h,0}(\mu_v, \mu_v)^{1/2} \leq C_\tau \|v\|_V$, where C_τ depends on τ_0 and can be made small by reducing this parameter. Note that the classical condition that a is coercive on the kernel of b can be misleading when working on cut meshes.

A4. *Approximation.* Let p and l denote the polynomial degrees of the spaces V_h and Λ_h respectively. Assume that there is an V-stable interpolation operator $\pi_h \colon H^1(\Omega) \to V_h$ satisfying

$$\|v - \pi_h v\|_V \lesssim h^r |v|_{H^{r+1}(\Omega)}, \quad r = \min(p, t_u - 1), \ v \in H^{t_u}(\Omega), \tag{7.30}$$

with $p \geq 1$ and $t_u \geq 1$ and an interpolation operator $\varpi_h \colon \Lambda \to \Lambda_h$ such that

$$\|\mu - \varpi_h \mu\|_\Lambda + \|\varpi_h \mu\|_{s_h} \lesssim h^{r+1/2} |\mu|_{H^r(\Omega_0)}, \quad r = \min(l+1, t_\mu), \; \mu \in H^{t_\mu}(\Omega_0), \tag{7.31}$$

with $l \geq 0$ and $t_\mu \geq 0$.

The approximation assumptions on V_h hold using the theory of Section 3.4. On Λ_h we typically need approximation in negative norm. On fitted meshes this is a standard result, and in the unfitted case we will show how to achieve (7.31) in the Section 7.6 below. The approximation result for the stabilization norm $\|\cdot\|_{s_h}$ is standard in the fitted case, and in the unfitted case it follows from arguments similar to those in Section 5.2 for the methods introduced below.

The stability of the form A_h is quantified in the global inf-sup condition.

Proposition 7.2. Assume that A2–A3 hold and that τ_0 is sufficiently small. Then, for all $v_h, \mu_h \in V_h \times \Lambda_h$,

$$|||(v_h, \mu_h)|||_\tau \lesssim \sup_{y, \eta \in V_h \times \Lambda_h} \frac{A[(v_h, \mu_h), (y, \eta)] + \tau_0 s_{h,0}(\mu_h, \eta)}{|||(y, \eta)|||_\tau}. \tag{7.32}$$

Proof. First, by (7.29),

$$c_a^2 \|v_h\|_V^2 + \tau_0 s_{h,0}(\mu_h, \mu_h) \leq A[(v_h, \mu_h), (v_h, \mu_h - \mu_v)] + \tau_0 s_{h,0}(\mu_h, \mu_h). \tag{7.33}$$

By the arithmetic–geometric inequality and the stability of μ_v, $\tau_0^{1/2} s_{h,0}(\mu_v, \mu_v)^{1/2} \leq C_\tau \|v_h\|_V$,

$$\tau_0 s_{h,0}(\mu_h, \mu_v) \leq C_\tau^2 \tau_0 / 2 c_a^{-2} s_{h,0}(\mu_h, \mu_h) + 1/2 c_a^2 \|v_h\|_V^2. \tag{7.34}$$

Then we see that by taking τ_0 small so that $C_\tau^2 / c_a^2 < 1$,

$$c_a^2 1/2 \|v_h\|_V^2 + 1/2 \tau_0 s_{h,0}(\mu_h, \mu_h) \leq A[(v_h, \mu_h), (v_h, \mu_h - \mu_v)] + \tau_0 s_{h,0}(\mu_h, \mu_h - \mu_v). \tag{7.35}$$

Next (7.28) implies that there exists $x_h \in V_h$, with $\|x_h\|_V = M_b \|\mu_h\|_\Lambda$ such that, with c_b^{-1} the hidden constant of (7.28),

$$1/2 c_b^2 \|\mu_h\|_\Lambda^2 \leq b(\mu_h, x_h) + \tau_0 s_{h,0}(\mu_h, \mu_h). \tag{7.36}$$

To see this, take squares of both sides of (7.28):

$$c_b{}^2 \|\mu_h\|_\Lambda^2 \leq \left(\frac{b(\mu_h, v_h)}{\|v_h\|_V} + \tau_0^{1/2} s_{h,0}(\mu_h, \mu_h)^{1/2} \right)^2, \tag{7.37}$$

$$c_b{}^2 \|\mu_h\|_\Lambda^2 \leq 2 \left(\frac{b(\mu_h, v_h)^2}{\|v_h\|_V^2} + \tau_0 s_{h,0}(\mu_h, \mu_h) \right). \tag{7.38}$$

Using the continuity of b, the first term on the right-hand side is bounded by

$$\left(\frac{b(\mu_h, v_h)}{\|v_h\|_V} \right)^2 \leq b(\mu_h, v_h / \|v_h\|_V) M_b \|\mu_h\|_\Lambda. \tag{7.39}$$

Take $x_h = M_b \|\mu_h\|_\Lambda v_h / \|v_h\|_V$. As a consequence,

$$1/2 c_b{}^2 \|\mu_h\|_\Lambda^2 \leq A[(v_h, \mu_h), (x_h, 0)] - a(v_h, x_h) + \tau_0 s_{h,0}(\mu_h, \mu_h). \quad (7.40)$$

Using the continuity of a, from (7.26) followed by the arithmetic–geometric inequality and the stability property of x_h, we have

$$a(v_h, x_h) \leq c_b{}^{-2} M_a^2 M_b^2 \|v_h\|_V^2 + \frac{c_b{}^2}{4} \|\mu_h\|_\Lambda^2. \quad (7.41)$$

It follows that

$$c_b{}^2/4 \|\mu_h\|_\Lambda^2 - c_b{}^{-2} M_a^2 M_b^2 \|v_h\|_V^2 \leq A[(v_h, \mu_h), (x_h, 0)] + \tau_0 s_{h,0}(\mu_h, \mu_h). \quad (7.42)$$

Adding (7.35) and (7.42) together, using a weight $\epsilon > 0$ on the second relation, we see that

$$\begin{aligned}
\left(1/2 - \epsilon c_a^{-2} c_b^{-2} M_a^2 M_b^2\right) c_a^2 \|v_h\|_V^2 &+ (1/2 - \epsilon) \tau_0 s_{h,0}(\mu_h, \mu_h) + \epsilon c_b{}^2/4 \|\mu_h\|_\Lambda^2 \\
&\leq A[(v_h, \mu_h), (v_h + \epsilon x_h, \mu_h - \mu_v)] + \tau_0 s_{h,0}(\mu_h, \mu_h - \mu_v). \quad (7.43)
\end{aligned}$$

Choosing

$$\epsilon < \min\left(1/2, (c_a c_b)^2 / \left(2 M_a^2 M_b^2\right)\right), \quad (7.44)$$

we see that

$$\|\|(v_h, \mu_h)\|\|_\tau^2 \lesssim A[(v_h, \mu_h), (v_h + \epsilon x_h, \mu_h - \mu_v)] + \tau_0 s_{h,0}(\mu_h, \mu_h - \mu_v). \quad (7.45)$$

We conclude by observing that by using a triangle inequality and the stabilities of x_h and μ_v, we obtain

$$\|\|(v_h + \epsilon x_h, \mu_h - \mu_v)\|\|_\tau \leq \|\|(v_h, \mu_h)\|\|_\tau + \|\|(\epsilon x_h, \mu_v)\|\|_\tau \lesssim \|\|(v_h, \mu_h)\|\|_\tau. \quad (7.46)$$

$\square$

We can now prove a best approximation estimate for the discretization of (7.5)–(7.6).

Theorem 7.3. Assume that A1–A4 hold and that τ_0 is small so that Proposition 7.2 holds. Then

$$\|\|(u - u_h, \lambda - \lambda_h)\|\|_0 \lesssim \inf_{(v_h, \mu_h) \in V_h \times \Lambda_h} \left(\|\|(u - v_h, \lambda - \mu_h)\|\|_0 + \tau_0^{1/2} \|\mu_h\|_{s_h}\right), \quad (7.47)$$

$$\|\lambda_h\|_{s_h} \lesssim \inf_{(v_h, \mu_h) \in V_h \times \Lambda_h} \left(\|\|(u - v_h, \lambda - \mu_h)\|\|_0 + \tau_0^{1/2} \|\mu_h\|_{s_h}\right), \quad (7.48)$$

and if the regularity assumption (7.16) holds and $\min(p, l+1) \geq t \geq 1$, then

$$\|\|(u - u_h, \lambda - \lambda_h)\|\|_0 + \|\lambda_h\|_{s_h} \lesssim h^t \left(\|f\|_{H^{t-1}(\Omega)} + \|g\|_{H^{t+1/2}(\Omega_0)}\right). \quad (7.49)$$

Proof. Using the triangle inequality, we have

$$\|\|(u - u_h, \lambda - \lambda_h)\|\|_0 \lesssim \|\|(u - v_h, \lambda - \mu_h)\|\|_0 + \|\|(v_h - u_h, \mu_h - \lambda_h)\|\|_0. \quad (7.50)$$

Recalling the consistency (7.25), we see that

$$A[(v_h - u_h, \mu_h - \lambda_h), (y, \eta)] + \tau_0 s_{h,0}(\mu_h - \lambda_h, \eta)$$
$$= A[(v_h - u, \mu_h - \lambda), (y, \eta)] + \tau_0 s_{h,0}(\mu_h, \eta). \qquad (7.51)$$

The first bound now follows by Proposition 7.2, the consistency (7.51) and the continuity of A and $s_{h,0}$, leading to

$$|||(v_h - u_h, \mu_h - \lambda_h)|||_\tau \lesssim |||(u - v_h, \lambda - \mu_h)|||_0 + \tau_0^{1/2}\|\mu_h\|_{s_h}. \qquad (7.52)$$

The second bound is an immediate consequence of the triangle inequality and (7.52):

$$\|\lambda_h\|_{s_h} \le \|\lambda_h - \mu_h\|_{s_h} + \|\mu_h\|_{s_h} \le \tau_0^{-1/2}|||(v_h - u_h, \mu_h - \lambda_h)|||_\tau + \|\mu_h\|_{s_h}. \qquad (7.53)$$

The *a priori* error estimate is a consequence of the approximation estimates (7.30)–(7.31). $\qquad\square$

Note that of the assumptions A1–A4 necessary for the abstract analysis, it is only the stability (7.28) in A3 that cannot easily be shown to hold in the CutFEM framework using the theory of the previous sections. The coercivity (7.29) follows by taking $\mu_v = \alpha \int_{\Omega_0} v\,\mathrm{d}s$ and applying the Poincaré inequality:

$$\|v\|_V \lesssim \alpha^{1/2}\|\nabla v\|_\Omega + \left|\alpha^{1/2} \int_{\Omega_0} v\,\mathrm{d}s\right|. \qquad (7.54)$$

Note that

$$\|\mu_v\|_\Lambda \lesssim \alpha^{1/2}\left|\int_{\Omega_0} v\,\mathrm{d}s\right| \lesssim \|v\|_V, \qquad (7.55)$$

using a global trace inequality on the domain Ω. The inequality

$$\tau_0^{1/2} s_{h,0}(\mu_v, \mu_v)^{1/2} \le C_\tau \|v\|_V \qquad (7.56)$$

will be satisfied by the forms introduced below, but we observe here that the scaling of the parameter must be $\tau_0 = \hat{\tau}_0 \alpha^{-1}$, where $\hat{\tau}_0$ is a dimensionless parameter that can be chosen small and $C_\tau \propto \hat{\tau}_0$. For approximation error estimates in the bulk, we refer to Section 3.4. Estimates in negative norm for unfitted surface approximations will be derived in Section 7.6. The consistency (7.25) holds by construction, and the continuity (7.26)–(7.27) follows using the Cauchy–Schwarz inequality for the forms a and s and by using the scaling in α, the Cauchy–Schwarz inequality and a global trace inequality for b, as in (7.9). In the following sections we will therefore focus exclusively on assumption A3: how to obtain stable Lagrange multiplier discretizations on cut meshes. This discussion will use the model problem of the previous section but can easily be extended to the applications of the next section.

When working on cut meshes and using stabilization, it is inconvenient to work directly in the $H^{-1/2}(\Omega_0)$-norm. It is easier to prove stability in the h-weighted

L^2-norm in the spirit of Pitkäranta (1980). An important observation is that the low frequencies of μ_h can always be controlled provided that the bulk space has approximation properties, and that therefore it is enough to prove stability in the weighted L^2-norm. Below we will work directly in the $H^{-1/2}(\Omega_0)$- and $H^1(\Omega)$-norms. Hence there is no α and no τ_0 weight in front of the stabilization.

Lemma 7.4. For all $\mu_h \in \Lambda_h$,

$$\|\mu_h\|_{H^{-1/2}(\Omega_0)} \lesssim \|h^{1/2}\mu_h\|_{\Omega_0} + \sup_{v \in V_h \setminus \{0\}} \frac{b(\mu_h, v)}{\|v\|_{H^1(\Omega)}}. \tag{7.57}$$

Proof. Since $\Lambda_h \subset \Lambda$,

$$\|\mu_h\|_{H^{-1/2}(\Omega_0)} \lesssim \sup_{v \in V \setminus \{0\}} \frac{b(\mu_h, v)}{\|v\|_{H^1(\Omega)}}. \tag{7.58}$$

We must show that the right-hand side is upper-bounded by the right-hand side of (7.57). Given $v \in H^1(\Omega)$, let $v^e = E_B v$ denote its stable extension to Ω_h, from Section 3.4, such that $\|v^e\|_{H^1(\Omega_h)} \lesssim \|v\|_{H^1(\Omega)}$. Let $\pi_h v^e$ be an H^1-stable interpolant of v^e with optimal approximation. Then

$$b(\mu_h, v) = b(\mu_h, v - \pi_h v^e) + b(\mu_h, \pi_h v^e). \tag{7.59}$$

For the first term on the right-hand side we use the Cauchy–Schwarz inequality, the multiplicative trace inequality and approximation

$$b(\mu_h, v - \pi_h v^e) \lesssim \|h^{1/2}\mu_h\|_{\Omega_0} h^{-1/2} \|v - \pi_h v^e\|_{\Omega_0}, \tag{7.60}$$

$$\|v - \pi_h v^e\|_{\Omega_0} \lesssim \|v^e - \pi_h v^e\|_{\Omega_h}^{1/2} \|\nabla(v^e - \pi_h v^e)\|_{\Omega_h}^{1/2} \lesssim h^{1/2} \|v\|_{H^1(\Omega)}. \tag{7.61}$$

For the second term we use

$$\|\pi_h v^e\|_{H^1(\Omega)} \leq \|\pi_h v^e\|_{H^1(\Omega_h)} \lesssim \|v^e\|_{H^1(\Omega_h)} \lesssim \|v\|_{H^1(\Omega)}. \tag{7.62}$$

Then

$$b(\mu_h, v) \lesssim \|h^{1/2}\mu_h\|_{\Omega_0} \|v\|_{H^1(\Omega)} + \frac{\|v\|_{H^1(\Omega)}}{\|\pi_h v^e\|_{H^1(\Omega)}} b(\mu_h, \pi_h v^e). \tag{7.63}$$

The proof follows by dividing through by $\|v\|_{H^1(\Omega)}$ and taking the sup over $v \in H^1(\Omega)$. $\qquad\square$

A naive way of achieving control of the high-frequency part in the formulation (7.22) is to use the stabilization term

$$s_{h,0}(\mu_h, \lambda_h) = (h^{1/2}\mu_h, \lambda_h)_{\Omega_0}. \tag{7.64}$$

This, however, results in a non-consistent method that is equivalent to the penalty method (after elimination of the multiplier). The lack of consistency restricts the method to $O(h^{1/2})$ convergence (Corti *et al.* 2024) and it is therefore not suitable to use in combination with cut elements. Below we will focus on stabilization methods that achieve stability while being weakly consistent to the right order.

7.5. Λ_h defined on a surface mesh $\Sigma_{\tilde{h}}$

We let $\Sigma_{\tilde{h}}$ denote a decomposition of each component $\Omega_{0,i}$ of Ω_0 in shape-regular (curved) simplices F such that $\mathrm{diam}(F) = O(\tilde{h})$. We let $\hat{F} \subset \mathbb{R}^{d-1}$ denote a reference element and define a differentiable map $T_F \colon \hat{F} \to F$. As before, V_h is taken as the unfitted finite element space in the bulk. We may then define a multiplier space by

$$\Lambda_{\tilde{h}} = \left\{ v_h \in L^2(\Omega_0) \mid v_h \circ T_F^{-1} \in \mathbb{P}_l(\hat{F}) \text{ for all } F \in \Sigma_{\tilde{h}} \right\}. \qquad (7.65)$$

We will consider the formulation (7.22) with $\tau_0 = 0$. It is well known that the estimates (7.30)–(7.31) are satisfied by these spaces. The bound (7.28), on the other hand, depends on both V_h and $\Sigma_{\tilde{h}}$. In a nutshell: if $h/\tilde{h}$ is small enough then (7.28) is satisfied (Babuška 1972/73). To see this, observe that since $\Lambda_{\tilde{h}} \subset \Lambda$, we have

$$\|\mu_h\|_{H^{-1/2}(\Omega_0)} \lesssim \sup_{v \in V \setminus \{0\}} \frac{b(\mu_h, v)}{\|v\|_{H^1(\Omega)}}. \qquad (7.66)$$

Now we want to replace the sup over V by one over V_h. In view of Lemma 7.4, this follows if we can bound the term $h^{1/2}\|\mu_h\|_{\Omega_0}$. Following Babuška (1973), for this term we will apply an inverse inequality.

Lemma 7.5. For all $q_h \in \Lambda_{\tilde{h}}$,

$$\|q_h\|_{\Omega_0} \lesssim \tilde{h}^{-1/2}\|q_h\|_{H^{-1/2}(\Omega_0)}. \qquad (7.67)$$

Proof. The proof of the lemma follows Lemma 3.3 of Nédélec (1976). For each element $F \in \Sigma_{\tilde{h}}$, let $\varphi_F = \hat{\varphi}(T^{-1}(x))$ be the function which is zero on ∂F and such that $\hat{\varphi}(\hat{x}) = \mathrm{dist}(\hat{x}, \partial \hat{F})$. Then, by the finite-dimensionality of q_h,

$$\|q_h\|_{\Omega_0}^2 \lesssim \int_{\Omega_0} q_h \sum_{F \in \Sigma_{\tilde{h}}} \varphi_F q_h \, \mathrm{d}s, \quad \left\| \sum_{F \in \Sigma_{\tilde{h}}} \varphi_F q_h \right\|_{\Omega_0}^2 \lesssim \|q_h\|_{\Omega_0}^2. \qquad (7.68)$$

First note that by duality

$$\|q_h\|_{\Omega_0}^2 \lesssim \int_{\Omega_0} q_h \sum_{F \in \Sigma_{\tilde{h}}} \varphi_F q_h \, \mathrm{d}s \lesssim \|q_h\|_{H^{-1/2}(\Omega_0)} \left\| \sum_{F \in \Sigma_{\tilde{h}}} \varphi_F q_h \right\|_{H^{1/2}(\Omega_0)}. \qquad (7.69)$$

Now apply the interpolation inequality (Taylor 2023, Proposition 3.1)

$$\|v\|_{H^s(\Omega_0)}^2 \lesssim \|v\|_{H^{s-1/2}(\Omega_0)}\|v\|_{H^{s+1/2}(\Omega_0)} \qquad (7.70)$$

with $s = 1/2$,

$$\left\| \sum_{F \in \Sigma_{\tilde{h}}} \varphi_F q_h \right\|_{H^{1/2}(\Omega_0)} \lesssim \left\| \sum_{F \in \Sigma_{\tilde{h}}} \varphi_F q_h \right\|_{\Omega_0}^{1/2} \left\| \sum_{F \in \Sigma_{\tilde{h}}} \varphi_F q_h \right\|_{H^1(\Omega_0)}^{1/2}. \qquad (7.71)$$

For the last term on the right-hand side, we see that

$$\left\|\sum_{F\in\Sigma_{\tilde{h}}}\varphi_F q_h\right\|_{H^1(\Omega_0)}^2 = \sum_{F\in\Sigma_{\tilde{h}}}\|\varphi_F q_h\|_{H^1(F)}^2. \tag{7.72}$$

Considering the H^1-seminorm, we see that

$$|\varphi_F q_h|_{H^1(F)}^2 = \int_F |\nabla_x(\hat{\varphi}(T_F^{-1}(x))q_h(T_F^{-1}(x)))|^2\,\mathrm{d}x$$
$$= \int_{\hat{F}} |J^{-1}\nabla_{\hat{x}}(\hat{\varphi}(\hat{x})q_h(\hat{x}))|^2|J|\,\mathrm{d}\hat{x}, \tag{7.73}$$

where J^{-1} is the Jacobian of T_F^{-1} and $|J|$ is the absolute value of the determinant of the Jacobian of the mapping T_F. Then, using an inverse inequality on $\hat{F}$, we see that since $\|J^{-1}\|_{L^\infty(F)} \lesssim h_F^{-1}$ and $\|J^{-1}\|_{L^\infty(\hat{F})}\|J\|_{L^\infty(\hat{F})} = O(1)$, we have

$$|\varphi_F q_h|_{H^1(F)}^2 \lesssim \|J^{-1}\|_{L^\infty(F)}^2\|J\|_{L^\infty(\hat{F})}\|q_h\|_{L^2(\hat{F})}^2$$
$$\lesssim h_F^{-2}\|J^{-1}\|_{L^\infty(F)}\|J\|_{L^\infty(\hat{F})}\|q_h\|_{L^2(F)}^2. \tag{7.74}$$

Collecting the above bounds, we see that

$$\|q_h\|_{\Omega_0}^2 \lesssim \|q_h\|_{H^{-1/2}(\Omega_0)}\|q_h\|_{\Omega_0}\tilde{h}^{-1/2}, \tag{7.75}$$

which proves the claim. $\qquad\square$

Applying Lemma 7.5 in the first term on the right-hand side of (7.57), it follows that $h^{1/2}\|\mu_h\|_{\Omega_0} \lesssim h^{1/2}\tilde{h}^{-1/2}\|\mu_h\|_{H^{-1/2}(\Omega_0)}$. Therefore

$$\left(1 - Ch^{1/2}\tilde{h}^{-1/2}\right)\|\mu_h\|_{H^{-1/2}(\Omega_0)} \lesssim \sup_{v\in V_h\setminus\{0\}}\frac{b(\mu_h,v)}{\|v\|_{H^1(\Omega)}}. \tag{7.76}$$

Here the inverse constant C depends on the mesh geometry of $\Sigma_{\tilde{h}}$. Clearly, for

$$Ch^{1/2}\tilde{h}^{-1/2} < 1, \tag{7.77}$$

the condition (7.28) is satisfied.

We conclude that for $h^{1/2}\tilde{h}^{-1/2}$ sufficiently small, the spaces V_h and $\Lambda_{\tilde{h}}$ satisfy the inequality (7.28) and hence Theorem 7.3 holds for this choice. Note that this analysis can be made local, allowing for mesh refinement using the ideas of Pitkäranta (1980).

Violation of the mesh condition: interior penalty stabilization. This time Λ_h is defined by (7.65) on a shape-regular surface mesh Σ_h violating the mesh condition (7.77). Hence it will not satisfy the inf-sup condition (7.28) with V_h. However, under the *a priori* assumption that the space $\Lambda_{\tilde{h}}$ satisfying the inf-sup condition exists, it is easy to design stabilized formulations where the distance to the space satisfying the inf-sup condition is penalized, in the spirit of Brezzi and Fortin (2001). Such stabilized formulations were first introduced for interface problems

and fictitious domain problems by Burman and Hansbo (2010a,b), then further developed by Barrenechea and Chouly (2012), Burman (2014) and Fournié and Lozinski (2017).

Note that from Lemma 7.4 it follows that only $\|h^{1/2}\mu_h\|_{\Omega_0}$ has to be controlled. Let $\pi_{\tilde{h}}\colon L^2(\Omega_0) \to \Lambda_{\tilde{h}}$ denote the L^2-projection on the inf-sup stable space $\Lambda_{\tilde{h}}$, such that $b(\pi_{\tilde{h}}\mu, \xi_h) = b(\mu, \xi_h)$ for all $\xi_h \in \Lambda_{\tilde{h}}$. Then

$$\|h^{1/2}\mu_h\|_{\Omega_0}^2 = \|h^{1/2}(\mu_h - \pi_{\tilde{h}}\mu_h)\|_{\Omega_0}^2 + \|h^{1/2}\pi_{\tilde{h}}\mu_h\|_{\Omega_0}^2. \tag{7.78}$$

Functions in $\Lambda_{\tilde{h}}$ satisfy an inverse inequality and the inf-sup condition (7.28), with $\tau_0 = 0$ therefore

$$\|h^{1/2}\pi_{\tilde{h}}\mu_h\|_{\Omega_0} \lesssim \|\pi_{\tilde{h}}\mu_h\|_{H^{-1/2}(\Omega_0)} \lesssim \sup_{v \in V_h \setminus \{0\}} \frac{b(\pi_{\tilde{h}}\mu_h, v)}{\|v\|_{H^1(\Omega)}}, \tag{7.79}$$

and

$$b(\pi_{\tilde{h}}\mu_h, v) = b(\pi_{\tilde{h}}\mu_h - \mu_h, v - \pi_{\tilde{h}}v) + b(\mu_h, v). \tag{7.80}$$

Using the Cauchy–Schwarz inequality and the approximation property of $\pi_{\tilde{h}}$, $\|v_h - \pi_{\tilde{h}}v_h\|_{\Omega_0} \lesssim \tilde{h}^{1/2}\|v_h\|_{H^{1/2}(\Omega_0)}$, followed by a trace inequality, we have

$$b(\pi_{\tilde{h}}\mu_h - \mu_h, v - \pi_{\tilde{h}}v) \lesssim \|h^{1/2}(\mu_h - \pi_{\tilde{h}}\mu_h)\|_{\Omega_0}\|v\|_{H^1(\Omega)}. \tag{7.81}$$

We conclude that the following proposition holds.

Proposition 7.6. Assume that $\tilde{h}/h = O(1)$. Then, for all $\mu_h \in \Lambda_h$,

$$\|\mu_h\|_{H^{-1/2}(\Omega_0)} \lesssim \|h^{1/2}(\mu_h - \pi_{\tilde{h}}\mu_h)\|_{\Omega_0} + \sup_{v \in V_h \setminus \{0\}} \frac{b(\mu_h, v)}{\|v\|_{H^1(\Omega)}}. \tag{7.82}$$

It follows that for $s_{h,0}(\mu_h, \mu_h)^{1/2}$ equivalent to $\|h^{1/2}(\mu_h - \pi_{\tilde{h}}\mu_h)\|_{\Omega_0}$, the inf-sup condition will be satisfied. The other assumptions for the analysis are verified as in Section 7.5. One possibility for the design of the stabilization is to decompose the boundary in (possibly overlapping) patches of diameter $\tilde{h}$ and penalize the difference of the multiplier and its projection on a polynomial on the patch (Barrenechea and Chouly 2012). This approach, however, requires explicit knowledge of the necessary size of $\tilde{h}/h$. Next we will show how to design an operator $s_{h,0}$ that does not require such explicit knowledge of the space $\Lambda_{\tilde{h}}$. This can be achieved using the stabilization operators discussed in Section 5.2. We will give an example using penalties on gradient jumps, but any equivalent stabilizing form may be used such as (5.16).

Lemma 7.7. Assume that the meshes $\Sigma_{\tilde{h}}$ and Σ_h are defined as unions of tessellations $\hat{\Sigma}_{\tilde{h},i}$ and $\hat{\Sigma}_{h,i}$ of $\hat{\Omega}_{0,i}$. Also assume that the associated spaces $\Lambda_{\tilde{h}}$ and Λ_h are defined using (7.65), with the mappings $T_{\tilde{F}} = \hat{x} \circ \hat{T}_{\tilde{F}}$ for all $\tilde{F} \in \Sigma_{\tilde{h}}$ and $T_F = \hat{x} \circ \hat{T}_F$ for all $F \in \Sigma_h$. Here $\hat{T}_F$ and $\hat{T}_{\tilde{F}}$ are affine maps that map the reference element $\hat{F}$ to a simplex $F \in \Sigma_h$ and $\tilde{F} \in \Sigma_{\tilde{h}}$, respectively.

Assume that $\tilde{h}/h = O(1)$. For all $\mu_h \in \Lambda_h$,

$$\|h^{1/2}(\mu_h - \pi_{\tilde{h}}\mu_h)\|_{\Omega_0} \lesssim s_{h,0}(\mu_h, \mu_h)^{1/2}, \qquad (7.83)$$

with

$$s_{h,0}(\mu_h, \lambda_h) = \sum_{i=1}^{N} \sum_{F \in \hat{\Sigma}_{h,i}} \int_{\partial F \setminus \partial \hat{\Omega}_{0,i}} \left(\sum_{j=0}^{l} h^{2j+2} \left[D_n^j \mu_h \right] \left[D_n^j \lambda_h \right] \right) ds, \qquad (7.84)$$

where l is the polynomial degree of the space Λ_h, D_n^j denotes the jth normal derivative on the boundary of F in the mesh $\hat{\Sigma}_{h,i}$ in the reference plane $\hat{\Omega}_{0,i}$, and $[D_n^0 \mu_h] = [\mu_h]$.

Proof. It is enough to consider one of the $\hat{\Sigma}_{h,i}$. For each face $F \subset \hat{\Sigma}_{\tilde{h},i}$, we let $\mathcal{E}$ denote the set of edges of $\hat{\Sigma}_{h,i}$ intersecting F. We map F to the reference element $\hat{F}$ with $|\hat{F}| = 1$. The set of scaled edges is denoted by $\hat{\mathcal{E}}$. The cardinality of $\hat{\mathcal{E}}$ is uniformly upper-bounded for all F and h by the shape regularity of the elements in $\hat{\Sigma}_{h,i}$ and since $\tilde{h}/h = O(1)$. The spaces Λ_h and $\Lambda_{\tilde{h}}$ use the same parametrization of $\hat{\Omega}_{0,i}$ and therefore $\eta_h = \mu_h - \pi_{\tilde{h}}\mu_h$ is a polynomial with zero average on $F \in \hat{\Sigma}_{\tilde{h},i}$. Let $\hat{\eta}_h$ denote the η_h function after scaling to $\hat{F}$. It follows that by norm equivalence on discrete spaces,

$$\|\hat{\eta}_h\|_{\hat{F}}^2 \lesssim \sum_{e \in \hat{\mathcal{E}}} \sum_{j=0}^{k} \int_e \left(\left[D_{\hat{x}}^j \hat{\mu}_h \right]|_e \right)^2 ds, \qquad (7.85)$$

where the hidden constant depends on the cardinality of $\hat{\mathcal{E}}$, i.e. on the shape-regularity of the meshes $\hat{\Sigma}_{h,i}$ and $\hat{\Sigma}_{\tilde{h},i}$ and the ratio $h/\tilde{h}$. Then note that $[\hat{\mu}_h]|_e = 0$ implies that the jumps of tangential derivatives of all orders are zero too. Scaling back to F and summing over $F \in \hat{\Sigma}_{\tilde{h},i}$, it follows that

$$\|h^{1/2}(\mu_h - \pi_{\tilde{h}}\mu_h)\|_{\Omega_{0,i}}^2 \lesssim \sum_{F \in \hat{\Sigma}_{h,i}} \int_{\partial F \setminus \partial \hat{\Omega}_{0,i}} \left(\sum_{j=1}^{k} h^{2j+2} \left[D_n^j \mu_h \right]^2 \right) ds. \qquad (7.86)$$

The conclusion follows after summing over i. $\qquad \square$

Violation of the mesh condition: Barbosa–Hughes stabilization. Another approach to stabilization of the Lagrange multiplier was introduced by Barbosa and Hughes (1991, 1992). The idea was to circumvent the inf-sup condition by adding a least-squares term penalizing the distance from the multiplier to the normal derivative of the bulk variable on the boundary. In the context of unfitted finite element methods this approach has been considered by several authors (Haslinger and Renard 2009, Fournié and Lozinski 2017). Observe that by Lemma 7.4 the stabilization must ensure control of $\|h^{1/2}\mu_h\|_{\Omega_0}$. The idea is to modify the penalty term (7.64) using that formally $\lambda = -\alpha n \cdot \nabla u$ on the boundary. Let

$$s_{h,0}(v_h, \mu_h, y, \zeta) = (h(\mu_h + n \cdot \alpha \nabla v_h), \zeta + \xi n \cdot \alpha \nabla y)_{\Omega_0}. \qquad (7.87)$$

Clearly, then, for a sufficiently smooth exact solution (u, λ) the stabilization is consistent, since $s_{h,0}(u, \lambda, y, \zeta) = 0$ for all $y \in V_h$ and $\zeta \in \Lambda_h$. Here the parameter $\xi \in \{-1, 0, 1\}$ defines different flavours of the method. Since the stabilization depends on both bulk and surface variables, it does not enter the framework above directly. In particular, for the non-symmetric variants the norm $|||(\cdot, \cdot)|||$ must be modified as well as the continuity of $s_{h,0}$. Most importantly, the method destroys the advantage of the previous multiplier method, in which the bulk variable does not need to be stabilized for accuracy. To see this, observe that

$$s_{h,0}(v_h, \mu_h, v_h, \mu_h) \geq \frac{3-\xi}{4}\|h^{1/2}\mu_h\|^2_{\Omega_0} - \alpha^2\|h^{1/2}n \cdot \nabla v_h\|^2_{\Omega_0}. \qquad (7.88)$$

The first term gives the necessary control of the h-weighted L^2-norm of the multiplier. The second term on the right-hand side must be controlled using the coercivity of the form a. This cannot be done without some stabilizing modification.

- *Ghost penalty.* Note that by the trace inequality,

$$\|h^{1/2}n \cdot \nabla v_h\|^2_{\Omega_0} \leq C_T\|\nabla v_h\|^2_{\Omega_h}. \qquad (7.89)$$

A ghost penalty term can be added to a, $a_h = a + s_{h,0}$ so that

$$a_h(v_h, v_h) - \epsilon\tau_0\alpha^2\|h^{1/2}n \cdot \nabla v_h\|^2_{\Omega_0} \geq \alpha\|v_h\|^2_{\Omega_h} - \epsilon\tau_0\alpha^2\|h^{1/2}n \cdot \nabla v_h\|^2_{\Omega_0}$$
$$\geq (\alpha - C_T\epsilon\tau_0\alpha^2)\|\nabla v_h\|^2_{\Omega_h}. \qquad (7.90)$$

The stability of Proposition 7.2 is then achieved for $\epsilon\tau_0 \propto \alpha^{-1}$ small enough.

- *Local extension.* On some triangle T with a bad cut, the functions $v_h|_T$, $y|_T$ of (7.87) can be taken as extensions from elements with large intersection with the physical domain, $S_h v_h|_T$ and $S_h y|_T$. Here, recall the mapping S_h of Section 4.3. That is, if we let w_h denote a function in V_h then $v_h|_T = (w_h|_{S_h(T)})^e$ and similarly for the test function y. This implies the trace inequality

$$\|h^{1/2}n \cdot \nabla v_h\|^2_{\Omega_0} \lesssim \|\nabla v_h\|^2_{\Omega}, \qquad (7.91)$$

and stability is achieved without ghost penalty stabilization. This extension approach was first considered in Haslinger and Renard (2009).

An important aspect of the Barbosa–Hughes stabilization is that it produces stable discretizations for any space Λ_h. This was exploited in Stenberg (1995) to eliminate the multiplier. Indeed, for $\Lambda_h = L^2(\Omega_0)$, on every $E = \Omega_0 \cap T$ we may use the equation

$$(u_h, \mu)_{\Omega_0} + \tau_0 s_{h,0}(u_h, \lambda, 0, \mu) = (g, \mu)_{\Omega_0} \qquad (7.92)$$

to deduce that

$$\lambda|_E = -n \cdot \alpha\nabla u_h|_E + (\tau_0 h)^{-1}(g - u_h)|_E. \qquad (7.93)$$

Eliminating λ in the formulation, we get

$$a(u_h, v) - (n \cdot \alpha \nabla u_h, v)_{\Omega_0} - \xi(n \cdot \alpha \nabla v, u_h)_{\Omega_0} + ((\tau_0 h)^{-1} u_h, v)_{\Omega_0}$$
$$= (f, v)_\Omega + (g, (\tau_0 h)^{-1} v - \xi n \cdot \alpha \nabla v)_{\Omega_0}, \tag{7.94}$$

and recognize Nitsche's method, with ξ leading to the different variants, symmetric ($\xi = 1$), skew-symmetric ($\xi = -1$) and incomplete ($\xi = 0$). If, as proposed above, the $n \cdot \nabla u_h$ and $n \cdot \nabla v$ contributions in the boundary terms are replaced by normal derivatives taken on extended functions $S_h u_h$ and $S_h v$, the method is stable without further stabilization. This last method, which mirrors the construction for the Barbosa–Hughes method using extension, coincides with the approach proposed in Buffa, Puppi and Vázquez (2020).

7.6. Λ_h defined by the trace on the bulk mesh $\mathcal{T}_{h,0}$

If the geometry is given implicitly, e.g. via a level set function, it can be inconvenient to create a surface mesh, in particular if the interface moves. It is then advantageous to define the multiplier using an approximation space defined on the bulk mesh but restricted to the cut elements. This type of approximation was introduced in Burman and Hansbo (2010a) and applied to problems with a moving boundary in von Wahl and Richter (2023). In this section assume that Ω_0 is smooth. How to handle complications due to corners will be discussed later. We recall $\mathcal{T}_{h,0}$ from equation (2.65), the collection of elements in the bulk mesh intersected by the boundary Ω_0. We assume that all elements in $\mathcal{T}_{h,0}$ are connected through at least one face with another element in $\mathcal{T}_{h,0}$. If this is not the case, the set can be enriched with some elements whose vertices are intersected by the interface. Now define Λ_h using a finite element space defined on the elements in $\mathcal{T}_{h,0}$. The simplest possible choice is to take, for $p \geq 2$,

$$\Lambda_h = \{\mu_h|_{\Omega_0} \in H^1(\Omega_0) \mid \mu_h \in H^1(\Omega_{h,0}) \text{ and } \mu_h|_T \in \mathbb{P}_l(T) \text{ for all } T \in \mathcal{T}_{h,0}\} \tag{7.95}$$

for $1 \leq l \leq p$. That is, we let the functions in Λ_h be defined by the traces on Ω_0 of functions in a bulk space of polynomial order at most p, where we recall that p is the polynomial degree of the space V_h. Even though the functions in Λ_h are constructed on the bulk mesh, we write $\Lambda_h \subset \Lambda$, here considering the restriction to Ω_0. For stabilization and in the analysis, on the other hand, it is necessary to use the fact that the functions in Λ_h are constructed on the bulk mesh. Observe that $\Lambda_h|_{\Omega_0}$ is not a linear space but a frame in the spirit of TraceFEM. This means that even if (7.28) should hold, the linear system may not be uniquely invertible and we have to resort to a stabilized formulation.

Approximation estimates. Using this trace space requires special care in designing the interpolation operator ϖ_h if error estimates are desired in the $H^{-1/2}$-norm. Error estimates for the L^2-norm can readily be derived using a standard bulk interpolant applied to the extended function as in Section 3. We recall the interpolant π_h

from (3.29) and consider the following bound for the h-weighted L^2-norm, for $\mu \in H^{t_\mu}(\Omega_0)$:

$$\|h^{1/2}(\mu - \pi_h \mu)\|_{\Omega_0} \lesssim h^{r+1/2}|\mu|_{H^r(\Omega_0)}, \quad r = \min(l+1, t_\mu) \geq 1/2. \qquad (7.96)$$

To obtain an interpolant that also has optimal approximation in the $H^{-1/2}(\Omega_0)$-norm, one may proceed as follows. Let $\mathcal{T}_{h,0}$ be decomposed into N disjoint patches P_i of diameter $O(h)$ in the direction tangential to Ω_0. Assume that each patch is sufficiently large that there is a piecewise affine positive bump function φ_i, $i = 1, \ldots, N$, with support in the patch and $\int_{P_i \cap \Omega_0} \varphi_i = 1$. We refer to Burman *et al.* (2024*a*) for further details of this construction. Define

$$\varpi_h \mu = \pi_h \mu + \sum_{i=1}^{N} \xi_i \varphi_i. \qquad (7.97)$$

We now determine the ξ_i so that $\varpi_h \mu$ satisfies a patch test on the $P_i \cap \Omega_0$,

$$\int_{P_i \cap \Omega_0} (\mu - \varpi_h \mu)\, \mathrm{d}s = 0, \quad \text{that is, } \xi_i = -\left(\int_{P_i \cap \Omega_0} \varphi_i\, \mathrm{d}s\right)^{-1} \int_{P_i \cap \Omega_0} (\mu - \pi_h \mu)\, \mathrm{d}s. \qquad (7.98)$$

We then obtain the following approximation result.

Lemma 7.8. For $\mu \in H^{t_\mu}(\Omega_0)$, $t_\mu \geq 1/2$,

$$\|\mu - \varpi_h \mu\|_{H^{-1/2}(\Omega_0)} \lesssim h^{r+1/2}|\mu|_{H^r(\Omega_0)}, \quad r = \min(l+1, t_\mu) \geq 1/2. \qquad (7.99)$$

Proof. By definition,

$$\|\mu - \varpi_h \mu\|_{H^{-1/2}(\Omega_0)} = \sup_{v \in H^{1/2}(\Omega_0)\setminus\{0\}} \frac{(\mu - \varpi_h \mu, v)_{\Omega_0}}{\|v\|_{H^{1/2}(\Omega_0)}}. \qquad (7.100)$$

Using the construction of ϖ_h, we have

$$(\mu - \varpi_h \mu, v)_{\Omega_0} = \sum_{i=1}^{N} (\mu - \varpi_h \mu, v - \bar{v}_i)_{P_i \cap \Omega_0}, \qquad (7.101)$$

where

$$\bar{v}_i = |P_i \cap \Omega_0|^{-1} \int_{P_i \cap \Omega_0} v\, \mathrm{d}s. \qquad (7.102)$$

Noting that $\|v - \bar{v}_i\|_{P_i \cap \Omega_0} \lesssim h^{1/2}\|v\|_{H^{1/2}(\Omega_0)}$, it follows that

$$\|\mu - \varpi_h \mu\|_{H^{-1/2}(\Omega_0)} \lesssim \|h^{1/2}(\mu - \varpi_h \mu)\|_{\Omega_0}. \qquad (7.103)$$

For the estimate in the L^2-norm, we have

$$\|h^{1/2}(\mu - \varpi_h \mu)\|_{\Omega_0} \lesssim \|h^{1/2}(\mu - \pi_h \mu)\|_{\Omega_0} + h^{d/2}\left(\sum_{i=1}^{N} \xi_i^2\right)^{1/2}. \qquad (7.104)$$

For the first term on the right-hand side we apply (7.96). For the second term we observe that using Cauchy–Schwarz inequality,

$$|\xi_i| \lesssim h^{-(d-1)} \left| \int_{P_i \cap \Omega_0} (\mu - \pi_h \mu) \, ds \right| \lesssim h^{-(d-1)/2} \|\mu - \pi_h \mu\|_{P_i \cap \Omega_0}, \qquad (7.105)$$

and hence

$$h^d \sum_{i=1}^N \xi_i^2 \lesssim h \|\mu - \pi_h \mu\|_{\Omega_0}^2, \qquad (7.106)$$

and we conclude by applying the previously derived bound on the approximation error in the L^2-norm. $\qquad \square$

Stabilization and stability. To stabilize the trace variable, we recall the stabilization forms of Section 5. For example, consider the normal stabilization on the bulk,

$$s_{h,0}(\lambda_h, \mu_h) = \sum_{T \in \mathcal{T}_{h,0}} \int_T h^2 \nabla \lambda_h \cdot n_{\Omega_0}^e \nabla \mu_h \cdot n_{\Omega_0}^e \, dx, \qquad (7.107)$$

for which the following stability estimate holds:

$$\|\mu_h\|_{\Omega_{h,0}}^2 \lesssim \|h^{1/2} \mu_h\|_{\Omega_0}^2 + s_{h,0}(\mu_h, \mu_h). \qquad (7.108)$$

In this case we directly prove a discrete inf-sup condition in the h-weighted L^2-norm exploiting the fact that traces of functions in V_h are in Λ_h. This allows us to conclude that (7.28) holds by applying Lemma 7.4.

Proposition 7.9. For all $\mu_h \in \Lambda_h$,

$$\|h^{1/2} \mu_h\|_{\Omega_0} \lesssim \sup_{v \in V_h \setminus \{0\}} \frac{b(\mu_h, v)}{\|v\|_{H^1(\Omega)}} + s_{h,0}(\mu_h, \mu_h)^{1/2}. \qquad (7.109)$$

Proof. First let v_μ be defined to be equal to $h\mu_h$ in $\mathcal{T}_{h,0}$, with all the nodal degrees of freedom in $\mathcal{T}_h \setminus \overline{\mathcal{T}_{h,0}}$ set to zero. Then it is easy to see that

$$\|v_\mu\|_{\Omega_h} \lesssim \|h\mu_h\|_{\Omega_{h,0}} \quad \text{and} \quad \|v_\mu\|_{H^1(\Omega_h)} \lesssim \|\mu_h\|_{\Omega_{h,0}}. \qquad (7.110)$$

In the second inequality we applied a standard inverse inequality. It then follows by (7.110) and the bound (7.108) that

$$\|v_\mu\|_{H^1(\Omega_h)} \lesssim \|\mu_h\|_{\Omega_{h,0}} \lesssim \|h^{1/2} \mu_h\|_{\Omega_0} + s_{h,0}(\mu_h, \mu_h)^{1/2}. \qquad (7.111)$$

Using this inequality and the construction of v_μ, we see that

$$\|v_\mu\|_{H^1(\Omega_h)} \|h^{1/2} \mu_h\|_{\Omega_0} \lesssim \|h^{1/2} \mu_h\|_{\Omega_0}^2 + s_{h,0}(\mu_h, \mu_h) = b(\mu_h, v_\mu) + s_{h,0}(\mu_h, \mu_h). \qquad (7.112)$$

Dividing through by $\|v_\mu\|_{H^1(\Omega_h)}$ and noting that

$$\frac{b(\mu_h, v_\mu)}{\|v_\mu\|_{H^1(\Omega_h)}} \leq \frac{b(\mu_h, v_\mu)}{\|v_\mu\|_{H^1(\Omega)}}, \qquad (7.113)$$

it only remains to bound the term

$$\frac{s_{h,0}(\mu_h, \mu_h)}{\|v_\mu\|_{H^1(\Omega_h)}}. \tag{7.114}$$

Noting that by construction

$$s_{h,0}(\mu_h, \mu_h)^{1/2} \lesssim \|h\mu_h\|_{H^1(\Omega_{h,0})} \lesssim \|v_\mu\|_{H^1(\Omega_h)}, \tag{7.115}$$

we obtain

$$\frac{s_{h,0}(\mu_h, \mu_h)}{\|v_\mu\|_{H^1(\Omega_h)}} \lesssim s_{h,0}(\mu_h, \mu_h)^{1/2}. \tag{7.116}$$

$\square$

Discontinuous multiplier space. One can also consider the case of a discontinuous multiplier defined on the bulk mesh. For $0 \le l \le k$, let

$$\Lambda_{D,h} = \{\mu_h|_{\Omega_0} \in L^2(\Omega_0) \mid \mu_h \in L^2(\Omega_{h,0}) \text{ and } \mu_h|_T \in \mathbb{P}_l(T) \text{ for all } T \in \mathcal{T}_{h,0}\}. \tag{7.117}$$

Methods using discontinuous multipliers on the bulk mesh can be analysed by combining the arguments of Sections 7.5 and 7.6. The key idea is to exploit the inf-sup stability of the continuous bulk space approximation space, Λ_h, and penalize the distance from a function in $\Lambda_{D,h}$ to Λ_h. Let $I_C \colon \Lambda_{D,h} \to \Lambda_h$ (where Λ_h is the bulk-based space defined in (7.95)) denote the discrete quasi-interpolant defined by taking nodal averages in the nodes of $\mathcal{T}_{h,0}$ of the functions in $\Lambda_{D,h}$. It then follows by discrete interpolation that

$$\|\mu_h - I_C\mu_h\|^2_{\Omega_{h,0}} \lesssim s_J(\mu_h, \mu_h), \tag{7.118}$$

with the jump penalty defined by

$$s_J(\mu_h, \lambda_h) = \sum_{F \in \mathcal{F}_{h,0}} h([\mu_h], [\lambda_h])_F, \tag{7.119}$$

where $\mathcal{F}_{h,0}$ denotes the set of interior faces F in $\mathcal{T}_{h,0}$, i.e. faces such that for some $T, T' \in \mathcal{T}_{h,0}$, $F = T \cap T'$. Then let $\tilde{I}_C \colon \Lambda_{D,h} \to \Lambda_h$ be defined by taking I_C and adding local bubbles to the interpolant, as in the construction of the interpolant of Lemma 7.8. It is straightforward to show (7.118) for $\tilde{I}_C$. One may then show a discrete approximation result in the $H^{-1/2}$-norm.

Lemma 7.10. For all $\mu \in \Lambda_{D,h}$,

$$\|\mu_h - \tilde{I}_C\mu_h\|^2_{H^{-1/2}(\Omega_0)} \lesssim \|\mu_h - I_C\mu_h\|^2_{\Omega_{h,0}} \lesssim s_J(\mu_h, \mu_h). \tag{7.120}$$

Proof. The proof is similar to that of Lemma 7.8, using (7.118) instead of approximation. By definition,

$$\|\mu_h - \tilde{I}_C\mu_h\|_{H^{-1/2}(\Omega_0)} = \sup_{v \in H^{1/2}(\Omega_0)\setminus\{0\}} \frac{(\mu_h - \tilde{I}_C\mu_h, v)_{\Omega_0}}{\|v\|_{H^{1/2}(\Omega_0)}}. \tag{7.121}$$

Using the construction of $\tilde{I}_C$, we have

$$(\mu_h - \tilde{I}_C\mu_h, v)_{\Omega_0} = \sum_{i=1}^{N} (\mu - \tilde{I}_C\mu, v - \bar{v}_i)_{P_i \cap \Omega_0} \lesssim \|h^{1/2}(\mu_h - \tilde{I}_C\mu_h)\|_{\Omega_0} \|v\|_{H^{1/2}(\Omega_0)}.$$

(7.122)

Observing that, by the arguments of Lemma 7.8,

$$\|h^{1/2}(\mu_h - \tilde{I}_C\mu_h)\|_{\Omega_0} \lesssim \|\mu_h - I_C\mu_h\|_{\Omega_{h,0}},$$

(7.123)

we conclude by applying (7.118). $\square$

Proposition 7.11. For all $\mu_h \in \Lambda_{D,h}$,

$$\|h^{1/2}\mu_h\|_{\Omega_0} \lesssim \sup_{v \in V_h \setminus \{0\}} \frac{b(\mu_h, v)}{\|v\|_{H^1(\Omega)}} + s_D(\mu_h, \mu_h)^{1/2},$$

(7.124)

where $s_D = s_{h,0} + s_J$, with $s_{h,0}$ defined in equation (7.107).

Proof. By the triangle inequality,

$$\|h^{1/2}\mu_h\|_{\Omega_0} \le \|h^{1/2}\tilde{I}_C\mu_h\|_{\Omega_0} + \|h^{1/2}(\mu_h - \tilde{I}_C\mu_h)\|_{\Omega_0}.$$

(7.125)

By Proposition 7.9,

$$\|h^{1/2}\tilde{I}_C\mu_h\|_{\Omega_0} \lesssim \sup_{v \in V_h \setminus \{0\}} \frac{b(\tilde{I}_C\mu_h, v)}{\|v\|_{H^1(\Omega)}} + s_{h,0}(\tilde{I}_C\mu_h, \tilde{I}_C\mu_h)^{1/2}.$$

(7.126)

Adding and subtracting μ_h and using the duality in b,

$$b(\tilde{I}_C\mu_h, v) \lesssim b(\mu_h, v) + \|\mu_h - \tilde{I}_C\mu_h\|_{H^{-1/2}(\Omega_0)} \|v\|_{H^{1/2}(\Omega_0)},$$

(7.127)

and since $s_{h,0}(\mu_h - \tilde{I}_C\mu_h, \mu_h - \tilde{I}_C\mu_h) \lesssim \|\mu_h - \tilde{I}_C\mu_h\|_{\Omega_{h,0}}^2$,

$$s_{h,0}(\tilde{I}_C\mu_h, \tilde{I}_C\mu_h)^{1/2} \lesssim s_{h,0}(\mu_h, \mu_h)^{1/2} + \|\mu_h - \tilde{I}_C\mu_h\|_{\Omega_{h,0}}.$$

(7.128)

Collecting the bounds, using $\|v\|_{H^{1/2}(\Omega_0)} \lesssim \|v\|_{H^1(\Omega)}$ and applying Lemma 7.10, we conclude that

$$\|h^{1/2}\mu_h\|_{\Omega_0} \lesssim \sup_{v \in V_h \setminus \{0\}} \frac{b(\mu_h, v)}{\|v\|_{H^1(\Omega)}} + s_{h,0}(\mu_h, \mu_h)^{1/2} + s_J(\mu_h, \mu_h)^{1/2}.$$

(7.129)

$\square$

Numerical illustration. We consider a problem with discontinuous multiplier space defined as piecewise constant functions on the elements cut by the boundary, and the field variable is approximated by C^0-continuous $P1$-elements. The penalty operator s_J defined in (7.119) is applied. For constant multipliers the stabilizer (7.107) is zero. The mesh domain is shown in Figure 7.1, meshing a circle of radius $r_0 = 1/2$ with centre at $(0.1, 0)$. On this domain we pose a problem with $\alpha = 1$ and right-hand side and boundary conditions corresponding to the exact solution $u = 9(r_0^3 - z^3)$, where $z = \sqrt{(x - 1/10)^2 + (2y/3)^2}$.
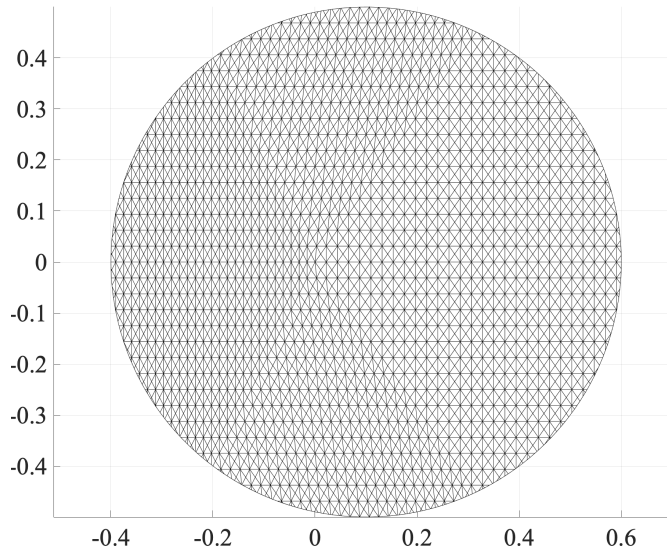
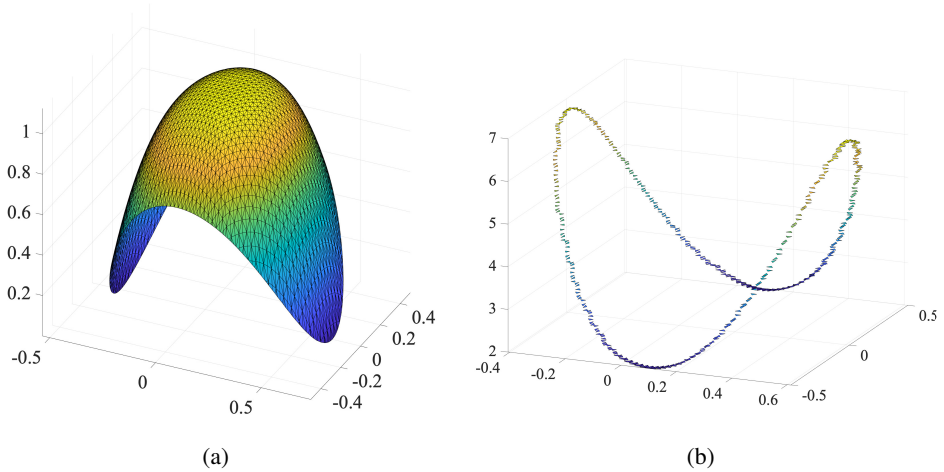Figure 7.1. The mesh domain for the numerical illustration.

| (a) | (b) |

Figure 7.2. The numerical solution of the field variable (a) and multiplier (b) with $\tau_0 = 10^{-1}$.

In Figure 7.2 we show the solution for a stable choice of τ_0, and in Figure 7.3 with a τ_0 chosen too small. We note the effect on the accuracy of the multiplier, whereas the field variable is not affected. Finally, in Figure 7.4 we show the field variable obtained without stabilization; the lack of stability is then affecting the field variable as well.

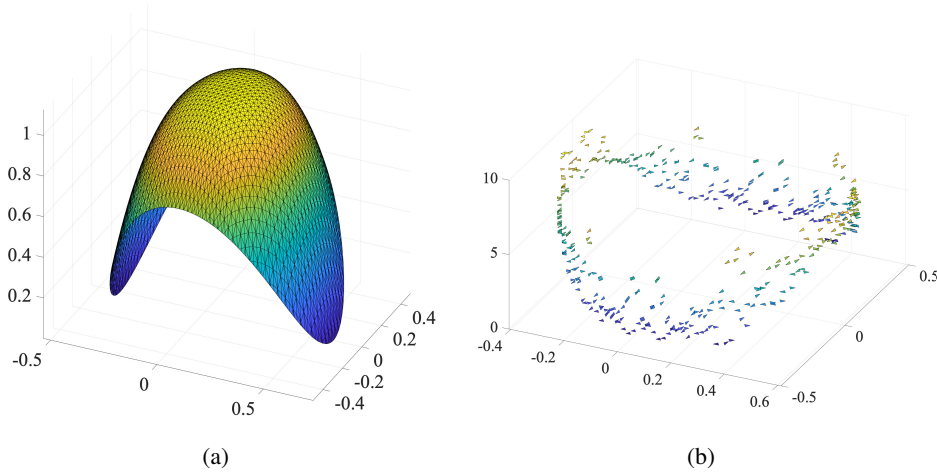(a)   (b)

Figure 7.3. The numerical solution of the field variable (a) and multiplier (b) with $\tau_0 = 10^{-4}$.
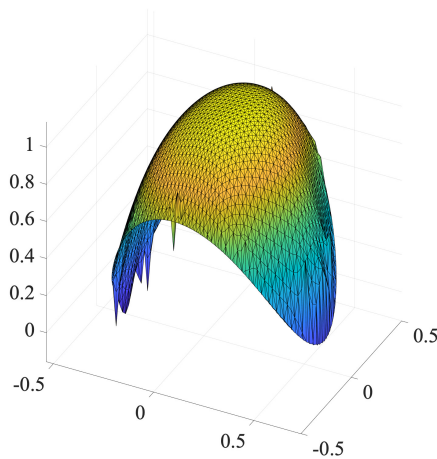

Figure 7.4. The numerical solution of the field variable with $\tau_0 = 0$.

7.7. Domains with corners

To get an optimally convergent method in the case where the domain has corners, the multiplier must be allowed to jump across the corner. The arguments of Section 7.5, where the boundary is meshed, carry over to this case without modification. Note that for the inf-sup stable case of Section 7.5, special care must be taken to satisfy the inf-sup condition also when corners are present. The stabilized methods do not have this concern.

In the case where the multiplier is defined on the bulk mesh, the situation is more delicate. Define $\mathcal{T}_{h,0,i} = \{T \in \widetilde{\mathcal{T}}_h \mid T \cap \Omega_{0,i} \neq \emptyset\}$ and $\Omega_{h,0,i} = \cup_{T \in \mathcal{T}_{h,0,i}} T$. The multiplier space must be defined as the union of the spaces

$$\Lambda_{h,i} = \{v_h|_{\Omega_{0,i}} \in H^1(\Omega_{0,i}) \mid v_h \in H^1(\Omega_{h,0,i}) \text{ and } v_h|_T \in \mathbb{P}_l(T) \text{ for all } T \in \mathcal{T}_{h,0,i}\}, \tag{7.130}$$

$0 \leq l \leq p-1$, $i = 1, \ldots, N$, i.e. $\Lambda_h = \cup_{i=1}^N \Lambda_{h,i}$. The previous argument can then only be used to obtain control of the multiplier in the interior of each $\Omega_{0,i}$. As in the bulk fictitious domain problem, full control of the multiplier over $\sum_{i=1}^N \|\cdot\|_{\Omega_{h,0,i}}^2$ is obtained by adding a ghost penalty term to the multiplier, extending the stability obtained by the inf-sup argument up to the boundary $\partial\Omega_{0,i}$ of $\Omega_{0,i}$. We will sketch this in the case of the continuous multiplier and for $p \geq 2$; for the case $p = 1$ and discontinuous multiplier with $l = 0$, we refer to Burman and Hansbo (2010a). It is enough to show stability on one of the $\Omega_{0,i}$. We assume that the stabilization $s_{h,0}$ consists of terms defined independently on each $\Omega_{0,i}$ that do not couple the different $\Lambda_{h,i}$. Let $\xi_i \in V_h$ be a piecewise affine function such that $\xi_i|_T = 0$ for $T \in \mathcal{T}_{h,0,i}$ with $T \cap \partial\Omega_{0,i} \neq \emptyset$ and set $\xi_i = 1$ in the remaining nodes in $\mathcal{T}_{h,0,i}$. ξ_i is extended to a function in V_h by setting ξ_i to zero in all remaining nodes in $\mathcal{T}_h \setminus \overline{\mathcal{T}}_{h,0,i}$. It follows that $v_\mu = \xi_i \mu_h^e \in V_h$, where $\mu_h \in \Lambda_{h,i}$ and μ_h^e denotes the canonical extension to Ω_h setting internal degrees of freedom to zero. We then have

$$\|h^{1/2}\mu_h \xi_i^{1/2}\|_{\Omega_{0,i}}^2 = (\mu_h, h\mu_h \xi_i)_{\Omega_{0,i}}. \tag{7.131}$$

Hence, using the same argument as in Section 7.6, we obtain for all $\mu_h \in \Lambda_h$,

$$\sum_{i=1}^N \|h^{1/2}\mu_h \xi_i^{1/2}\|_{\Omega_{0,i}} \lesssim \sup_{v \in V_h \setminus \{0\}} \frac{b(\mu_h, v)}{\|v\|_{H^1(\Omega)}} + s_{h,0}(\mu_h, \mu_h)^{1/2}. \tag{7.132}$$

We then recall from Section 4 that there exists a stabilization $s_{0,i}$ with the property that

$$\|h^{1/2}\mu_h\|_{\Omega_{h,0,i}} \lesssim \|h^{1/2}\mu_h \xi_i^{1/2}\|_{\Omega_{0,i}} + s_{0,i}(\mu_h, \mu_h)^{1/2}, \tag{7.133}$$

and we have the stability:

$$\|h^{1/2}\mu_h\|_{\Omega_0} \lesssim \sup_{v \in V_h \setminus \{0\}} \frac{b(\mu_h, v)}{\|v\|_{H^1(\Omega)}} + s_{h,0}(\mu_h, \mu_h)^{1/2} + s_{0,i}(\mu_h, \mu_h)^{1/2}. \tag{7.134}$$

Note that, as in the bulk case, the ghost penalty is used here to extend the stability of an $O(h)$ layer close to the boundary of the $\Omega_{0,i}$, where it would otherwise fail. To summarize, in the presence of corners the stabilizer acts to counter two different sources of instability. First it ensures the inf-sup condition (7.28), but only in the interior of each $\Omega_{0,i}$. Then another stabilizing form of ghost penalty type must be applied to ensure stability up to the boundary of $\Omega_{0,i}$. In particular, for low-order elements a stabilizing form can be designed that serves both purposes.

8. Further examples and hybridization

In this section we illustrate how the cut finite element Lagrange multiplier method can be applied to the model problems of Section 2. First we consider the two-domain problem with discontinuous diffusivity using a Neumann–Dirichlet coupling, then a bulk–surface problem. Finally we will show how the Lagrange multiplier approach can be used to create a method for multi-domain problems using Dirichlet–Neumann coupling when a cut finite element solver for the fictitious domain boundary value problem is available.

8.1. Example: elliptic problem with discontinuous coefficient

We consider the interface model problem discussed in Section 2.2. There are two coupling conditions, (2.19), $[u] = g_0$, and (2.20), $[n \cdot \alpha \nabla u] = f_0$, that have to be expressed in the form of a multiplier and a constraint equation. We have some liberty in doing this, depending on which one of the conditions (2.19) and (2.20) is built into boundary conditions imposed by the PDE in the bulk in each subdomain. If the condition (2.19) is imposed weakly we say that it is a Dirichlet coupling, and if (2.20) is imposed weakly we say that it is a Neumann coupling. This reflects the fact that the local problems to be solved in a domain decomposition approach are Dirichlet problems in the former case and Neumann problems in the latter.

Neumann coupling. The classical way is to introduce an equation imposing the condition (2.19) on the primal variable:

$$(u_1 - u_2, \mu)_{\Omega_0} = (g_0, \mu)_{\Omega_0}. \tag{8.1}$$

This leads to the Lagrange multiplier formulation (2.33)–(2.34) derived in Section 2.2. We recall it here for the readers' convenience: find $(u_1, u_2, \lambda) \in V_1 \times V_2 \times \Lambda$ such that

$$\sum_{i=1}^{2} (\alpha_i \nabla u_i, \nabla v_i)_{\Omega_i}, + (\lambda, v_1 - v_2)_{\Omega_0} = \sum_{i=1}^{2} (f_i, v_i)_{\Omega_i} + (f_0, \langle v \rangle_*)_{\Omega_0}, \tag{8.2}$$

$$(u_1 - u_2, \mu)_{\Omega_0} = (g_0, \mu)_{\Omega_0}, \tag{8.3}$$

for all $(v_1, v_2, \mu) \in V_1 \times V_2 \times \Lambda$, where V_1, V_2 were defined in (2.23) and $\Lambda = H^{-1/2}(\Omega_0)$.

We see that by (2.20) we can set

$$\lambda = -n_1 \cdot \alpha_1 \nabla u_1|_{\Omega_0} + \eta_2 f_0 = n_2 \cdot \alpha_2 \nabla u_2|_{\Omega_0} - \eta_1 f_0, \tag{8.4}$$

and with this notation

$$(-\alpha_i \Delta u_i, v_i)_{\Omega_i} = \underbrace{(\alpha_i \nabla u_i, \nabla v_i)_{\Omega_i}}_{a_i(u_i, v_i)} + \underbrace{((-1)^{i+1} \lambda, v_i)_{\Omega_0}}_{b_i(\lambda, v_i)} - (\eta_{(3-i)} f_0, v_i)_{\Omega_0}. \tag{8.5}$$

This defines the following local Neumann problem: find $u_i \in V_i$ such that

$$a_i(u_i, v_i) = -b_i(\lambda, v_i) + (f_i, v_i)_{\Omega_i} + (\eta_{3-i} f_0, v_i)_{\Omega_0} \quad \text{for all } v_i \in V_i. \tag{8.6}$$

To connect with the earlier derivation, observe that we also have

$$\lambda = \eta_1 \lambda + \eta_2 \lambda = -\eta_1 n_1 \cdot \alpha_1 \nabla u_1|_{\Omega_0} + \eta_2 n_2 \cdot \alpha_2 \nabla u_2|_{\Omega_0} = -\langle n \cdot \alpha \nabla u \rangle. \quad (8.7)$$

This immediately leads to a formulation of the form (2.33)–(2.34) by defining

$$a(u, v) = \sum_{i=1}^{2} (\alpha_i \nabla u_i, \nabla v_i)_{\Omega_i} \quad \text{and} \quad b(\mu, v) = (\mu, v_1 - v_2)_{\Omega_0}. \quad (8.8)$$

The right-hand side for each subdomain Ω_i is defined by

$$l_i(v_i) = (f_i, v_i)_{\Omega_i} + (\eta_{3-i} f_0, v_i)_{\Omega_0}. \quad (8.9)$$

This is the classical mortar coupling where the equation (2.19) is imposed through the added constraint equation and (2.20) is imposed weakly. Well-posedness in the spaces V_i, $i = 1, 2$ and Λ follows using the arguments of the previous section.

CutFEM formulation of the Neumann coupling. For the discretization of (8.2)–(8.3), we recall the space W_h defined by (2.39) for the approximation of u_i, $i = 1, 2$. For a multiplier space Λ_h and a stabilizing form satisfying the approximation assumption (7.31), the formulation is now given as follows: find $u_h = (u_{h,1}, u_{h,2}) \in W_h$ and $\lambda_h \in \Lambda_h$ such that

$$a(u_h, v) + b(\lambda_h, v) = l(v) \qquad \text{for all } v = (v_1, v_2) \in W_h, \quad (8.10)$$

$$b(\mu, u_h) - \tau_{s,0} s_{h,0}(\lambda_h, \mu) = (g_0, \mu)_{\Omega_0} \quad \text{for all } \mu \in \Lambda_h, \quad (8.11)$$

where the forms a, b and l are defined above. For the analysis we introduce the norms

$$\|v\|_V^2 = \sum_{i=1}^{2} \alpha_i \|v_i\|_{H^1(\Omega_i)}^2, \quad (8.12)$$

$$\|\mu\|_\Lambda^2 = \alpha_{\min}^{-1} \|\mu\|_{H^{-1/2}(\Omega_0)}^2, \quad \alpha_{\min} = \min(\alpha_1, \alpha_2). \quad (8.13)$$

The coercivity of a holds by choosing $\mu_v = \alpha_{\min} \int_{\Omega_0} [v_h] \, ds$ and proceeding as for the fictitious domain case. To see that the continuity (7.26) holds, we apply the Cauchy–Schwarz inequality to a, and for b we observe that

$$b(\mu, v) = (\mu, [v])_{\Omega_0}$$

$$\leq \alpha_{\min}^{-1/2} \|\mu\|_{H^{-1/2}(\Omega_0)} \alpha_{\min}^{1/2} \sum_{i=1}^{2} \|v_i\|_{H^1(\Omega_i)}$$

$$\lesssim \|\mu\|_\Lambda \|v\|_V. \quad (8.14)$$

If the multiplier space Λ_h and the stabilization $s_{h,0}$ are chosen so that the condition (7.28) is satisfied for the space $V_{h,i}$, such that $\alpha_i = \alpha_{\min}$ and the parameter

$\tau_{s,0} = \tau_0 \alpha_{\min}^{-1}$, then Theorem 7.3 holds. If robustness with respect to the contrast is not necessary, either side can be used to satisfy the inf-sup condition. If the spaces satisfy the inf-sup condition without stabilization, optimal preconditioners can be derived using the framework of Bertoluzza and Burman (2023). The design of efficient preconditioners for the stabilized system is an open problem.

8.2. Example: bulk–surface coupling

We now revisit a model for the interaction of concentrations in the bulk and on the surface, with a prescribed jump between the two similar to (2.55)–(2.57). This time, to simplify the problem setting, the surface PDE acts on the boundary as a non-local boundary condition. This is a model for proton transport in cell membranes introduced in Georgievskii, Medvedev and Stuchebrukhov (2002), with absorption in the bulk. Below we will apply a Neumann-type coupling for this problem. For simplicity, we let Ω be a smooth subset of $\mathbb{R}^3$ with boundary Ω_0 and outward-pointing normal n. The model we consider takes the form

$$-\nabla \cdot (\alpha_B \nabla u_B) + u_B = f_B \quad \text{in } \Omega, \tag{8.15}$$

$$-\nabla_0 \cdot (\alpha_S \nabla_0 u_S) + n \cdot \alpha_B \nabla u_B = f_S \quad \text{on } \Omega_0, \tag{8.16}$$

$$\varsigma n \cdot \alpha_B \nabla u_B + b_B u_B - b_S u_S = 0 \quad \text{on } \Omega_0. \tag{8.17}$$

Here ∇ is the $\mathbb{R}^3$ gradient and ∇_0 is the tangent gradient associated with Ω_0 defined by

$$\nabla_0 = P_0 \nabla, \tag{8.18}$$

with $P_0 = P_0(x)$ the projection of $\mathbb{R}^3$ onto the tangent plane of Ω_0 at $x \in \Omega_0$, defined by

$$P_0 = I - n \otimes n. \tag{8.19}$$

Further, b_B, b_S, α_B and α_S are positive constants, and $f_B : \Omega \to \mathbb{R}$ and $f_S : \Omega_0 \to \mathbb{R}$ are given square-integrable functions. To see how the problem can be cast in the abstract framework, we define the spaces $V_S = H^1(\Omega_0)$, $V_B = H^1(\Omega)$ and $\Lambda = H^{-1/2}(\Omega_0)$ (the dual of the space of traces on Ω_0 of functions in V_B). Then we multiply (8.15) by a test function $v_B \in V_B$ and (8.16) by a test function $v_S \in V_S$, to obtain

$$(-\nabla \cdot (\alpha_B \nabla u_B) + u_B, v_B)_\Omega$$
$$= (\alpha_B \nabla u_B, \nabla v_B)_\Omega + (u_B, v_B)_\Omega - (n \cdot (\alpha_B \nabla u_B), v_B)_{\Omega_0} \tag{8.20}$$

and, noting that the surface Ω_0 is closed,

$$(-\nabla_0 \cdot (\alpha_S \nabla_0 u_S), v_S)_\Omega + (n \cdot (\alpha_B \nabla u_B), v_S)_{\Omega_0}$$
$$= (\alpha_S \nabla_0 u_S, \nabla_0 v_S)_{\Omega_0} + (n \cdot (\alpha_B \nabla u_B), v_S)_{\Omega_0}. \tag{8.21}$$

It follows that the last term in the above equations couples the two systems, so we define $\lambda = -n \cdot (\alpha_B \nabla u_B)$. Then we introduce the weak forms $a_B \colon V_B \times V_B \to \mathbb{R}$ and $a_S \colon V_S \times V_S \to \mathbb{R}$,

$$a_B(u_B, v_B) = b_B((\alpha_B \nabla u_B, \nabla v_B)_\Omega + (u_B, v_B)_\Omega), \qquad (8.22)$$

$$a_S(u_S, v_S) = b_S(\alpha_S \nabla_0 u_S, \nabla_0 v_S)_{\Omega_0}, \qquad (8.23)$$

and the coupling form

$$b(v, \mu) = (\mu, b_B v_B - b_S v_S)_{\Omega_0}. \qquad (8.24)$$

We let $b(v_B, \mu) = (\mu, b_B v_B)_{\Omega_0}$ and $b(v_S, \mu) = -(\mu, b_S v_S)_{\Omega_0}$. The weak formulation may then be written as follows: find $\{u_B, u_S, \lambda\} \in V_B \times V_S \times \Lambda$ such that

$$a_B(u_B, v_B) + b(v_B, \lambda) = (b_B f_B, v_B)_\Omega \quad \text{for all } v_B \in V_B, \qquad (8.25)$$

$$a_S(u_S, v_S) + b(v_S, \lambda) = (b_S f_S, v_S)_{\Omega_0} \quad \text{for all } v_S \in V_S, \qquad (8.26)$$

$$-\varsigma(\lambda, \mu)_{\Omega_0} + b(u, \mu) = 0 \qquad \text{for all } \mu \in \Lambda. \qquad (8.27)$$

Consider the norms

$$\|v\|_V^2 = b_B \alpha_B \|v_B\|_\Omega^2 + b_S \alpha_S \|v_S\|_{\Omega_0}^2, \quad \|\mu\|_\Lambda^2 = (b_B \alpha_B)^{-1} \|\mu\|_{H^{-1/2}(\Omega_0)}^2. \qquad (8.28)$$

The Poincaré inequality for u_S can be shown using arguments similar to those in Section 3.8. This formulation is well-posed in the indicated spaces using the arguments of the previous section. By using equation (8.27) one may, however, eliminate the multiplier to arrive at a formulation similar to that of equation (2.62). The advantage of keeping the multiplier is that the formulation is robust for all $\varsigma \to 0$. In applications, typically ς may be very small.

CutFEM formulation of the bulk–surface coupling. A discretization for the bulk–surface problem is most easily achieved by choosing the spaces $V_{h,B}$ and Λ_h together with a possible stabilization $s_{h,0}$ so that an optimal unfitted fictitious domain method of the type discussed in Section 7 is obtained, using these spaces in a formulation similar to (7.17)–(7.18). For the approximation space of u_S and the form a_S, it is convenient to use a discretization of a surface PDE, with stabilization similar to that proposed in Sections 2.3 and 5. Together this leads to a formulation that will satisfy the error estimate of Theorem 7.3.

Observe that it is not possible to choose the multiplier space to be inf-sup stable with the space used for discretization of the PDE on the surface, (8.26). Such a choice will lead to inf-sup stability in the weaker $H^{-1}(\Omega_0)$-norm instead of $H^{-1/2}(\Omega_0)$ and suboptimal estimates.

8.3. Combining local Dirichlet solvers to solve multidomain problems

Assume now that we have at our disposal solvers for the fictitious domain problem, using either a Lagrange multiplier approach or Nitsche's method (see Sections 2.1 and 7.4), and we want to use these codes as building blocks in a multidomain solver.

Since a Dirichlet condition is imposed by the local solvers the coupling will instead become of Dirichlet–Neumann type. Then (2.20) is imposed through the added constraint and (2.19) is imposed weakly. This leads to the following bilinear form for the local solver if Lagrange multipliers are used:

$$A_i(u_i, \phi_i, v_i, \psi_i) = \underbrace{(\alpha_i \nabla u_i, \nabla v_i)_{\Omega_i}}_{a_i(u_i, v_i)} + (\phi_i, v_i)_{\Omega_0} - (\psi_i, u_i)_{\Omega_0}, \qquad (8.29)$$

where $u_i, v_i \in V_i = H^1(\Omega_i)$ and $\phi_i, \psi_i \in \Lambda_i = H^{-1/2}(\partial\Omega_i \cap \Omega_0)$. Since by (2.19) we may define $\lambda = u_1 - \eta_1 g_0 = u_2 + \eta_2 g_0 = \eta_2 u_1 + \eta_1 u_2 = \langle u \rangle_*$ on Ω_0, where λ is in the space $\Lambda = H^{1/2}(\Omega_0)$, consisting of traces of functions in V_i on Ω_0, with $i = 1$ or 2, we must have, for $i = 1, 2$,

$$A_i(u_i, \phi_i, v_i, \psi_i)$$
$$= (f_i, v_i)_\Omega - (\lambda, \psi_i)_{\Omega_0} + (\eta_i(-1)^i g_0, \psi_i)_{\Omega_0} \quad \text{for all } (v_i, \psi_i) \in V_i \times \Lambda_i. \quad (8.30)$$

Observe that this coincides with the formulation (7.5)–(7.6) for the imposition of the Dirichlet boundary data $\lambda - \eta_i(-1)^i g_0$. In this case, the spaces V_i and Λ_i must satisfy the inf-sup condition (7.11) separately on the two subdomains. To close the system we add the equation for the constraint (2.20). Since in this case $\phi_i = -n_i \cdot \alpha_i \nabla u_i$, the constraint equation can be written $(\phi_1 + \phi_2, \mu)_{\Omega_0} = -(f_0, \mu)_{\Omega_0}$, for all $\mu \in \Lambda$.

We see that the resulting method can be interpreted as a coupling scheme of the form (2.33)–(2.34) if $u = \{(u_i, \phi_i)\}_{i=1}^2$, $v = \{(v_i, \psi_i)\}_{i=1}^2$ and where the $a(u, v) = \sum_{i=1}^2 A_i(u_i, \phi_i, v_i, \psi_i)$, with A_i defined by (8.29) and $b(\lambda, \psi) = (\lambda, \psi_1 + \psi_2)_{\Omega_0}$. We write the scheme as follows: find $(u_i, \phi_i) \in (V_i \times \Lambda_i)$, $\lambda \in \Lambda$ such that for $i = 1, 2$

$$A_i(u_i, \phi_i, v_i, \psi_i) + (\lambda, \psi_i)_{\Omega_0} = l_i(v_i, \psi_i) \quad \text{for all } v_i, \psi_i \in V_i \times \Lambda_i, \qquad (8.31)$$

where $l_i(v_i, \psi_i) = (f_i, v_i)_\Omega + (g_0, \eta_i(-1)^i \psi_i)_{\Omega_0}$, and

$$(\phi_1 + \phi_2, \mu)_{\Omega_0} = -(f_0, \mu)_{\Omega_0} \quad \text{for all } \mu \in \Lambda. \qquad (8.32)$$

The spaces V_i, Λ_i must satisfy the inf-sup condition (7.11) for $i = 1, 2$. The space Λ must also satisfy an inf-sup condition with either Λ_1 or Λ_2.

This Dirichlet coupling is what is sometimes known as the three fields formulation (Brezzi and Marini 1994, Bertoluzza 2003, 2016). The analysis of the previous section cannot be immediately applied to this case, but the results still follow using similar arguments and we refer to the above works for details. The formulation (8.31)–(8.32) may appear significantly more complicated than (8.2)–(8.3), but the objectives of the two formulations are different. Assume that a method for the approximation of a boundary value problem with Dirichlet data is available. Then this solver serves as a building block for the local problem (8.31) of the coupled problem. In (8.2)–(8.3), local solvers use Neumann boundary conditions.

CutFEM formulation of the Dirichlet coupling. To discretize (8.31)–(8.32), we replace the spaces V_i, Λ_i, $i = 1, 2$ and Λ by their discrete unfitted counterparts $W_h, \Lambda_{h,i}$, $i = 1, 2$ and Λ_h as before. We arrive at the following formulation: find $(u_{h,i}, \phi_{h,i}) \in (V_{h,i} \times \Lambda_{h,i})$ and $\lambda_h \in \Lambda_h$ such that for $i = 1, 2$

$$A_{h,i}(u_{h,i}, \phi_{h,i}, v_i, \psi_i) + (\lambda_h, \psi_i)_{\Omega_0} = l_i(v_{h,i}, \psi_i), \qquad (8.33)$$

for all $v_i, \psi_i \in V_{h,i} \times \Lambda_{h,i}$, and where

$$A_{h,i}(u_{h,i}, \phi_{h,i}, v_i, \psi_i) = A_i(u_{h,i}, \phi_{h,i}, v_i, \psi_i) + \tau_{s,0,i} s_{h,0,i}(\phi_{h,i}, \psi_i) \qquad (8.34)$$

with A_i defined in (8.29), and

$$(\phi_{h,1} + \phi_{h,2}, \mu)_{\Omega_0} - \tau_{s,0} s_{h,0}(\lambda_h, \mu) = -(f_0, \mu)_{\Omega_0} \quad \text{for all } \mu \in \Lambda_h. \qquad (8.35)$$

Then, assuming that the pairs $V_{h,i}, \Lambda_{h,i}$ and the stabilizer $s_{h,0}$ are chosen to satisfy the inf-sup condition (7.28) for the local solvers, and that Λ_h together with one of the $\Lambda_{h,i}$ satisfies the inf-sup condition (7.28), we obtain a result similar to that of Theorem 7.3.

Clearly the above approach is attractive only if two unfitted solvers using multipliers are already available for the two local problems. Otherwise the accumulation of inf-sup conditions may be intimidating. To reduce the number of multipliers on the discrete level, one may proceed by formal elimination on the discrete level in the spirit of Stenberg (1995).

For the spaces Λ_i, instead of introducing additional variables we then use $\phi_i = -n_i \cdot \alpha_i \nabla u_i$ to substitute ϕ_i in the discrete approximation for some approximation of the flux $-n_i \cdot \alpha_i \nabla u_i$. Any stabilization associated with the ϕ_i is omitted. We propose two substitutions that result in different hybridized Nitsche methods.

- The simplest approach is to make the direct substitution $\phi_{h,i} = -n_i \cdot \alpha_i \nabla u_{h,i}$ and $\psi_i = -n_i \cdot \alpha_i \nabla v_i$, where $u_{h,i}$ and $v_{h,i}$ are functions in $V_{h,i}$. This leads to a hybridized version of the penalty-free skew-symmetric Nitsche method first analysed in Burman (2012) and in the unfitted framework in Boiveau, Burman, Claus and Larson (2018), which takes the following form: find $\{(u_{h,1}, u_{h,2}), \lambda_h\} \in W_h \times \Lambda_h$ such that

$$A_i(u_{h,i}, -n_i \cdot \alpha_i \nabla u_{h,i}, v_i, -n_i \cdot \alpha_i \nabla v_i) - (\lambda_h, n_i \cdot \alpha_i \nabla v_i)_{\Omega_0}$$
$$+ \tau_{s,i} s_{h,i}(u_{h,i}, v_i) = l_i(v_i, -n_i \cdot \alpha_i \nabla v_i) \quad \text{for } i = 1, 2, \qquad (8.36)$$

$$\sum_{i=1}^{2} (\mu, n_i \cdot \alpha_i \nabla u_{h,i})_{\Omega_0} + \tau_{s,0} s_{h,0}(\lambda_h, \mu) = (f_0, \mu)_{\Omega_0}, \qquad (8.37)$$

for all $\{(v_1, v_2), \mu\} \in W_h \times \Lambda_h$. Now only Λ_h and one of the sides need to satisfy the inf-sup condition using the flux functions $n_i \cdot \alpha_i \nabla v_{h,i}$. On unfitted

meshes the inf-sup stability only holds together with a ghost penalty (Boiveau *et al.* 2018). Then an unfitted method that is stable with optimal approximation estimates in the H^1-norm is obtained, as was shown in Boiveau, Burman and Claus (2017) and Boiveau *et al.* (2018). Writing out the terms in A_i, this formulation can be written as

$$\sum_{i=1}^{2} \big(a_i(u_{h,i}, v_i) - (n_i \cdot \alpha_i \nabla u_{h,i}, v_i - \mu)_{\Omega_0} + (n_i \cdot \alpha_i \nabla v_i, u_{h,i} - \lambda_h)_{\Omega_0}$$
$$+ \tau_{s,i} s_{h,i}(u_{h,i}, v_i) \big) + \tau_{s,0} s_{h,0}(\lambda_h, \mu)$$
$$= \sum_{i=1}^{2} l_i(v_i, -n_i \cdot \alpha_i \nabla v_i) + (f_0, \mu)_{\Omega_0}. \tag{8.38}$$

- Approximating $\phi_{h,i} \approx \hat{\phi}_{h,i}(u_{h,i}, \lambda_h) = -n_i \cdot \alpha_i \nabla u_{h,i} + \beta_0/2\alpha_i h^{-1}(u_{h,i} - \lambda_h)$ for some positive real dimensionless parameter $\beta_0 > 0$, and for $\hat{\psi}_i(v_i, \mu) = n_i \cdot \alpha_i \nabla v_i - \beta_0/2\alpha_i h^{-1}(v_i - \mu)$, leads to the hybridized Nitsche method originally introduced in Egger (2009) and applied as proposed here in the framework of CutFEM in Burman *et al.* (2019*a*). It takes the following form: find $\{(u_{h,1}, u_{h,2}), \lambda_h\} \in W_h \times \Lambda_h$ such that, for $i = 1, 2$,

$$A_i(u_{h,i}, \hat{\phi}_{h,i}, v_i, \hat{\psi}_i) + \tau_{s,i} s_{h,i}(u_{h,i}, v_i) + (\lambda_h, \hat{\psi}_i)_{\Omega_0} = l_i(v_i, \hat{\psi}_i), \tag{8.39}$$
$$(\mu, \hat{\phi}_{h,1} + \hat{\phi}_{h,2})_{\Omega_0} - \tau_{s,0} s_{h,0}(\lambda_h, \mu) = -(f_0, \mu)_{\Omega_0}, \tag{8.40}$$

for all $\{(v_1, v_2), \mu\} \in W_h \times \Lambda_h$. Writing out the terms in A_i, this formulation can be written as

$$\sum_{i=1}^{2} \big(a_i(u_{h,i}, v_i) - (n_i \cdot \alpha_i \nabla u_{h,i}, v_i - \mu)_{\Omega_0} - (n_i \cdot \alpha_i \nabla v_i, u_{h,i} - \lambda_h)_{\Omega_0}$$
$$+ (\beta_0/h\alpha_i(u_{h,i} - \lambda_h), v_i - \mu)_{\Omega_0} + \tau_{s,i} s_{h,i}(u_{h,i}, v_i) \big)$$
$$+ \tau_{s,0} s_{h,0}(\lambda_h, \mu) \big)$$
$$= \sum_{i=1}^{2} l_i(v_i, \hat{\psi}_i) + (f_0, \mu)_{\Omega_0}. \tag{8.41}$$

For results on stability and optimal error estimates we refer to Burman *et al.* (2019*b*). The conditioning of the Schur complement (i.e. when the bulk degrees of freedom have been eliminated) was shown to be optimal irrespective of the mesh interface intersection in the unfitted case too.

We have now derived both the Neumann and the Dirichlet coupling with Lagrange multipliers and two hybridized Nitsche methods. Finally, we can eliminate the hybridization variable in the hybridized Nitsche method. Using the definition of
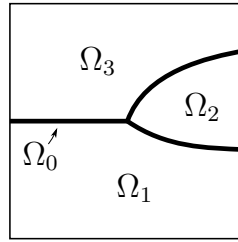
Figure 8.1. Illustration of the model problem geometry. The unit square $[0, 1]^2$ is divided into three subdomains, Ω_1, Ω_2 and Ω_3, according to the figure with material coefficients $\alpha_1 = 1$, $\alpha_2 = 2$ and $\alpha_3 = 3$.

the trace variable we can also eliminate λ_h. Recall the weighted average $\langle v \rangle_* = \eta_2 v_1 + \eta_1 v_2$. Now replace λ_h with $\langle u_h \rangle_*$ and the associated test function μ with $\langle v \rangle_*$ in (8.41), and take $\tau_{s,0} = 0$. Writing out the resulting method, we arrive at our original formulation of Nitsche's method (2.40).

Numerical example hybridization: three subdomains. To illustrate the performance of the hybridized methods, we will reproduce a numerical example from Burman *et al.* (2019b, Section 5.2). The method (8.41) is applied to an interface problem, with $f = 1$, $f_0 = g_0 = 0$, coupling three different subdomains. The unit square is partitioned into three subdomains Ω_i, $i = 1, 2, 3$ with a different constant material coefficient α_i in each subdomain; see Figure 8.1. In this problem we have three interface subdomains. We consider the following two unfitted mesh constructions (for details see Burman *et al.* 2019b, Section 5.1).

- *Global background grid.* Here active meshes associated with each subdomain are extracted from the same background grid; see Figure 8.2. We use $Q2$-elements on each mesh. Note that all subdomains have cut elements and that some skeleton subdomains are curved within elements. In this setting there are no locking effects due to non-matching approximation spaces when choosing the penalty parameter β large. A sample solution and the magnitude of its gradient are presented in Figure 8.3.

- *Single element interfaces.* Here the mesh and the space on each subdomain is constructed independently, some as quadrilateral meshes with $Q2$-elements and some as triangular meshes with $P2$-elements. On each skeleton subdomain we use a single $Q4$-element. Sample meshes in this set-up are visualized in Figure 8.4 and the corresponding numerical solution is presented in Figure 8.5.
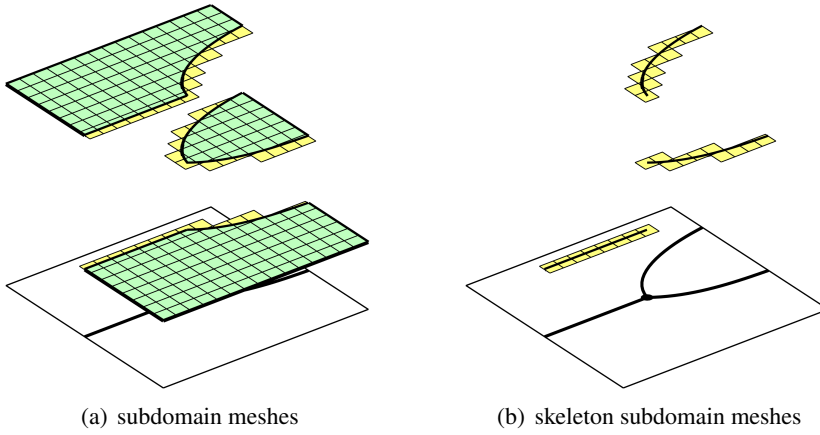
(a) subdomain meshes   (b) skeleton subdomain meshes

Figure 8.2. Meshes in the three subdomain example extracted from a global background grid. (a) Unfitted meshes with $Q2$-elements. (b) Skeleton subdomain meshes also with $Q2$-elements.
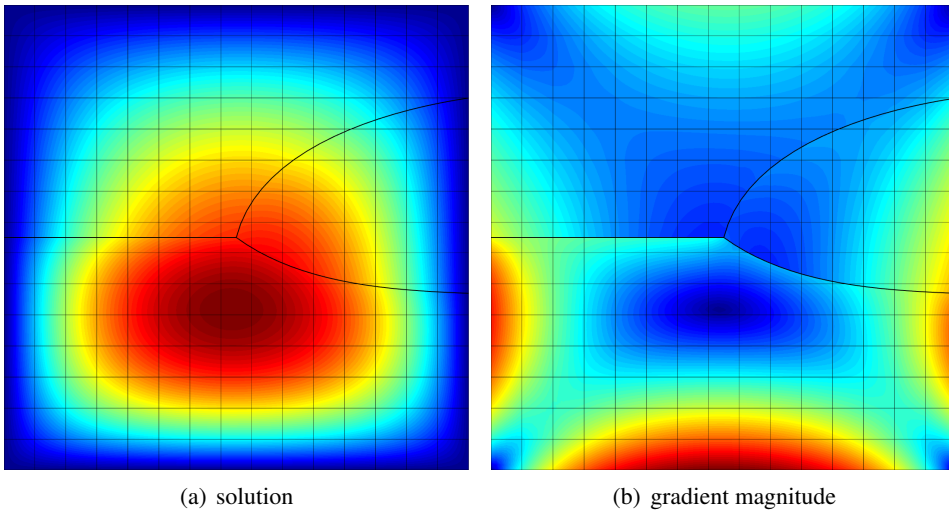

(a) solution   (b) gradient magnitude

Figure 8.3. Approximate solution (a) and the gradient magnitude (b) in the three subdomains using the construction illustrated in Figure 8.2.

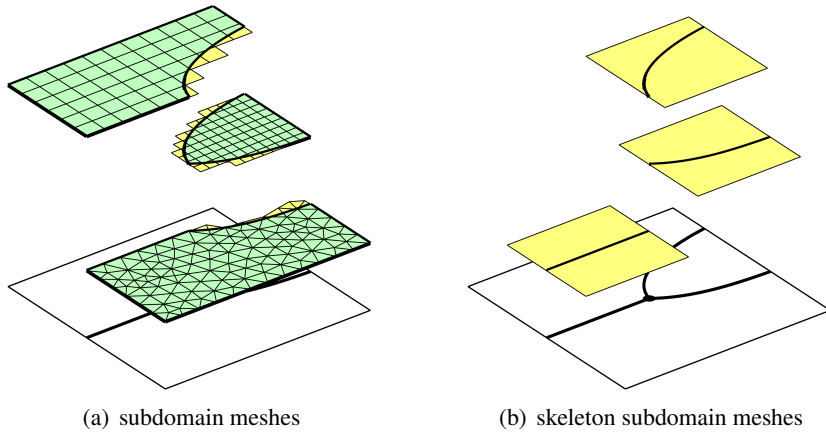(a) subdomain meshes   (b) skeleton subdomain meshes

Figure 8.4. Meshes are constructed independently for each subdomain in the three subdomain example: (a) $Q2$-elements on quadrilateral meshes for subdomain Ω_2 and Ω_3, and $P2$-elements on triangular meshes for the subdomain Ω_1. (b) Each skeleton subdomain is embedded in a single $Q4$-element.

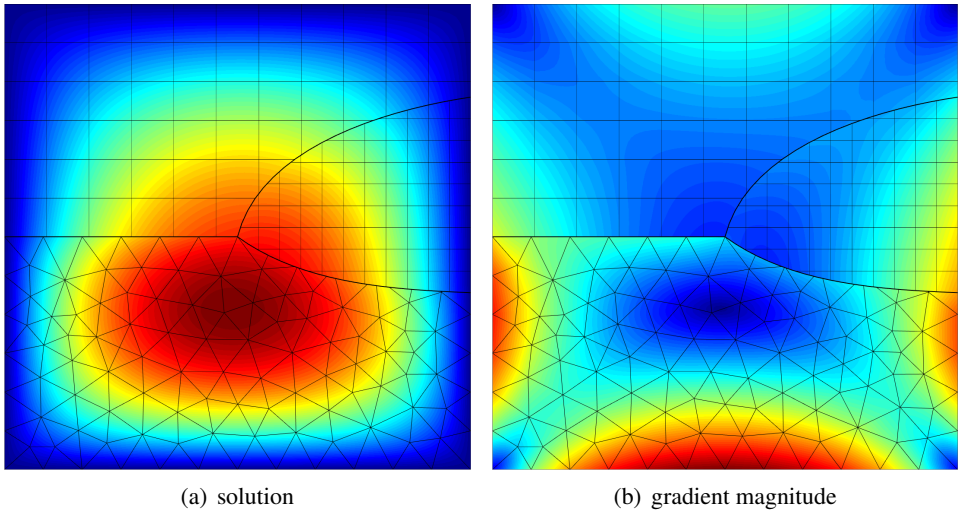(a) solution   (b) gradient magnitude

Figure 8.5. Approximate solution (a) and the gradient magnitude (b) in the three subdomains using the construction illustrated in Figure 8.4.

9. CutFEM in time-dependent domains

For time-dependent PDEs in evolving domains in $\mathbb{R}^d$, three main strategies have been proposed in connection with cut finite element discretizations.

The first strategy approximates the material derivative by following the characteristics, allowing information from previous time steps to be retrieved. This approach is combined with cut finite element discretizations in space by Hansbo *et al.* (2015*a*), where a convection–diffusion equation on a moving interface is considered. The method in Hansbo *et al.* (2015*a*) uses backward Euler, and the unfitted scheme is proved to be first-order accurate in the L^2-norm. More recently, this strategy has been extended to a fourth-order backward differentiation formula (BDF) and applied to convection–diffusion equations in a moving bulk domain in Ma, Zhang and Zheng (2022). In this extension, the moving boundary is explicitly represented using cubic spline interpolation, and integrals on cut elements are subdivided, with high-order Gauss–Legendre quadrature applied. The resulting scheme is fourth-order accurate in the energy norm, as demonstrated in Ma *et al.* (2022).

The second strategy involves approximating the time-dependent PDE in an unfitted space–time domain. The discontinuous Galerkin (DG) method is used in time, combined with an unfitted spatial discretization, allowing the space–time domain to be partitioned into space–time slabs. Approximations can then be computed one time slab at a time. Space–time unfitted finite element methods have been presented in Chessa and Belytschko (2004) and Lehrenfeld and Reusken (2013) for bulk problems and in Grande (2014), Olshanskii and Reusken (2014) and Olshanskii, Reusken and Xu (2014) for PDEs on evolving surfaces. For both bulk and surface problems, first-order accuracy is shown in the energy norm, and second-order convergence is demonstrated in a weaker norm than the L^2-norm.

Implementing these unfitted space–time methods requires integration over $\mathbb{R}^{d+1}$-dimensional space–time elements, which may have complex shapes due to the unfitted evolving boundary; see e.g. Lehrenfeld (2015) for an implementation in three space dimensions for a bulk problem. It is important to note that these methods use approximation spaces defined by restrictions of finite element spaces from a space–time unfitted mesh to the space–time domain where the PDE is defined. This differs slightly from cut finite element discretizations, where the approximation spaces are defined on the entire active mesh, not just where the PDE is defined.

To simplify the implementation of space–time methods and avoid integration over $\mathbb{R}^{d+1}$-dimensional space–time elements, a time-stepping strategy can be used. In the framework of CutFEM, Hansbo *et al.* (2016) and Zahedi (2017) demonstrate that space–time integrals can be approximated by first applying a quadrature rule in time, provided that appropriate stabilization terms are included in the weak formulation. These terms help to extend and control the solution across all the elements of a suitably defined active mesh. The method extends CutFEM, originally developed

for stationary domains, to time-dependent domains by approximating the solution over an active mesh that encompasses the time-dependent domain over a small time interval. Numerical studies have shown that this scheme is stable and robust with respect to the position of the boundary relative to the mesh. It has been successfully applied to multiphase flow problems in Frachon and Zahedi (2019, 2023). In Zahedi (2017), high-order discretizations for surface PDEs are presented, using an explicit representation of the interface via spline interpolation and the introduction of appropriate stabilization terms. For high-order discretization of bulk problems in a moving domain represented by a level set function, Heimann *et al.* (2023) propose a method based on isoparametric mapping for integration on cut elements. They also introduce adaptive quadrature rules for time integration that adjust to the evolution of the moving domain. In Frachon and Zahedi (2023), Reynolds' transport theorem is applied to achieve mass conservation for surface PDEs. Additionally, Myrbäck and Zahedi (2024) propose mass-conservative high-order discretizations for both bulk and surface PDEs, also leveraging Reynolds' transport theorem to derive a weak formulation that inherently ensures mass conservation. To ensure convergence and robustness, especially for high-order elements and independent of the cut configuration, this weak formulation must be efficiently stabilized (Myrbäck and Zahedi 2024). For integration on cut elements, represented by the level set method, Gaussian quadrature rules based on the algorithm of Saye (2015) are used. The third strategy also includes methods based on the method of lines, where time derivatives are replaced by finite difference schemes. Lehrenfeld and Olshanskii (2019) proposed an unfitted discretization, where the time derivative is discretized using BDF1, combined with a cut finite element method in space. This method utilizes an active mesh that covers the time-dependent domain from the previous time step. For BDF1, which is an implicit Euler discretization in time, optimal error estimates are derived for the solution in the H^1-norm in space, as detailed in Lehrenfeld and Olshanskii (2019). We show here that when BDF1 is used, the scheme is identical to the one presented in Hansbo *et al.* (2016) when the lowest-order elements in time (i.e. piecewise constant polynomials) and a first-order quadrature rule are used. See also Remark 3.2 in Frachon and Zahedi (2019). In Lou and Lehrenfeld (2022), the focus is on high-order BDF schemes and the use of isoparametric mapping for integration on cut elements.

To illustrate this third strategy based on time-stepping, we first consider a bulk problem, followed by a coupled bulk–surface problem.

9.1. A space–time method using time-stepping by quadrature

Let us first consider the following bulk problem: given $\Omega(t)$ with boundary $\Omega_0(t)$, evolving with velocity $\boldsymbol{\beta}_{\Omega_0}$ for $t \in [0, T]$, find $u : [0, T] \times \Omega(t) \to \mathbb{R}$ such that

$$\partial_t u + \nabla \cdot (\boldsymbol{\beta} u - \alpha \nabla u) = f \qquad \text{in } \Omega(t), \tag{9.1}$$

$$\boldsymbol{n} \cdot \alpha \nabla u = 0 \qquad \text{on } \Omega_0(t), \tag{9.2}$$

$$u(0, \boldsymbol{x}) = u_0(\boldsymbol{x}) \quad \text{in } \Omega(0). \tag{9.3}$$

Here, $\boldsymbol{\beta}$ is the fluid velocity, and we assume $\boldsymbol{\beta} \cdot \boldsymbol{n} = \boldsymbol{\beta}_{\Omega_0} \cdot \boldsymbol{n}$ on $\Omega_0(t)$, and that $\Omega_0(t)$ is a closed, smooth surface.

Recall Reynolds' transport theorem:

$$\frac{\mathrm{d}}{\mathrm{d}t} \int_{\Omega(t)} u \, \mathrm{d}\boldsymbol{x} = \int_{\Omega(t)} \partial_t u \, \mathrm{d}\boldsymbol{x} + \int_{\Omega_0(t)} \boldsymbol{n} \cdot \boldsymbol{\beta}_{\Omega_0} u \, \mathrm{d}s. \qquad (9.4)$$

Combining (9.4) with the given PDE (9.1), using the divergence theorem, and the condition $\boldsymbol{\beta} \cdot \boldsymbol{n} = \boldsymbol{\beta}_{\Omega_0} \cdot \boldsymbol{n}$ on $\Omega_0(t)$, applying the boundary condition (9.2), and finally integrating in time yields the mass conservation law:

$$\int_{\Omega(T)} u \, \mathrm{d}\boldsymbol{x} - \int_{\Omega(0)} u \, \mathrm{d}\boldsymbol{x} = \int_0^T \int_{\Omega(t)} f \, \mathrm{d}\boldsymbol{x} \, \mathrm{d}t. \qquad (9.5)$$

We now present the methods introduced in Hansbo *et al.* (2016) and Myrbäck and Zahedi (2024), followed by a discussion of the methods in Lehrenfeld and Olshanskii (2019) and Olshanskii and von Wahl (2024), which are based on finite difference approximations of the time derivative using BDF1, and how they are related.

Let $I_n = [t_{n-1}, t_n] \subset [0, T]$ be a time interval and let $V = H^1(\cup_{t \in I_n} \{t\} \times \Omega(t))$. By multiplying the PDE by $v \in V$, integrating in space and time, and applying integration by parts in space, we obtain the weak formulation:

$$\int_{I_n} (\partial_t u + \nabla \cdot (\boldsymbol{\beta} u), v)_{\Omega(t)} \, \mathrm{d}t + \int_{I_n} (\alpha \nabla u, \nabla v)_{\Omega(t)} \, \mathrm{d}t = \int_{I_n} (f, v)_{\Omega(t)} \, \mathrm{d}t. \qquad (9.6)$$

Next, applying Reynolds' transport theorem to the product uv and integrating over I_n, we obtain

$$(u, v)_{\Omega(t_n)} - (u, v)_{\Omega(t_{n-1})}$$
$$= \int_{I_n} (\partial_t u + \nabla \cdot (\boldsymbol{\beta} u), v)_{\Omega(t)} \, \mathrm{d}t + \int_{I_n} (u, \partial_t v + \boldsymbol{\beta} \cdot \nabla v)_{\Omega(t)} \, \mathrm{d}t. \qquad (9.7)$$

By combining (9.7) with the weak formulation (9.6), we arrive at

$$(u, v)_{\Omega(t_n)} - (u, v)_{\Omega(t_{n-1})}$$
$$- \int_{I_n} (u, \partial_t v + \boldsymbol{\beta} \cdot \nabla v)_{\Omega(t)} \, \mathrm{d}t + \int_{I_n} (\alpha \nabla u, \nabla v)_{\Omega(t)} \, \mathrm{d}t = \int_{I_n} (f, v)_{\Omega(t)} \, \mathrm{d}t. \qquad (9.8)$$

We now define two cut finite element discretizations, one based on the weak formulation (9.6), as presented in the works of Hansbo *et al.* (2016) and Zahedi (2017), and the other based on the weak formulation (9.8), as introduced in Myrbäck (2022) and Myrbäck and Zahedi (2024).

We will demonstrate that the advantage of the cut finite element discretization based on the weak formulation (9.8) is that it inherently ensures mass conservation. However, this approach requires efficient stabilization to maintain robustness and accuracy.

Mesh and finite element spaces. To define a cut finite element discretization, we need to specify the active mesh, the finite element space and the weak formulation. We use discontinuous elements in time, meaning that the approximate solution will be computed one time slab at a time, with each solution depending on the solution from the previous time slab. This approach avoids the need to solve a fully coupled problem over the entire time interval $[0, T]$.

Let $0 = t_0 < t_1 < \cdots < t_N = T$ be a partition of $I = [0, T]$ into time intervals $(t_{n-1}, t_n]$, each of length $\Delta t_n = t_n - t_{n-1}$ for $n = 1, \ldots, N$. Let $\widetilde{\Omega}$ be the computational domain, which is assumed to be easy to mesh and such that $\Omega(t) \subset \widetilde{\Omega}$ for all $t \in I$. Let $\widetilde{\mathcal{T}}_h$ denote the background mesh of $\widetilde{\Omega}$, which is unfitted with respect to the boundary $\Omega_0(t)$.

For simplicity, we assume that the background mesh $\widetilde{\mathcal{T}}_h$ is time-independent and generated independently of the position of $\Omega_0(t)$. However, depending on the specific application, a time-dependent background mesh may be required for efficiency. For instance, the mesh diameter h near $\Omega_0(t)$ may need to be smaller than that of elements farther away from the boundary.

For $t \in I$, the mesh associated with $\Omega(t)$ and $\Omega_0(t)$ is defined as

$$\mathcal{T}_h(t) = \{T \in \widetilde{\mathcal{T}}_h : T \cap \Omega(t) \neq \emptyset\}, \quad \mathcal{T}_{h,0}(t) = \{T \in \widetilde{\mathcal{T}}_h : T \cap \Omega_0(t) \neq \emptyset\}. \quad (9.9)$$

We define active meshes associated with each domain and each time interval $I_n = [t_{n-1}, t_n]$, as

$$\mathcal{T}_h^n = \bigcup_{t \in I_n} \{\mathcal{T}_h(t)\} = \{T \in \widetilde{\mathcal{T}}_h : T \cap \Omega(t) \neq \emptyset \text{ for some } t \in I_n\}, \quad (9.10)$$

$$\mathcal{T}_{h,0}^n = \bigcup_{t \in I_n} \{\mathcal{T}_{h,0}(t)\} = \{T \in \widetilde{\mathcal{T}}_h : T \cap \Omega_0(t) \neq \emptyset \text{ for some } t \in I_n\}. \quad (9.11)$$

Each active mesh constitutes an active domain:

$$\Omega_h^n = \bigcup_{T \in \mathcal{T}_h^n} T, \quad \Omega_{h,0}^n = \bigcup_{T \in \mathcal{T}_{h,0}^n} T. \quad (9.12)$$

For a visualization of the active meshes $\mathcal{T}_h^n$ and $\mathcal{T}_h^{n+1}$, along with the corresponding active domains associated with the time intervals I_n and I_{n+1}, refer to Figure 9.1. Note that $\Omega(t_n)$ is a subset of both the active domain Ω_h^n and the active domain Ω_h^{n+1}.

Let $V_{h,p_s}(\mathcal{T}_h^n)$ be the finite element space with basis functions of order p_s (in space), defined on the active mesh $\mathcal{T}_h^n$. For example, this could be the space spanned by Lagrange basis functions of order p_s. On a Cartesian mesh, one can use the tensor product space of Lagrange basis functions of order p_s in each spatial direction. Let $P_k(I_n)$ denote the space of polynomials of degree k in I_n. The space–time cut finite element space is then defined as

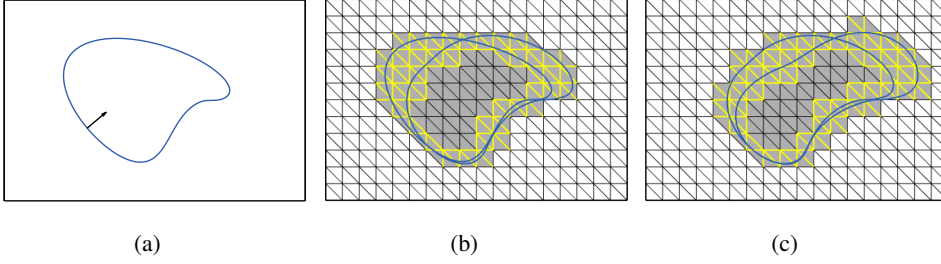$$W_h^n = P_{p_t}(I_n) \otimes V_{h,p_s}(\mathcal{T}_h^n). \quad (9.13)$$

Figure 9.1. (a) The initial configuration, i.e. $\Omega(0)$, embedded in the computational domain $\widetilde{\Omega}$. (b) The elements in the active mesh for the time interval I_n. The grey domain is Ω_h^n and the grey triangles belong to the set $\mathcal{T}_h^n$. Marked faces (in yellow) belong to elements in $\mathcal{T}_{h,0}^n$ that are involved in the stabilization process. The blue curves represent $\Omega_0(t_{n-1})$ and $\Omega_0(t_n)$. (c) Similar illustration for the time interval I_{n+1}, where the blue curves show the boundaries $\Omega_0(t_n)$ and $\Omega_0(t_{n+1})$. The grey domain is Ω_h^{n+1} and the grey triangles are the elements of the active mesh $\mathcal{T}_h^{n+1}$.

A function $v \in W_h^n$ has the form

$$v(t, \boldsymbol{x}) = \sum_{j=0}^{p_t} v_{h,j}(\boldsymbol{x}) \left(\frac{t - t_{n-1}}{\Delta t_n} \right)^j, \quad v_{h,j} \in V_{h,p_s}\left(\mathcal{T}_h^n\right), \ t \in I_n, \ \boldsymbol{x} \in \Omega_h^n. \quad (9.14)$$

Here,

$$v_{h,j}(\boldsymbol{x}) = \sum_{l=1}^{N_s} c_{l,j} \varphi_l(\boldsymbol{x}), \quad (9.15)$$

where $c_{l,j} \in \mathbb{R}$ and N_s is the number of degrees of freedom of $V_{h,p_s}\left(\mathcal{T}_h^n\right)$ for which $\{\varphi_l\}_{l=1}^{N_s}$ is a basis.

The weak formulation. For each $n = 1, \ldots, N$, given the solution from the previous time slab at $\Omega_h(t_{n-1})$, denoted by $u_h^-(t_{n-1}, \boldsymbol{x})$ (with $u_h^-(t_0, \boldsymbol{x}) = u_{h,0}(\boldsymbol{x})$ for $\boldsymbol{x} \in \Omega_h(0)$), and a quadrature rule with weights and nodes $\{(\omega_q, t_q^n)\}_{q=1}^{N_q}$, we seek $u_h \in W_h^n$ such that

$$A_h^n(u_h, v_h) + S_h^n(u_h, v_h) = L_h^n(v_h) \quad \text{for all } v_h \in W_h^n. \quad (9.16)$$

Following Hansbo *et al.* (2016) and Zahedi (2017), the weak formulation is derived from (9.6), and the solution u_h^- defined on the active mesh from the previous time slab is imposed onto the new active mesh $\mathcal{T}_h^n$ at $\Omega(t_{n-1})$. Stabilization is then used to extend the solution u_h to the entire active mesh Ω_h^n. Thus the weak formulation

is given by the forms

$$A_h^n(u, v) = (u, v)_{\Omega(t_{n-1})} + \sum_{q=1}^{N_q} \omega_q a\left(t_q^n, u, v\right), \qquad (9.17)$$

$$a(t, u, v) = (\partial_t u + \boldsymbol{\beta} \cdot \nabla u, v)_{\Omega(t)} + (\nabla \cdot \boldsymbol{\beta} u, v)_{\Omega(t)} + (\alpha \nabla u, \nabla v)_{\Omega(t)}, \qquad (9.18)$$

$$L^n(v) = (u_h^-, v)_{\Omega(t_{n-1})} + \sum_{q=1}^{N_q} \omega_q(f, v)_{\Omega(t_q^n)}, \qquad (9.19)$$

$$S_h^n(u, v) = \int_{I_n} \tau s_h^n(u, v) \, \mathrm{d}t = \sum_{q=1}^{N_q} \omega_q \tau s_h^n\left(u\left(t_q^n\right), v\left(t_q^n\right)\right). \qquad (9.20)$$

Here, $\tau > 0$ is a sufficiently large constant. The stabilization form can take the form of either the face-based or the element-based stabilization, defined in (4.5) and (4.15) respectively (with $m = 1$). In the case of full stabilization, all the faces in the mesh $\mathcal{T}_{h,0}^n$ that are shared by two elements in $\mathcal{T}_h^n$ belong to the set $\mathcal{F}_h$, as shown in Figure 9.1. Within a given time interval I_n, both the active mesh and the subset where stabilization is applied are time-independent. The quadrature rule is chosen to ensure that the integral in (9.20) can be computed exactly. For instance, when s_h is the element-based stabilization form, the quadrature rule must integrate polynomials of degree $2p_t$ exactly. In practice, higher-order quadrature rules are often chosen to ensure the accuracy of the other integrals in the weak formulation, which involve time-dependent domains. In the numerical examples we have used Lobatto quadrature.

Lowest-order elements in time. When using the lowest-order elements in time, i.e. $p_t = 0$, we have for $v \in W_h^n$ that

$$v(t, \boldsymbol{x}) = v_{h,0}(\boldsymbol{x}), \quad t \in I_n, \ \boldsymbol{x} \in \Omega_h^n, \ v_{h,0}(\boldsymbol{x}) \in V_{h,p_s}\left(\mathcal{T}_h^n\right), \qquad (9.21)$$

and thus $\partial_t v = 0$. We will show that using the one-point quadrature rule $(\omega_1, t_1^n) = (\Delta t, t_{n-1})$ in (9.16) yields the backward Euler discretization. For simplicity, let us take $f = 0$. The method from Hansbo *et al.* (2016) is then as follows: for each $n = 1, \ldots, N$, given the solution from the previous time slab $u_h^-(\boldsymbol{x})$ (with $u_h^-(\boldsymbol{x}) = u_{h,0}(\boldsymbol{x})$, for $n = 1$), find $u_h \in W_h^n$ such that

$$(u_h, v_h)_{\Omega(t_{n-1})} + \Delta t \, a(t_{n-1}, u_h, v_h) + \tau \Delta t s_h^n(u_h, v_h) = (u_h^-, v_h)_{\Omega(t_{n-1})}, \qquad (9.22)$$

for all $v_h \in V_{h,p_s}\left(\mathcal{T}_h^n\right)$, where

$$a(t, u, v) = (\boldsymbol{\beta} \cdot \nabla u, v)_{\Omega(t)} + (\alpha \nabla u, \nabla v)_{\Omega(t)} + (\nabla \cdot \boldsymbol{\beta} u, v)_{\Omega(t)}. \qquad (9.23)$$

Since discontinuous elements are used in time, the approximate solution is double-valued at each time instance $t = t_n$, with one solution from the left (from the time slab I_n) and one from the right (from I_{n+1}). Let $u_h^n(\boldsymbol{x})$ denote the solution

associated with the time slab I_{n+1}, and $u_h^{n-1}(\boldsymbol{x}) = u_h^-(\boldsymbol{x})$ (with $u_h^0(\boldsymbol{x}) = u_{h,0}(\boldsymbol{x})$ given). The solution u_h^n lies in W_h^{n+1} for $n = 1, \ldots, N$, and satisfies

$$\frac{\left(u_h^n, v_h\right)_{\Omega_h(t_n)} - \left(u_h^{n-1}, v_h\right)_{\Omega_h(t_n)}}{\Delta t} + a\left(t_n, u_h^n, v_h\right) + \tau s_h^{n+1}\left(u_h^n, v_h\right) = 0, \quad (9.24)$$

for all $v_h \in V_{h,p_s}\left(\mathcal{T}_h^{n+1}\right)$, which corresponds to the scheme proposed and analysed by Lehrenfeld and Olshanskii (2019) based on the BDF1 discretization in time.

Note that u_h^n is defined on the active mesh $\mathcal{T}_h^{n+1}$, which includes both $\Omega(t_n)$ and $\Omega(t_{n+1})$. Similarly u_h^{n-1} is well-defined on the entire active mesh $\mathcal{T}_h^n$ and hence on $\Omega(t_n)$. The active mesh, as defined in Lehrenfeld and Olshanskii (2019), is

$$\mathcal{T}_h^n = \{T \in \widetilde{\mathcal{T}}_h \colon \text{dist}(\boldsymbol{x}, \Omega(t_{n-1})) \leq \delta \text{ for some } \boldsymbol{x} \in T\}, \quad \Omega_h^n = \bigcup_{T \in \mathcal{T}_h^n} T, \quad (9.25)$$

where δ is proportional to Δt but chosen sufficiently large that $\Omega(t_n) \subset \Omega_h^n$. This definition of the active mesh should be compared with that in (9.10) (from Hansbo *et al.* 2016), as the two definitions differ. However, the key point in both cases is that $\Omega(t_n) \subset \Omega_h^n$, and the stabilization term controls the approximate solution over the entire active mesh.

Under the condition of a sufficiently small time step Δt, the following stability estimate (in the case $f = 0$) is derived by Lehrenfeld and Olshanskii (2019) (see Theorem 5.1):

$$\|u_h^N\|_{\Omega_h(t_N)}^2 + \Delta t \sum_{n=1}^N \left(\alpha/2\|\nabla u_h^n\|_{\Omega_h(t_n)}^2 + \tau s_h^{n+1}\left(u_h^n, u_h^n\right)\right) \leq \exp(c_T t_N)\|\|u_h^0\|\|_0^2,$$
$$(9.26)$$

where c_T is independent of h and Δt, and

$$\|\|u_h\|\|_0^2 = \|u_h\|_{\Omega_h(t_0)}^2 + \alpha/2\|\nabla u_h\|_{\Omega_h(t_0)}^2 + \tau s_h^1(u_h, u_h). \quad (9.27)$$

Here, $\Omega_h(t)$ is an approximation of $\Omega(t)$ such that $\text{dist}(\Omega(t_n), \Omega_h(t_n)) \lesssim h^{p_s+1}$. To derive this stability estimate, Lehrenfeld and Olshanskii (2019) rely on the stabilization form and also a strictly positive diffusion coefficient α (see Lehrenfeld and Olshanskii 2019, Lemma 5.4).

The conservative formulation. Following the weak form in (9.8), the bilinear form A_h^n in (9.16) can be defined as

$$A_h^n(u, v) = (u, v)_{\Omega(t_n)} + \sum_{q=1}^{N_q} \omega_q a_c\left(t_q^n, u, v\right), \quad (9.28)$$

$$a_c(t, u, v) = -(u, \partial_t v + \boldsymbol{\beta} \cdot \nabla v)_{\Omega(t_q^n)} + (\alpha \nabla u, \nabla v)_{\Omega(t_q^n)}. \quad (9.29)$$

The stabilization form is chosen such that $S_h^n(u, 1) = 0$. Thus, by taking $v_h = 1$ in the cut finite element discretization (9.16) with the bilinear form A_h^n as defined in

(9.28), we obtain

$$\int_{\Omega(t_n)} u_h \, \mathrm{d}\boldsymbol{x} - \int_{\Omega(t_{n-1})} u_h^- \, \mathrm{d}\boldsymbol{x} = \sum_{q=1}^{N_q} \omega_q \int_{\Omega(t_q^n)} f \, \mathrm{d}\boldsymbol{x}. \qquad (9.30)$$

Summing over all time intervals, we obtain the following discrete mass conservation:

$$\int_{\Omega(T)} u_h \, \mathrm{d}\boldsymbol{x} - \int_{\Omega(0)} u_0 \, \mathrm{d}\boldsymbol{x} = \sum_{n=1}^{N} \sum_{q=1}^{N_q} \omega_q \int_{\Omega(t_q^n)} f \, \mathrm{d}\boldsymbol{x}. \qquad (9.31)$$

Thus the cut finite element discretization based on the weak form in (9.8), which utilizes Reynolds' transport theorem, ensures mass conservation. In contrast, the discretization based on the weak form in (9.6) and the bilinear form A_h^n in (9.17) does not naturally conserve mass. However, the discrete mass conservation condition (9.30) can be imposed using a Lagrange multiplier, as done in Hansbo *et al.* (2016), Zahedi (2017).

Numerical simulations have shown that this conservative formulation is more sensitive to the position of the boundary relative to the computational mesh. As a result, stronger stabilization, smaller time steps or more quadrature points are often required, particularly when using higher-order elements beyond linear elements. To address this, the formulation is combined with macro-element stabilization. This approach enables efficient stabilization of both bulk and surface problems, applying more stabilization where needed without increasing the overall error. Macro-element stabilization was introduced in Larson and Zahedi (2023) and extended to time-dependent problems in Myrbäck and Zahedi (2024).

Next, we extend these discretizations to coupled bulk–surface problems.

9.2. Coupled bulk–surface problems

The same strategy can be used to solve coupled bulk–surface problems in evolving domains. Consider the following problem modelling the dynamics of soluble surfactants: find $u_B \colon I \times \Omega(t) \to \mathbb{R}^d$ and $u_S \colon I \times \Omega_0(t) \to \mathbb{R}^{d-1}$ such that

$$\partial_t u_B + \nabla \cdot (\boldsymbol{\beta} u_B) - \nabla \cdot (\alpha \nabla u_B) = f_B \qquad \text{in } I \times \Omega(t), \qquad (9.32)$$

$$\partial_t u_S + \boldsymbol{\beta} \cdot \nabla u_S + (\nabla_0 \cdot \boldsymbol{\beta}) u_S - \nabla_0 \cdot (\alpha_0 \nabla_0 u_S) = f_S + f_C \qquad \text{on } I \times \Omega_0(t), \qquad (9.33)$$

$$-\boldsymbol{n} \cdot (\alpha \nabla u_B) = f_C \qquad \text{on } I \times \Omega_0(t), \qquad (9.34)$$

$$u_B(0, \boldsymbol{x}) = u_{B,0}(\boldsymbol{x}) \qquad \text{in } \Omega(0), \qquad (9.35)$$

$$u_S(0, \boldsymbol{x}) = u_{S,0}(\boldsymbol{x}) \qquad \text{on } \Omega_0(0). \qquad (9.36)$$

Here, α and α_0 are the bulk and surface diffusion coefficients, respectively, and f_B and f_S are source terms. The operator ∇_0 denotes the tangential gradient. The coupling term f_C describes the exchange of surfactants between the bulk and the

surface. An example is the Langmuir isotherm,

$$f_C = b_B u_B - b_S u_S - b_{BS} u_B u_S, \tag{9.37}$$

where b_B, b_S and b_{BS} are physical constants related to the adsorption and desorption of the surfactant. The case of $b_{BS} = 0$ gives the linear Henry coupling model.

As before, we define active meshes corresponding to the evolution of each subdomain in a small time slab. On these active meshes, we define finite element spaces consisting of discontinuous elements in time and continuous elements in space. One may also use discontinuous elements in space. Recall the definitions of $\mathcal{T}_h^n$ and $\mathcal{T}_{h,0}^n$ from (9.10) and (9.11), respectively. Let $V_{h,p_s}(\mathcal{T}_h^n)$ be as before, i.e. the finite element space with basis functions of order p_s (in space), defined on the active mesh $\mathcal{T}_h^n$. Similarly, define $V_{h,p_s}(\mathcal{T}_{h,0}^n)$ as the finite element space with basis functions of order p_s (in space), defined on the active mesh $\mathcal{T}_{h,0}^n$. On a Cartesian mesh, we use the tensor product space of Lagrange basis functions of order p_s in each spatial direction.

Recall the space $P_p(I_n)$; we now define the space–time cut finite element space for the coupled problem as

$$W_h^n = \left(P_{p_t}(I_n) \otimes V_{h,p_s}(\mathcal{T}_h^n)\right) \times \left(P_{p_t}(I_n) \otimes V_{h,p_s}(\mathcal{T}_{h,0}^n)\right), \tag{9.38}$$

where $v \in W_h^n$ is of the form $v = (v_B, v_S)$.

The cut finite element method reads as follows: for each $n = 1, \dots, N$, given the solution from the previous time slab at $\Omega_h(t_{n-1})$ and $\Omega_{h,0}(t_{n-1})$, which is $u_h^- = (u_{h,B}^-, u_{h,S}^-)$ (with $u_h^- = (u_{B,0}, u_{S,0})$ for $n = 1$), and a quadrature rule with weights and nodes $\{(\omega_q, t_q^n)\}_{q=1}^{N_q}$, find $u_h \in W_h^n$ such that

$$A_h^n(u_h, v) + S_h^n(u_h, v) = L_h^n(v) \quad \text{for all } v_h \in W_h^n. \tag{9.39}$$

Here, as before, we have

$$L^n(v) = b_B(u_{B,h}^-, v_B)_{\Omega(t_{n-1})} + b_S(u_{S,h}^-, v_S)_{\Omega_0(t_{n-1})}$$
$$+ \sum_{q=1}^{N_q} \omega_q b_B(f_B, v_B)_{\Omega(t)} + \sum_{q=1}^{N_q} \omega_q b_S(f_S, v_S)_{\Omega_0(t)}, \tag{9.40}$$

$$S_h^n(w, v) = \sum_{q=1}^{N_q} \omega_q \left(b_B s_h^n\left(w_B(t_q^n), v_B(t_q^n)\right) + b_{BS} s_{h,0}^n\left(w_S(t_q^n), v_S(t_q^n)\right)\right), \tag{9.41}$$

and we can have a non-conservative formulation with the bilinear form A and a,

similar to equations (9.17) and (9.18), but including the surface terms

$$A_h^n(\mathbf{w}, \mathbf{v}) = b_B(w_B, v_B)_{\Omega(t_{n-1})} + b_S(w_S, v_S)_{\Omega_0(t_{n-1})} + \sum_{q=1}^{N_q} \omega_q a\big(t_q^n, \mathbf{u}, \mathbf{v}\big), \quad (9.42)$$

$$\begin{aligned}
a(t, \mathbf{w}, \mathbf{v}) = {} & b_B(\partial_t w_B + \boldsymbol{\beta} \cdot \nabla w_B, v_B)_{\Omega(t)} + b_S(\partial_t w_S + \boldsymbol{\beta} \cdot \nabla w_S, v_S)_{\Omega_0(t)} \\
& + b_B(\alpha \nabla w_B, \nabla v_B)_{\Omega(t)} + b_S(\alpha_0 \nabla_0 w_S, \nabla v_S)_{\Omega_0(t)} \\
& + (b_B w_B - b_S w_S - b_{BS} w_B w_S, b_B v_B - b_S v_S)_{\Omega_0(t)},
\end{aligned} \quad (9.43)$$

or a conservative formulation with A and a similar to equations (9.28) and (9.29):

$$A_h^n(\mathbf{w}, \mathbf{v}) = b_B(w_B, v_B)_{\Omega(t_n)} + b_S(w_S, v_S)_{\Omega_0(t_n)} + \sum_{q=1}^{N_q} \omega_q a\big(t_q^n, \mathbf{u}, \mathbf{v}\big), \quad (9.44)$$

$$\begin{aligned}
a(t, \mathbf{w}, \mathbf{v}) = {} & -b_B(w_B, \partial_t v_B + \boldsymbol{\beta} \cdot \nabla v_B)_{\Omega(t)} - b_S(w_S, \partial_t v_S + \boldsymbol{\beta} \cdot \nabla v_S)_{\Omega_0(t)} \\
& + b_B(\alpha \nabla w_B, \nabla v_B)_{\Omega(t)} + b_S(\alpha_0 \nabla_0 w_S, \nabla_0 v_S)_{\Omega_0(t)} \\
& + (b_B w_B - b_S w_S - b_{BS} w_B w_S, b_B v_B - b_S v_S)_{\Omega_0(t)}.
\end{aligned} \quad (9.45)$$

Thus we have two different methods for discretizing the problem: a non-conservative and a conservative cut finite element discretization. Stabilization is associated with each subdomain. Examples of stabilization forms s_h^n for the bulk are as before. For the numerical examples of this bulk–surface problem, we will use (4.15) (with $m = 1$ and $\tau > 0$ a sufficiently large constant). A macro-element stabilization with $\gamma = 0.7$ is used to classify elements as large (see Section 4). Examples of stabilization terms for the surface problem are given in Section 5. We choose the following stabilization term:

$$s_{h,0}^n(v(t), w(t)) = \sum_{F \in \mathcal{F}_h} \tau_{0,F} h^{-3}([v], [w])_{P(F)} + \sum_{j=1}^{p_s} \tau_0 h^{2(j-1)} \big(\nabla_n^j v, \nabla_n^j w\big)_{\Omega_0(t)}.$$

$$(9.46)$$

Here, $\tau_{0,F} > 0$ and $\tau_0 > 0$ are sufficiently large constants, and compared to the bulk stabilization, $\mathcal{F}_h$ now contains only the interior faces in $\mathcal{T}_{h,0}^n$ in the case of full stabilization.

Due to (9.37), we have a linear problem if $b_{BS} = 0$ and a non-linear problem if $b_{BS} \neq 0$, which can be solved using Newton's method, as described in Hansbo *et al.* (2016) for the non-conservative scheme and Myrbäck and Zahedi (2024) for the conservative scheme. Myrbäck and Zahedi (2024) have shown that in every Newton iteration, mass conservation holds for the linearized solution of the conservative scheme.

Next, we consider numerical examples to illustrate the conservation error and the convergence order of the two methods.

9.3. Numerical example

We consider two numerical examples in this section. The first example involves the bulk problem defined by equations (9.1)–(9.3), and the second example involves the coupled bulk–surface problem defined by equations (9.33)–(9.36). The code used to generate the numerical results in this section is available in Frachon and Myrbäck (2024).

Bulk problem. We consider an example of two colliding spheres from Olshanskii and von Wahl (2024). The two spheres have radius 0.5 and are centred at $(0, 0, t - 3/4)$ and $(0, 0, 3/4 - t)$, respectively. The velocity field is defined as

$$\boldsymbol{\beta} = \begin{cases} (0, 0, -1) & \text{if } (z > 0 \text{ and } t \leq 0.75) \text{ or } (z \leq 0 \text{ and } t > 0.75), \\ (0, 0, 1) & \text{if } (z \leq 0 \text{ and } t \leq 0.75) \text{ or } (z > 0 \text{ and } t > 0.75), \end{cases} \tag{9.47}$$

and the diffusion coefficient $\alpha = 0.1$. The initial solution is $u_0 = \text{sign}(z)$, and the source term $f = 0$ in equation (9.1).

We discretize equation (9.1)–(9.3) over time t in $I = [0, 1.5]$ using the method from equation (9.16) with $p_t = p_s = 1$ and Simpson's rule for quadrature. Recall that for $p_t = 0$ and using a one-point quadrature rule, the method is equivalent to backward Euler time-stepping. Therefore, in the lowest-order case, the non-conservative method from Hansbo *et al.* (2016), i.e. with A_h^n as in equation (9.17), is equivalent to the method proposed in Lehrenfeld and Olshanskii (2019), while the conservative method from Myrbäck (2022) and Myrbäck and Zahedi (2024), i.e. using A_h^n as in equation (9.28), is equivalent to the method proposed in Olshanskii and von Wahl (2024).

The computational domain is $\widetilde{\Omega} = [-0.6, 0.6] \times [-0.6, 0.6] \times [-1.35, 1.35]$, and we generate a uniform background mesh of tetrahedra with $h = 0.5625$. We choose $\Delta t = h/3$ and $\tau = 0.1$. The two spheres and the solution u_h at times $t = 0, 0.25, 0.75, 1.5$ are shown in Figure 9.2. The conservation error is measured as

$$e_c(t_n) = \left| \int_{\Omega(t_n)} u_h \, d\boldsymbol{x} - \int_{\Omega(0)} u_0 \, d\boldsymbol{x} \right|, \tag{9.48}$$

and shown for t_n, the endpoint of each time interval $I_n = [t_{n-1}, t_n]$, in Figure 9.3. The conservation error for the conservative method is of the order of machine epsilon, while the error for the non-conservative method increases rapidly as the two spheres approach and merge. In the non-conservative method, a Lagrange multiplier can be used to set $\int_{\Omega(t_n)} u_h$ at each time instance t_n, as in Hansbo *et al.* (2016), in order to prevent this mass loss.

Coupled bulk–surface problem. Consider the coupled bulk–surface problem given by equations (9.33)–(9.36), with the following parameters: the initial surface $\Omega_0(0)$
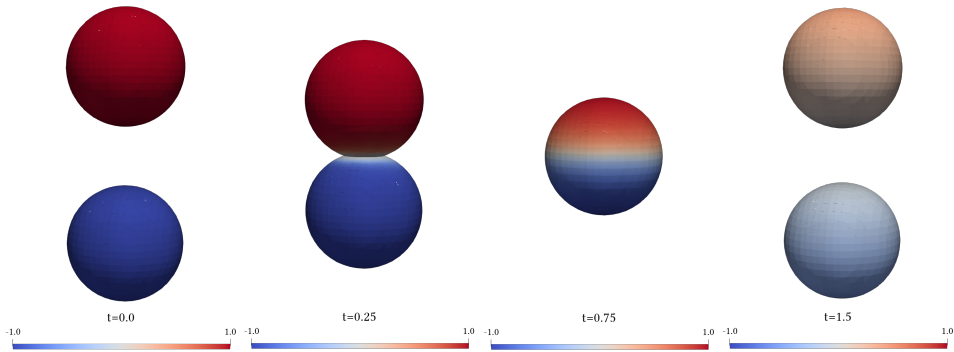
Figure 9.2. Bulk problem: two colliding spheres. The solution u_h using the conservative method (equation (9.16) with A_h^n as in (9.29)) with linear elements in time and space, i.e. $p_t = p_s = 1$, and Simpson's quadrature rule.
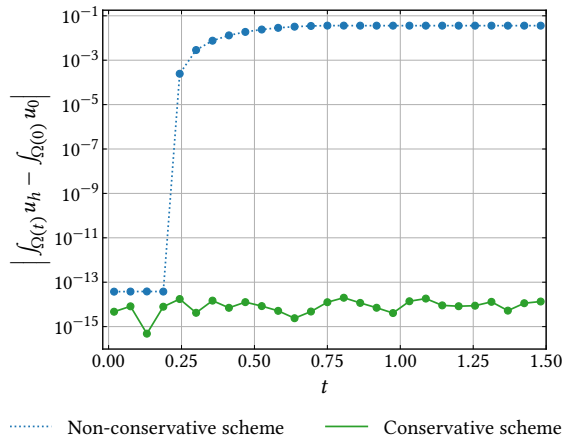

Figure 9.3. Bulk problem: two colliding spheres. The conservation error as a function of time.

is a circle centred at $(0, 0)$ with radius 1, the velocity field is $\boldsymbol{\beta} = (0, 1-x^2)$, $\alpha = 0.01$, $\alpha_0 = 1$, $b_B = b_S = b_{BS} = 1$. The domain $\Omega(t)$ is defined by

$$\Omega(t) = \{(x, y) \mid \phi(x, y) < 0\}, \quad \text{where } \phi(x, y) = x^2 + (y - (1 - x^2)t)^2 - 1. \quad (9.49)$$

We choose the source terms so that the exact solution in the bulk is

$$u_B = 0.5 + 0.4 \cos(\pi x) \cos(\pi y) \cos(2\pi t), \quad (9.50)$$

and u_S is chosen to satisfy the coupling condition (9.34). The problem is solved for $t \in [0, 1]$, with the computational domain $\widetilde{\Omega} = [-1.5, 1.5] \times [-3.5, 3.5]$, and we use a uniform Cartesian mesh. The time step is chosen as $\Delta t = h/3$, and a tolerance of 10^{-10} is used in Newton's method to solve the nonlinear problem.
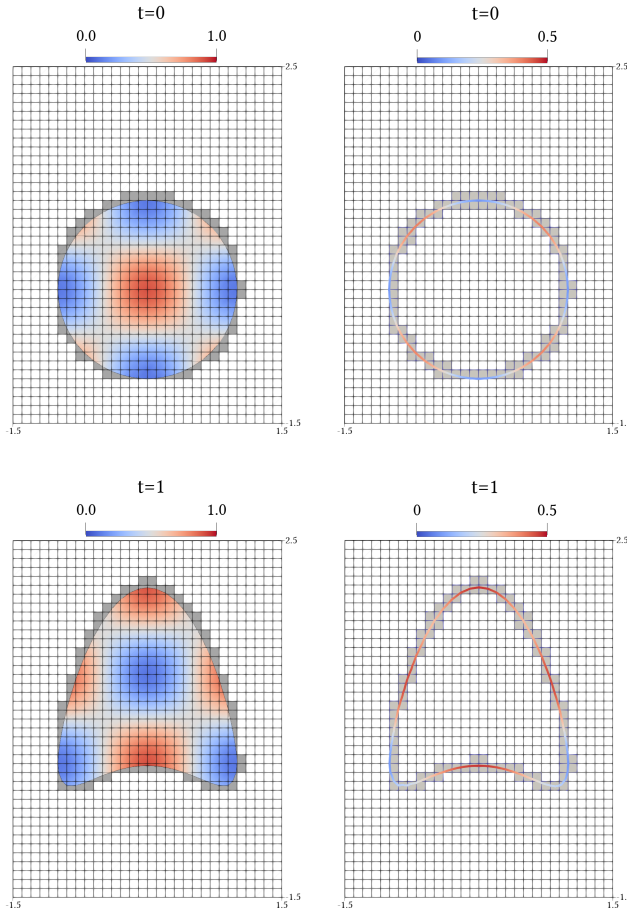
Figure 9.4. Coupled bulk–surface problem. The initial solution and the approximate solution $(u_{h,B}, u_{h,S})$ at the final time $t = 1$, using the space–time method defined in equation (9.39) with a as in (9.45), $p_t = p_s = 1$, and Simpson's quadrature rule.

For $p_t = p_s = 1$ we apply Simpson's quadrature rule and set $\tau = \tau_{0,F} = \tau_0 = 1$. The approximate solutions for the bulk and surface, as well as the background mesh and the active meshes, are shown at the initial and final times for the mesh size $h = 0.1$ in Figure 9.4.

In Figure 9.5 we show the convergence order of the non-conservative and conservative schemes. Both the bulk and surface solutions show optimal convergence order. For $p_t = p_s = 2$ we use a five-point Lobatto quadrature rule in time for the non-conservative scheme and a nine-point Lobatto quadrature for the conservative method. For the conservative scheme we also use higher stabilization constants $(\tau_{0,F} = 10)$. To prevent an increase in the L^2-error due to the large stabilization

(a) non-conservative scheme
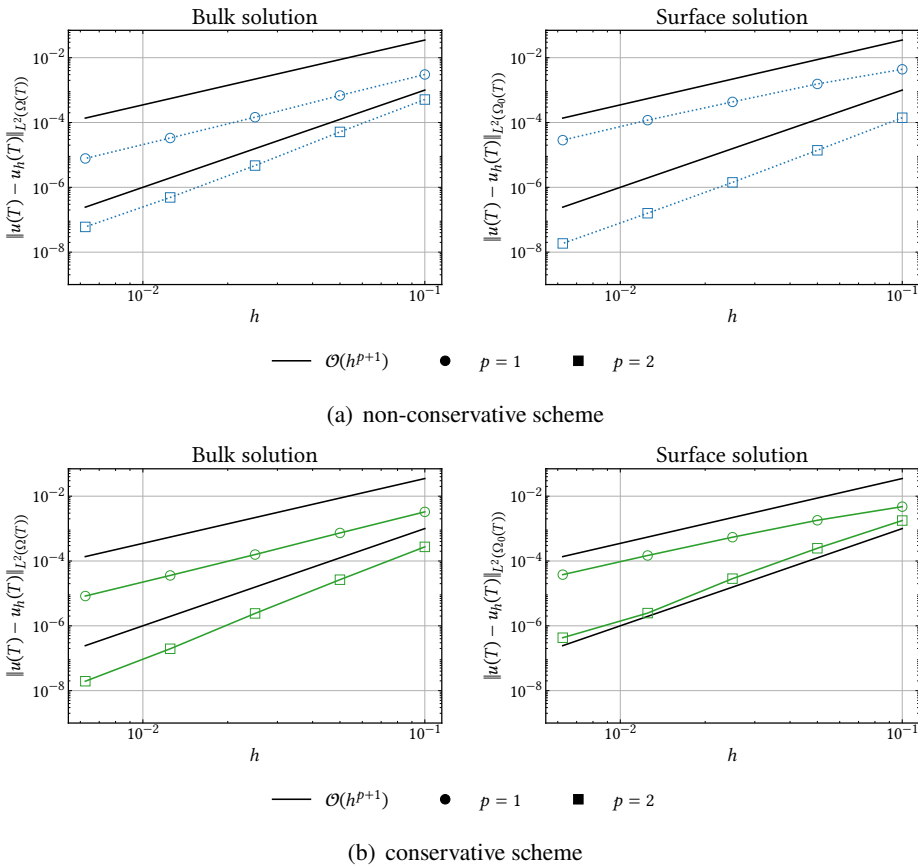

(b) conservative scheme

Figure 9.5. Coupled bulk–surface problem. The L^2-error at the final time $T = 1$ as a function of mesh size h, illustrating the convergence order of the bulk solution (left), where $u = u_B$, and the surface solution (right), where $u = u_S$. Results for (a) the non-conservative method, and (b) the conservative method. Circles represent results with $p = p_t = p_s = 1$, and squares represent results with $p = p_t = p_s = 2$.

parameter, we apply macro-element stabilization, ensuring that strong stabilization is only applied where necessary.

The conservation error is measured as

$$
e_c(t_n) = \left| \int_{\Omega(t_n)} u_{B,h} \, \mathrm{d}\boldsymbol{x} - \int_{\Omega(0)} u_{B,0} \, \mathrm{d}\boldsymbol{x} + \int_{\Omega_0(t_n)} u_{h,S} \, \mathrm{d}s - \int_{\Omega_0(0)} u_{S,0} \, \mathrm{d}s \right.
$$
$$
\left. - \sum_{n=1}^{N_t} \sum_{q=1}^{N_q} \omega_q \left(\int_{\Omega(t_q^n)} f_B \, \mathrm{d}\boldsymbol{x} - \int_{\Omega_0(t_q^n)} f_S \, \mathrm{d}s \right) \right|. \tag{9.51}
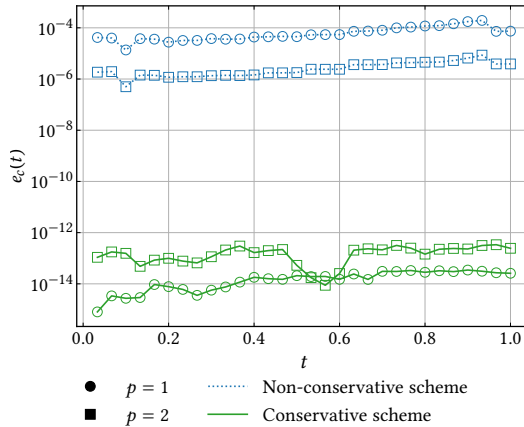$$

Figure 9.6. Coupled bulk–surface problem: the conservation error as a function of time. Circles represent results with $p = p_t = p_s = 1$, and squares represent results with $p = p_t = p_s = 2$.

Here N_t is such that $N_t \Delta t = t_n$, where t_n is the endpoint of each time interval $I_n = [t_{n-1}, t_n]$. The conservation error is shown in Figure 9.6. The conservation error for the conservative method is of the order of machine epsilon, while the error for the non-conservative method depends on the mesh size and the polynomial order used in the approximation space.

References

C. Ager, B. Schott, M. Winter and W. A. Wall (2019), A Nitsche-based cut finite element method for the coupling of incompressible fluid flow with poroelasticity, *Comput. Methods Appl. Mech. Engrg* **351**, 253–280.

J. Ahlkrona and D. Elfverson (2021), A cut finite element method for non-Newtonian free surface flows in 2D: Application to glacier modelling, *J. Comput. Phys. X* **11**, art. 100090.

C. Annavarapu, M. Hautefeuille and J. E. Dolbow (2012), A robust Nitsche's formulation for interface problems, *Comput. Methods Appl. Mech. Engrg* **225/228**, 44–54.

M. Anselmann and M. Bause (2022), Cut finite element methods and ghost stabilization techniques for space–time discretizations of the Navier–Stokes equations, *Int. J. Numer. Methods Fluids* **94**, 775–802.

E. Aulisa and J. Loftin (2023), Exact subdomain and embedded interface polynomial integration in finite elements with planar cuts, *Numer. Algorithms* **94**, 315–350.

I. Babuška (1972/73), The finite element method with Lagrangian multipliers, *Numer. Math.* **20**, 179–192.

I. Babuška (1973), The finite element method with penalty, *Math. Comp.* **27**, 221–228.

S. Badia, M. A. Caicedo, A. F. Martín and J. Principe (2021), A robust and scalable unfitted adaptive finite element framework for nonlinear solid mechanics, *Comput. Methods Appl. Mech. Engrg* **386**, art. 114093.

S. Badia, P. A. Martorell and F. Verdugo (2024), Space–time unfitted finite elements on moving explicit geometry representations, *Comput. Methods Appl. Mech. Engrg* **428**, art. 117091.

S. Badia, F. Verdugo and A. F. Martín (2018), The aggregated unfitted finite element method for elliptic problems, *Comput. Methods Appl. Mech. Engrg* **336**, 533–553.

H. J. C. Barbosa and T. J. R. Hughes (1991), The finite element method with Lagrange multipliers on the boundary: Circumventing the Babuška–Brezzi condition, *Comput. Methods Appl. Mech. Engrg* **85**, 109–128.

H. J. C. Barbosa and T. J. R. Hughes (1992), Circumventing the Babuška–Brezzi condition in mixed finite element approximations of elliptic variational inequalities, *Comput. Methods Appl. Mech. Engrg* **97**, 193–210.

N. Barrau, R. Becker, E. Dubach and R. Luce (2012), A robust variant of NXFEM for the interface problem, *C. R. Math. Acad. Sci. Paris* **350**, 789–792.

G. R. Barrenechea and F. Chouly (2012), A local projection stabilized method for fictitious domains, *Appl. Math. Lett.* **25**, 2071–2076.

J. W. Barrett and C. M. Elliott (1986), Finite element approximation of the Dirichlet problem using the boundary penalty method, *Numer. Math.* **49**, 343–366.

P. Bastian and C. Engwer (2009), An unfitted finite element method using discontinuous Galerkin, *Int. J. Numer. Methods Engrg* **79**, 1557–1576.

R. Becker, E. Burman and P. Hansbo (2009), A Nitsche extended finite element method for incompressible elasticity with discontinuous modulus of elasticity, *Comput. Methods Appl. Mech. Engrg* **198**, 3352–3360.

R. Becker, P. Hansbo and R. Stenberg (2003), A finite element method for domain decomposition with non-matching grids, *ESAIM Math. Model. Numer. Anal.* **37**, 209–225.

M. Berger (2017), Cut cells: Meshes and solvers, in *Handbook of Numerical Methods for Hyperbolic Problems*, Vol. 18 of Handbook of Numerical Analysis, Elsevier, pp. 1–22.

A. Bernland, E. Wadbro and M. Berggren (2018), Acoustic shape optimization using cut finite elements, *Int. J. Numer. Methods Engrg* **113**, 432–449.

N. Berre, M. E. Rognes and A. Massing (2024), Cut finite element discretizations of cell-by-cell EMI electrophysiology models, *SIAM J. Sci. Comput.* **46**, B527–B553.

S. Bertoluzza (2003), Analysis of a stabilized three-fields domain decomposition method, *Numer. Math.* **93**, 611–634.

S. Bertoluzza (2016), Analysis of a mesh-dependent stabilization for the three fields domain decomposition method, *Numer. Math.* **133**, 1–36.

S. Bertoluzza and E. Burman (2023), An abstract framework for heterogeneous coupling: stability, approximation and applications. Available at arXiv:2312.11733.

T. Boiveau and E. Burman (2015), A penalty-free Nitsche method for the weak imposition of boundary conditions in compressible and incompressible elasticity, *IMA J. Numer. Anal.* **36**, 770–795.

T. Boiveau, E. Burman and S. Claus (2017), Penalty-free Nitsche method for interface problems, in *Geometrically Unfitted Finite Element Methods and Applications*, Vol. 121 of Lecture Notes in Computational Science and Engineering, Springer, pp. 183–210.

T. Boiveau, E. Burman, S. Claus and M. Larson (2018), Fictitious domain method with boundary value correction using penalty-free Nitsche method, *J. Numer. Math.* **26**, 77–95.

S. P. A. Bordas, E. Burman, M. G. Larson and M. A. Olshanskii, eds (2017), *Geometrically Unfitted Finite Element Methods and Applications*, Vol. 121 of Lecture Notes in Computational Science and Engineering, Springer.

J. H. Bramble, T. Dupont and V. Thomée (1972), Projection methods for Dirichlet's problem in approximating polygonal domains with boundary-value corrections, *Math. Comp.* **26**, 869–879.

S. Brenner and R. Scott (2008), *The Mathematical Theory of Finite Element Methods*, Texts in Applied Mathematics, third edition, Springer.

E. Bretin, J. Chapelat, P.-Y. Outtier and Y. Renard (2022), Shape optimization of a linearly elastic rolling structure under unilateral contact using Nitsche's method and cut finite elements, *Comput. Mech.* **70**, 205–224.

F. Brezzi (1974), On the existence, uniqueness and approximation of saddle-point problems arising from Lagrangian multipliers, *Rev. Française Automat. Informat. Recherche Opérationnelle Sér. Rouge* **8**, 129–151.

F. Brezzi and M. Fortin (2001), A minimal stabilisation procedure for mixed finite element methods, *Numer. Math.* **89**, 457–491.

F. Brezzi and L. D. Marini (1994), A three-field domain decomposition method, in *Domain Decomposition Methods in Science and Engineering*, Vol. 157 of Contemporary Mathematics, American Mathematical Society, pp. 27–34.

A. Buffa, R. Puppi and R. Vázquez (2020), A minimal stabilization procedure for isogeometric methods on trimmed geometries, *SIAM J. Numer. Anal.* **58**, 2711–2735.

H. P. Bui, S. Tomar and S. P. A. Bordas (2019), Corotational cut finite element method for real-time surgical simulation: Application to needle insertion simulation, *Comput. Methods Appl. Mech. Engrg* **345**, 183–211.

E. Burman (2010), Ghost penalty, *C. R. Math. Acad. Sci. Paris* **348**, 1217–1220.

E. Burman (2012), A penalty-free nonsymmetric Nitsche-type method for the weak imposition of boundary conditions, *SIAM J. Numer. Anal.* **50**, 1959–1981.

E. Burman (2014), Projection stabilization of Lagrange multipliers for the imposition of constraints on interfaces and boundaries, *Numer. Methods Partial Differential Equations* **30**, 567–592.

E. Burman and A. Ern (2018), An unfitted hybrid high-order method for elliptic interface problems, *SIAM J. Numer. Anal.* **56**, 1525–1546.

E. Burman and M. A. Fernández (2014), An unfitted Nitsche method for incompressible fluid–structure interaction using overlapping meshes, *Comput. Methods Appl. Mech. Engrg* **279**, 497–514.

E. Burman and P. Hansbo (2010*a*), Fictitious domain finite element methods using cut elements, I: A stabilized Lagrange multiplier method, *Comput. Methods Appl. Mech. Engrg* **199**, 2680–2686.

E. Burman and P. Hansbo (2010*b*), Interior-penalty-stabilized Lagrange multiplier methods for the finite-element solution of elliptic interface problems, *IMA J. Numer. Anal.* **30**, 870–885.

E. Burman and P. Hansbo (2012), Fictitious domain finite element methods using cut elements, II: A stabilized Nitsche method, *Appl. Numer. Math.* **62**, 328–341.

E. Burman and P. Hansbo (2014), Fictitious domain methods using cut elements, III: A stabilized Nitsche method for Stokes' problem, *ESAIM Math. Model. Numer. Anal.* **48**, 859–874.

E. Burman and P. Hansbo (2017), Deriving robust unfitted finite element methods from augmented Lagrangian formulations, in *Geometrically Unfitted Finite Element Methods and Applications*, Vol. 121 of Lecture Notes in Computational Science and Engineering, Springer, pp. 1–24.

E. Burman and J. Preuss (2023), Unique continuation for an elliptic interface problem using unfitted isoparametric finite elements. Available at arXiv:2307.05210.

E. Burman and P. Zunino (2012), Numerical approximation of large contrast problems with the unfitted Nitsche method, in *Frontiers in Numerical Analysis*, Vol. 85 of Lecture Notes in Computational Science and Engineering, Springer, pp. 227–282.

E. Burman, M. Cicuttin, G. Delay and A. Ern (2021*a*), An unfitted hybrid high-order method with cell agglomeration for elliptic interface problems, *SIAM J. Sci. Comput.* **43**, A859–A882.

E. Burman, S. Claus and A. Massing (2015*a*), A stabilized cut finite element method for the three field Stokes problem, *SIAM J. Sci. Comput.* **37**, A1705–A1726.

E. Burman, S. Claus, P. Hansbo, M. G. Larson and A. Massing (2015*b*), CutFEM: Discretizing geometry and partial differential equations, *Int. J. Numer. Methods Engrg* **104**, 472–501.

E. Burman, G. Delay and A. Ern (2021*b*), An unfitted hybrid high-order method for the Stokes interface problem, *IMA J. Numer. Anal.* **41**, 2362–2387.

E. Burman, O. Duran and A. Ern (2022*a*), Unfitted hybrid high-order methods for the wave equation, *Comput. Methods Appl. Mech. Engrg* **389**, art. 114366.

E. Burman, D. Elfverson, P. Hansbo, M. G. Larson and K. Larsson (2017*a*), A cut finite element method for the Bernoulli free boundary value problem, *Comput. Methods Appl. Mech. Engrg* **317**, 598–618.

E. Burman, D. Elfverson, P. Hansbo, M. G. Larson and K. Larsson (2019*a*), Cut topology optimization for linear elasticity with coupling to parametric nondesign domain regions, *Comput. Methods Appl. Mech. Engrg* **350**, 462–479.

E. Burman, D. Elfverson, P. Hansbo, M. G. Larson and K. Larsson (2019*b*), Hybridized CutFEM for elliptic interface problems, *SIAM J. Sci. Comput.* **41**, A3354–A3380.

E. Burman, M. A. Fernández and F. M. Gerosa (2023*a*), Convergence analysis of an unfitted mesh semi-implicit coupling scheme for incompressible fluid–structure interaction, *Vietnam J. Math.* **51**, 37–69.

E. Burman, S. Frei and A. Massing (2022*b*), Eulerian time-stepping schemes for the nonstationary Stokes equations on time-dependent domains, *Numer. Math.* **150**, 423–478.

E. Burman, J. Guzmán, M. A. Sánchez and M. Sarkis (2018*a*), Robust flux error estimation of an unfitted Nitsche method for high-contrast interface problems, *IMA J. Numer. Anal.* **38**, 646–668.

E. Burman, P. Hansbo and M. Larson (2024*a*), Cut finite element method for divergence-free approximation of incompressible flow: A Lagrange multiplier approach, *SIAM J. Numer. Anal.* **62**, 893–918.

E. Burman, P. Hansbo and M. G. Larson (2015*c*), A stabilized cut finite element method for partial differential equations on surfaces: The Laplace–Beltrami operator, *Comput. Methods Appl. Mech. Engrg* **285**, 188–207.

E. Burman, P. Hansbo and M. G. Larson (2018*b*), A cut finite element method with boundary value correction, *Math. Comp.* **87**, 633–657.

E. Burman, P. Hansbo and M. G. Larson (2020*a*), Cut Bogner–Fox–Schmit elements for plates, *Adv. Model. Simul. Eng. Sci.* **7**, art. 27.

E. Burman, P. Hansbo and M. G. Larson (2020*b*), A cut finite element method for a model of pressure in fractured media, *Numer. Math.* **146**, 783–818.

E. Burman, P. Hansbo and M. G. Larson (2022*c*), CutFEM based on extended finite element spaces, *Numer. Math.* **152**, 331–369.

E. Burman, P. Hansbo and M. G. Larson (2022*d*), Explicit time stepping for the wave equation using CutFEM with discrete extension, *SIAM J. Sci. Comput.* **44**, A1254–A1289.

E. Burman, P. Hansbo and M. G. Larson (2022*e*), On the design of locking free ghost penalty stabilization and the relation to CutFEM with discrete extension. Available at arXiv:2205.01340.

E. Burman, P. Hansbo and M. G. Larson (2024*b*), Low regularity estimates for CutFEM approximations of an elliptic problem with mixed boundary conditions, *Math. Comp.* **93**, 35–54.

E. Burman, P. Hansbo, M. G. Larson and K. Larsson (2023*b*), Extension operators for trimmed spline spaces, *Comput. Methods Appl. Mech. Engrg* **403**, art. 115707.

E. Burman, P. Hansbo, M. G. Larson and A. Massing (2017*b*), A cut discontinuous Galerkin method for the Laplace–Beltrami operator, *IMA J. Numer. Anal.* **37**, 138–169.

E. Burman, P. Hansbo, M. G. Larson and A. Massing (2018*c*), Cut finite element methods for partial differential equations on embedded manifolds of arbitrary codimensions, *ESAIM Math. Model. Numer. Anal.* **52**, 2247–2282.

E. Burman, P. Hansbo, M. G. Larson and D. Samvin (2019*c*), A cut finite element method for elliptic bulk problems with embedded surfaces, *GEM Int. J. Geomath.* **10**, art. 10.

E. Burman, P. Hansbo, M. G. Larson and S. Zahedi (2016*a*), Cut finite element methods for coupled bulk–surface problems, *Numer. Math.* **133**, 203–231.

E. Burman, P. Hansbo, M. G. Larson, A. Massing and S. Zahedi (2016*b*), Full gradient stabilized cut finite element methods for surface partial differential equations, *Comput. Methods Appl. Mech. Engrg* **310**, 278–296.

E. Burman, C. He and M. G. Larson (2021*c*), Comparison of shape derivatives using CutFEM for ill-posed Bernoulli free boundary problem, *J. Sci. Comput.* **88**, art. 35.

E. Burman, C. He and M. G. Larson (2022*f*), *A posteriori* error estimates with boundary correction for a cut finite element method, *IMA J. Numer. Anal.* **42**, 333–362.

E. Cáceres, J. Guzmán and M. Olshanskii (2020), New stability estimates for an unfitted finite element method for two-phase Stokes problem, *SIAM J. Numer. Anal.* **58**, 2165–2192.

Y. Cai, J. Chen and N. Wang (2021), A Nitsche extended finite element method for the biharmonic interface problem, *Comput. Methods Appl. Mech. Engrg* **382**, art. 113880.

A. Cangiani, Z. Dong and E. H. Georgoulis (2021), *hp*-version discontinuous Galerkin methods on essentially arbitrarily-shaped elements, *Math. Comp.* **91**, 1–35.

D. Capatina and C. He (2021), Flux recovery for cut finite element method and its application in *a posteriori* error estimation, *ESAIM Math. Model. Numer. Anal.* **55**, 2759–2784.

M. Cenanovic, P. Hansbo and M. G. Larson (2016), Cut finite element modeling of linear membranes, *Comput. Methods Appl. Mech. Engrg* **310**, 98–111.

Z. Chen and Y. Liu (2023), An arbitrarily high order unfitted finite element method for elliptic interface problems with automatic mesh generation, *J. Comput. Phys.* **491**, art. 112384.

Z. Chen and Y. Liu (2024), An arbitrarily high order unfitted finite element method for elliptic interface problems with automatic mesh generation, Part II: Piecewise-smooth interfaces, *Appl. Numer. Math.* **206**, 247–268.

Z. Chen, K. Li and X. Xiang (2021), An adaptive high-order unfitted finite element method for elliptic interface problems, *Numer. Math.* **149**, 507–548.

Z. Chen, K. Li, M. Lyu and X. Xiang (2024), A high order unfitted finite element method for time-harmonic Maxwell interface problems, *Int. J. Numer. Anal. Model.* **21**, 822–849.

A. Y. Chernyshenko and M. A. Olshanskii (2020), An unfitted finite element method for the Darcy problem in a fracture network, *J. Comput. Appl. Math.* **366**, art. 112424.

J. Chessa and T. Belytschko (2004), Arbitrary discontinuities in space–time finite elements by level sets and X-FEM, *Int. J. Numer. Methods Engrg* **61**, 2595–2614.

S. Claus and P. Kerfriden (2018), A stable and optimally convergent LaTIn-CutFEM algorithm for multiple unilateral contact problems, *Int. J. Numer. Methods Engrg* **113**, 938–966.

S. Claus and P. Kerfriden (2019), A CutFEM method for two-phase flow problems, *Comput. Methods Appl. Mech. Engrg* **348**, 185–206.

S. Claus, S. Bigot and P. Kerfriden (2018), CutFEM method for Stefan–Signorini problems with application in pulsed laser ablation, *SIAM J. Sci. Comput.* **40**, B1444–B1469.

S. Claus, P. Kerfriden, F. Moshfeghifar, S. Darkner, K. Erleben and C. Wong (2021), Contact modeling from images using cut finite element solvers, *Adv. Model. Simul. Eng. Sci.* **8**, art. 13.

B. Cockburn and M. Solano (2012), Solving Dirichlet boundary-value problems on curved domains by extensions from subdomains, *SIAM J. Sci. Comput.* **34**, A497–A519.

D. C. Corti, G. Delay, M. A. Fernández, F. Vergnet and M. Vidrascu (2024), Low-order fictitious domain method with enhanced mass conservation for an interface Stokes problem, *ESAIM Math. Model. Numer. Anal.* **58**, 303–333.

S. Court (2019), A fictitious domain approach for a mixed finite element method solving the two-phase Stokes problem with surface tension forces, *J. Comput. Appl. Math.* **359**, 30–54.

F. de Prenter, C. Lehrenfeld and A. Massing (2018), A note on the stability parameter in Nitsche's method for unfitted boundary value problems, *Comput. Math. Appl.* **75**, 4322–4336.

S. B. Dilgen, J. S. Jensen and N. Aage (2021), Shape optimization of the time-harmonic response of vibroacoustic devices using cut elements, *Finite Elem. Anal. Des.* **196**, art. 103608.

M. Dryja (2003), On discontinuous Galerkin methods for elliptic problems with discontinuous coefficients, *Comput. Methods Appl. Math.* **3**, 76–85.

K. Dunn, R. Lui and M. Sarkis (2021), An unconditionally stable semi-implicit CutFEM for an interaction problem between an elastic membrane and an incompressible fluid, *Electron. Trans. Numer. Anal.* **54**, 296–322.

M. Duprez, V. Lleras and A. Lozinski (2023), A new ϕ-FEM approach for problems with natural boundary conditions, *Numer. Methods Partial Differential Equations* **39**, 281–303.

H. Egger (2009), A class of hybrid mortar finite element methods for interface problems with non-matching meshes. Preprint: AICES-2009-2.

C. Engwer, S. May, A. Nüßing and F. Streitbürger (2020), A stabilized DG cut cell method for discretizing the linear transport equation, *SIAM J. Sci. Comput.* **42**, A3677–A3703.

A. Ern and J.-L. Guermond (2006), Evaluation of the condition number in linear systems arising in finite element approximations, *ESAIM Math. Model. Numer. Anal.* **40**, 29–48.

M. Fabre, J. Pousin and Y. Renard (2016), A fictitious domain method for frictionless contact problems in elasticity using Nitsche's method, *SMAI J. Comput. Math.* **2**, 19–50.

S. Farina, S. Claus, J. S. Hale, A. Skupin and S. P. A. Bordas (2021), A cut finite element method for spatially resolved energy metabolism models in complex neuro-cell morphologies with minimal remeshing, *Adv. Model. Simul. Eng. Sci.* **8**, art. 5.

M. A. Fernández and M. Landajuela (2020), Splitting schemes and unfitted-mesh methods for the coupling of an incompressible fluid with a thin-walled structure, *IMA J. Numer. Anal.* **40**, 1407–1453.

M. A. Fernández and F. M. Gerosa (2021), An unfitted mesh semi-implicit coupling scheme for fluid–structure interaction with immersed solids, *Int. J. Numer. Methods Engrg* **122**, 5384–5408.

M. Fournié and A. Lozinski (2017), Stability and optimal convergence of unfitted extended finite element methods with Lagrange multipliers for the Stokes equations, in *Geometrically Unfitted Finite Element Methods and Applications*, Vol. 121 of Lecture Notes in Computational Science and Engineering, Springer, pp. 143–182.

T. Frachon and S. Myrbäck (2024), CutFEM-Library, *GitHub repository*. Available at https://github.com/CutFEM/CutFEM-Library.

T. Frachon and S. Zahedi (2019), A cut finite element method for incompressible two-phase Navier–Stokes flows, *J. Comput. Phys.* **384**, 77–98.

T. Frachon and S. Zahedi (2023), A cut finite element method for two-phase flows with insoluble surfactants, *J. Comput. Phys.* **473**, art. 111734.

T. Frachon, P. Hansbo, E. Nilsson and S. Zahedi (2024*a*), A divergence preserving cut finite element method for Darcy flow, *SIAM J. Sci. Comput.* **46**, A1793–A1820.

T. Frachon, E. Nilsson and S. Zahedi (2024*b*), Divergence-free cut finite element methods for Stokes flow, *BIT Numer. Math.* **64**, art. 39.

T.-P. Fries and T. Belytschko (2010), The extended/generalized finite element method: An overview of the method and its applications, *Int. J. Numer. Methods Engrg* **84**, 253–304.

T.-P. Fries and M. W. Kaiser (2023), On the simultaneous solution of structural membranes on all level sets within a bulk domain, *Comput. Methods Appl. Mech. Engrg* **415**, art. 116223.

P. Fu and G. Kreiss (2021), High order cut discontinuous Galerkin methods for hyperbolic conservation laws in one space dimension, *SIAM J. Sci. Comput.* **43**, A2404–A2424.

P. Fu, T. Frachon, G. Kreiss and S. Zahedi (2022), High order discontinuous cut finite element methods for linear hyperbolic conservation laws with an interface, *J. Sci. Comput.* **90**, art. 84.

P. Fu, G. Kreiss and S. Zahedi (2024), A bound preserving cut discontinuous Galerkin method for one dimensional hyperbolic conservation laws, *ESAIM Math. Model. Numer. Anal.* **58**, 1651–1680.

H. Garcke, R. Nürnberg and Q. Zhao (2023), Structure-preserving discretizations of two-phase Navier–Stokes flow using fitted and unfitted approaches, *J. Comput. Phys.* **489**, art. 112276.

W. Garhuom and A. Düster (2022), Non-negative moment fitting quadrature for cut finite elements and cells undergoing large deformations, *Comput. Mech.* **70**, 1059–1081.

Y. Georgievskii, E. S. Medvedev and A. A. Stuchebrukhov (2002), Proton transport via the membrane surface, *Biophys J.* **82**, 2833–2846.

B. Giovanardi, L. Formaggia, A. Scotti and P. Zunino (2017), Unfitted FEM for modelling the interaction of multiple fractures in a poroelastic medium, in *Geometrically Unfitted Finite Element Methods and Applications*, Vol. 121 of Lecture Notes in Computational Science and Engineering, Springer, pp. 331–352.

V. Girault and R. Glowinski (1995), Error analysis of a fictitious domain method applied to a Dirichlet problem, *Japan J. Indust. Appl. Math.* **12**, 487–514.

R. Glowinski, T.-W. Pan and J. Périaux (1994), A fictitious domain method for Dirichlet problem and applications, *Comput. Methods Appl. Mech. Engrg* **111**, 283–303.

J. Grande (2014), Eulerian finite element methods for parabolic equations on moving surfaces, *SIAM J. Sci. Comput.* **36**, B248–B271.

J. Grande, C. Lehrenfeld and A. Reusken (2018), Analysis of a high-order trace finite element method for PDEs on level set surfaces, *SIAM J. Numer. Anal.* **56**, 228–255.

S. Gross and A. Reusken (2023), Analysis of optimal preconditioners for CutFEM, *Numer. Linear Algebra Appl.* **30**, art. e2486.

R. Guo, Y. Lin and J. Zou (2023), Solving two-dimensional **H**(curl)-elliptic interface systems with optimal convergence on unfitted meshes, *European J. Appl. Math.* **34**, 774–805.

C. Gürkan and A. Massing (2019), A stabilized cut discontinuous Galerkin framework for elliptic boundary value and interface problems, *Comput. Methods Appl. Mech. Engrg* **348**, 466–499.

C. Gürkan, S. Sticko and A. Massing (2020), Stabilized cut discontinuous Galerkin methods for advection–reaction problems, *SIAM J. Sci. Comput.* **42**, A2620–A2654.

J. Guzmán and M. Olshanskii (2018), Inf-sup stability of geometrically unfitted Stokes finite elements, *Math. Comp.* **87**, 2091–2112.

A. Hansbo and P. Hansbo (2002), An unfitted finite element method, based on Nitsche's method, for elliptic interface problems, *Comput. Methods Appl. Mech. Engrg* **191**, 5537–5552.

A. Hansbo and P. Hansbo (2004), A finite element method for the simulation of strong and weak discontinuities in solid mechanics, *Comput. Methods Appl. Mech. Engrg* **193**, 3523–3540.

A. Hansbo, P. Hansbo and M. G. Larson (2003), A finite element method on composite grids based on Nitsche's method, *ESAIM Math. Model. Numer. Anal.* **37**, 495–514.

P. Hansbo (2005), Nitsche's method for interface problems in computational mechanics, *GAMM-Mitt.* **28**, 183–206.

P. Hansbo, T. Jonsson, M. G. Larson and K. Larsson (2017*a*), A Nitsche method for elliptic problems on composite surfaces, *Comput. Methods Appl. Mech. Engrg* **326**, 505–525.

P. Hansbo, M. G. Larson and K. Larsson (2017*b*), Cut finite element methods for linear elasticity problems, in *Geometrically Unfitted Finite Element Methods and Applications*, Vol. 121 of Lecture Notes in Computational Science and Engineering, Springer, pp. 25–63.

P. Hansbo, M. G. Larson and K. Larsson (2020), Analysis of finite element methods for vector Laplacians on surfaces, *IMA J. Numer. Anal.* **40**, 1652–1701.

P. Hansbo, M. G. Larson and S. Zahedi (2014), A cut finite element method for a Stokes interface problem, *Appl. Numer. Math.* **85**, 90–114.

P. Hansbo, M. G. Larson and S. Zahedi (2015*a*), Characteristic cut finite element methods for convection–diffusion problems on time dependent surfaces, *Comput. Methods Appl. Mech. Engrg* **293**, 431–461.

P. Hansbo, M. G. Larson and S. Zahedi (2015*b*), Stabilized finite element approximation of the mean curvature vector on closed surfaces, *SIAM J. Numer. Anal.* **53**, 1806–1832.

P. Hansbo, M. G. Larson and S. Zahedi (2016), A cut finite element method for coupled bulk–surface problems on time-dependent domains, *Comput. Methods Appl. Mech. Engrg* **307**, 96–116.

J. Haslinger and Y. Renard (2009), A new fictitious domain approach inspired by the extended finite element method, *SIAM J. Numer. Anal.* **47**, 1474–1499.

F. Heimann, C. Lehrenfeld and J. Preuß (2023), Geometrically higher order unfitted space–time methods for PDEs on moving domains, *SIAM J. Sci. Comput.* **45**, B139–B165.

P. Huang, H. Wu and Y. Xiao (2017), An unfitted interface penalty finite element method for elliptic interface problems, *Comput. Methods Appl. Mech. Engrg* **323**, 439–460.

H. Ji, F. Wang and J. Chen (2017), Unfitted finite element methods for the heat conduction in composite media with contact resistance, *Numer. Methods Partial Differential Equations* **33**, 354–380.

A. Johansson and M. G. Larson (2013), A high order discontinuous Galerkin Nitsche method for elliptic problems with fictitious boundary, *Numer. Math.*

T. Jonsson, M. G. Larson and K. Larsson (2017), Cut finite element methods for elliptic problems on multipatch parametric surfaces, *Comput. Methods Appl. Mech. Engrg* **324**, 366–394.

E. N. Karatzas, M. Nonino, F. Ballarin and G. Rozza (2022), A reduced order cut finite element method for geometrically parametrized steady and unsteady Navier–Stokes problems, *Comput. Math. Appl.* **116**, 140–160.

P. Kerfriden, S. Claus and I. Mihai (2020), A mixed-dimensional CutFEM methodology for the simulation of fibre-reinforced composites, *Adv. Model. Simul. Eng. Sci.* **7**, art. 18.

M. Kirchhart, S. Gross and A. Reusken (2016), Analysis of an XFEM discretization for Stokes interface problems, *SIAM J. Sci. Comput.* **38**, A1019–A1043.

M. Köppel, V. Martin and J. E. Roberts (2019*a*), A stabilized Lagrange multiplier finite-element method for flow in porous media with fractures, *GEM Int. J. Geomath.* **10**, art. 7.

M. Köppel, V. Martin, J. Jaffré and J. E. Roberts (2019*b*), A Lagrange multiplier method for a discrete fracture model for flow in porous media, *Comput. Geosci.* **23**, 239–253.

H. Kothari and R. Krause (2022), A generalized multigrid method for solving contact problems in Lagrange multiplier based unfitted finite element method, *Comput. Methods Appl. Mech. Engrg* **392**, art. 114630.

M. G. Larson and S. Zahedi (2019), Stabilization of high order cut finite element methods on surfaces, *IMA J. Numer. Anal.* **40**, 1702–1745.

M. G. Larson and S. Zahedi (2023), Conservative cut finite element methods using macroelements, *Comput. Methods Appl. Mech. Engrg* **414**, art. 116141.

C. Lehrenfeld (2015), The Nitsche XFEM-DG space–time method and its implementation in three space dimensions, *SIAM J. Sci. Comput.* **37**, A245–A270.

C. Lehrenfeld (2016), High order unfitted finite element methods on level set domains using isoparametric mappings, *Comput. Methods Appl. Mech. Engrg* **300**, 716–733.

C. Lehrenfeld and M. Olshanskii (2019), An Eulerian finite element method for PDEs in time-dependent domains, *ESAIM Math. Model. Numer. Anal.* **53**, 585–614.

C. Lehrenfeld and A. Reusken (2013), Analysis of a Nitsche XFEM-DG discretization for a class of two-phase mass transport problems, *SIAM J. Numer. Anal.* **51**, 958–983.

C. Lehrenfeld and A. Reusken (2017), Optimal preconditioners for Nitsche-XFEM discretizations of interface problems, *Numer. Math.* **135**, 313–332.

C. Lehrenfeld and A. Reusken (2018), Analysis of a high-order unfitted finite element method for elliptic interface problems, *IMA J. Numer. Anal.* **38**, 1351–1387.

C. Lehrenfeld, T. van Beeck and I. Voulis (2023), Analysis of divergence-preserving unfitted finite element methods for the mixed Poisson problem. Available at arXiv:2306.12722.

B. Liu (2021), A Nitsche stabilized finite element method: Application for heat and mass transfer and fluid–structure interaction, *Comput. Methods Appl. Mech. Engrg* **386**, art. 114101.

H. Liu, M. Neilan and M. Olshanskii (2023), A CutFEM divergence-free discretization for the Stokes problem, *ESAIM Math. Model. Numer. Anal.* **57**, 143–165.

Y. Lou and C. Lehrenfeld (2022), Isoparametric unfitted BDF–finite element method for PDEs on evolving domains, *SIAM J. Numer. Anal.* **60**, 2069–2098.

T. Ludescher, S. Gross and A. Reusken (2020), A multigrid method for unfitted finite element discretizations of elliptic interface problems, *SIAM J. Sci. Comput.* **42**, A318–A342.

C. Ma, Q. Zhang and W. Zheng (2022), A fourth-order unfitted characteristic finite element method for solving the advection–diffusion equation on time-varying domains, *SIAM J. Numer. Anal.* **60**, 2203–2224.

A. Main and G. Scovazzi (2018), The shifted boundary method for embedded domain computations, Part I: Poisson and Stokes problems, *J. Comput. Phys.* **372**, 972–995.

A. Massing, M. G. Larson, A. Logg and M. E. Rognes (2014), A stabilized Nitsche fictitious domain method for the Stokes problem, *J. Sci. Comput.* **61**, 604–628.

A. Massing, M. G. Larson, A. Logg and M. E. Rognes (2015), A Nitsche-based cut finite element method for a fluid–structure interaction problem, *Commun. Appl. Math. Comput. Sci.* **10**, 97–120.

A. Massing, B. Schott and W. A. Wall (2018), A stabilized Nitsche cut finite element method for the Oseen problem, *Comput. Methods Appl. Mech. Engrg* **328**, 262–300.

R. Massjung (2012), An unfitted discontinuous Galerkin method applied to elliptic interface problems, *SIAM J. Numer. Anal.* **50**, 3134–3162.

B. Maury (2009), Numerical analysis of a finite element/volume penalty method, *SIAM J. Numer. Anal.* **47**, 1126–1148.

S. May and M. Berger (2017), An explicit implicit scheme for cut cells in embedded boundary meshes, *J. Sci. Comput.* **71**, 919–943.

S. May and F. Laakmann (2024), Accuracy analysis for explicit–implicit finite volume schemes on cut cell meshes, *Commun. Appl. Math. Comput.* **6**, 2239–2264.

M. McCracken and C. Peskin (1980), A vortex method for blood flow through heart valves, *J. Comput. Phys.* **35**, 183–205.

E. Mikaeili, S. Claus and P. Kerfriden (2022), Concurrent multiscale analysis without meshing: Microscale representation with CutFEM and micro/macro model blending, *Comput. Methods Appl. Mech. Engrg* **393**, art. 114807.

N. Moës, J. Dolbow and T. Belytschko (1999), A finite element method for crack growth without remeshing, *Int. J. Numer. Methods Engrg* **46**, 131–150.

S. Myrbäck (2022), Conservative discontinuous cut finite element methods: Convection–diffusion problems in evolving bulk-interface domains. Master's thesis, KTH Royal Institute of Technology.

S. Myrbäck and S. Zahedi (2024), A high-order conservative cut finite element method for problems in time-dependent domains, *Comput. Methods Appl. Mech. Engrg* **431**, art. 117245.

J.-C. Nédélec (1976), Curved finite element methods for the solution of singular integral equations on surfaces in R^3, *Comput. Methods Appl. Mech. Engrg* **8**, 61–80.

J. A. Nitsche (1971), Über ein Variationsprinzip zur Lösung von Dirichlet-Problemen bei Verwendung von Teilräumen, die keinen Randbedingungen unterworfen sind, *Abh. Math. Univ. Hamburg* **36**, 9–15.

L. H. Odsæter, T. Kvamsdal and M. G. Larson (2019), A simple embedded discrete fracture-matrix model for a coupled flow and transport problem in porous media, *Comput. Methods Appl. Mech. Engrg* **343**, 572–601.

M. A. Olshanskii and A. Reusken (2014), Error analysis of a space–time finite element method for solving PDEs on evolving surfaces, *SIAM J. Numer. Anal.* **52**, 2092–2120.

M. A. Olshanskii and A. Reusken (2017), Trace finite element methods for PDEs on surfaces, in *Geometrically Unfitted Finite Element Methods and Applications*, Vol. 121 of Lecture Notes in Computational Science and Engineering, Springer, pp. 211–258.

M. A. Olshanskii and D. Safin (2016), Numerical integration over implicitly defined domains for higher order unfitted finite element methods, *Lobachevskii J. Math.* **37**, 582–596.

M. A. Olshanskii, A. Quaini, A. Reusken and V. Yushutin (2018), A finite element method for the surface Stokes problem, *SIAM J. Sci. Comput.* **40**, A2492–A2518.

M. A. Olshanskii, A. Reusken and J. Grande (2009), A finite element method for elliptic equations on surfaces, *SIAM J. Numer. Anal.* **47**, 3339–3358.

M. A. Olshanskii, A. Reusken and X. Xu (2014), An Eulerian space–time finite element method for diffusion problems on evolving surfaces, *SIAM J. Numer. Anal.* **52**, 1354–1377.

M. Olshanskii and H. von Wahl (2024), A conservative Eulerian finite element method for transport and diffusion in moving domains. Available at arXiv:2404.07130.

M. Olshanskii, Y. Palzhanov and A. Quaini (2023), A scalar auxiliary variable unfitted FEM for the surface Cahn–Hilliard equation, *J. Sci. Comput.* **97**, art. 57.

M. Olshanskii, A. Quaini and Q. Sun (2021), An unfitted finite element method for two-phase Stokes problems with slip between phases, *J. Sci. Comput.* **89**, art. 41.

S. Osher and R. P. Fedkiw (2001), Level set methods: An overview and some recent results, *J. Comput. Phys.* **169**, 463–502.

J. Parvizian, A. Düster and E. Rank (2007), Finite cell method: *h*- and *p*-extension for embedded domain problems in solid mechanics, *Comput. Mech.* **41**, 121–133.

C. S. Peskin (2002), The immersed boundary method, *Acta Numer.* **11**, 479–517.

J. Pitkäranta (1980), Local stability conditions for the Babuška method of Lagrange multipliers, *Math. Comp.* **35**, 1113–1129.

M. Poluektov and L. Figiel (2022), A cut finite-element method for fracture and contact problems in large-deformation solid mechanics, *Comput. Methods Appl. Mech. Engrg* **388**, art. 114234.

J. Preuß (2018), Higher order unfitted isoparametric space–time FEM on moving domains. Master's thesis, University of Göttingen.

A. Reusken (2008), Analysis of an extended pressure finite element space for two-phase incompressible flows, *Comput. Vis. Sci.* **11**, 293–305.

A. Reusken (2015), Analysis of trace finite element methods for surface partial differential equations, *IMA J. Numer. Anal.* **35**, 1568–1590.

M. Ruess, D. Schillinger, Y. Bazilevs, V. Varduhn and E. Rank (2013), Weakly enforced essential boundary conditions for NURBS-embedded and trimmed NURBS geometries on the basis of the finite cell method, *Int. J. Numer. Methods Engrg* **95**, 811–846.

R. I. Saye (2015), High-order quadrature methods for implicitly defined surfaces and volumes in hyperrectangles, *SIAM J. Sci. Comput.* **37**, A993–A1019.

R. I. Saye (2022), High-order quadrature on multi-component domains implicitly defined by multivariate polynomials, *J. Comput. Phys.* **448**, art. 110720.

B. Schott, C. Ager and W. A. Wall (2019), A monolithic approach to fluid–structure interaction based on a hybrid Eulerian-ALE fluid domain decomposition involving cut elements, *Int. J. Numer. Methods Engrg* **119**, 208–237.

J. A. Sethian (2001), Evolution, implementation, and application of level set and fast marching methods for advancing fronts, *J. Comput. Phys.* **169**, 503–555.

E. M. Stein (1970), *Singular Integrals and Differentiability Properties of Functions*, Vol. 30 of Princeton Mathematical Series, Princeton University Press.

R. Stenberg (1995), On some techniques for approximating boundary conditions in the finite element method, *J. Comput. Appl. Math.* **63**, 139–148.

S. Sticko and G. Kreiss (2016), A stabilized Nitsche cut element method for the wave equation, *Comput. Methods Appl. Mech. Engrg* **309**, 364–387.

S. Sticko and G. Kreiss (2019), Higher order cut finite elements for the wave equation, *J. Sci. Comput.* **80**, 1867–1887.

S. Sticko, G. Ludvigsson and G. Kreiss (2020), High-order cut finite elements for the elastic wave equation, *Adv. Comput. Math.* **46**, art. 45.

M. E. Taylor (2023), *Partial Differential Equations I: Basic Theory*, Vol. 115 of Applied Mathematical Sciences, third edition, Springer.

I. Tchinda Ngueyong and J. M. Urquiza (2024), Fictitious domain method: A stabilized post-processing technique for boundary-flux calculation using cut elements, *Comput. Methods Appl. Mech. Engrg* **418**, art. 116509.

I. Tchinda Ngueyong, J. M. Urquiza and D. Martin (2024*a*), A CutFEM method for phase change problems with natural convection, *Comput. Methods Appl. Mech. Engrg* **420**, art. 116713.

I. Tchinda Ngueyong, J. M. Urquiza and D. Martin (2024*b*), A Nitsche-based cut finite element solver for two-phase Stefan problems, *Int. J. Numer. Methods Engrg* **125**, art. e7408.

C. H. Villanueva and K. Maute (2017), CutFEM topology optimization of 3D laminar incompressible flow problems, *Comput. Methods Appl. Mech. Engrg* **320**, 444–473.

H. von Wahl and T. Richter (2023), Error analysis for a parabolic PDE model problem on a coupled moving domain in a fully Eulerian framework, *SIAM J. Numer. Anal.* **61**, 286–314.

H. von Wahl, T. Richter and C. Lehrenfeld (2022), An unfitted Eulerian finite element method for the time-dependent Stokes problem on moving domains, *IMA J. Numer. Anal.* **42**, 2505–2544.

E. Wadbro, S. Zahedi, G. Kreiss and M. Berggren (2013), A uniformly well-conditioned, unfitted Nitsche method for interface problems, *BIT Numer. Math.* **53**, 791–820.

M. Winter, B. Schott, A. Massing and W. A. Wall (2018), A Nitsche cut finite element method for the Oseen problem with general Navier boundary conditions, *Comput. Methods Appl. Mech. Engrg* **330**, 220–252.

H. Wu and Y. Xiao (2019), An unfitted *hp*-interface penalty finite element method for elliptic interface problems, *J. Comput. Math.* **37**, 316–339.

F. Yang (2024), The least squares finite element method for elasticity interface problem on unfitted mesh, *ESAIM Math. Model. Numer. Anal.* **58**, 695–721.

F. Yang and X. Xie (2024), An unfitted finite element method with direct extension stabilization for time-harmonic Maxwell problems on smooth domains, *Adv. Comput. Math.* **50**, art. 51.

S. Zahedi (2017), A space–time cut finite element method with quadrature in time, in *Geometrically Unfitted Finite Element Methods and Applications*, Vol. 121 of Lecture Notes in Computational Science and Engineering, Springer, pp. 281–306.

K. Zhang, W. Deng and H. Wu (2024), A CutFE-LOD method for the multiscale elliptic problems on complex domains, *J. Comput. Appl. Math.* **445**, art. 115820.

L. Zhang, A. Gerstenberger, X. Wang and W. K. Liu (2004), Immersed finite element method, *Comput. Methods Appl. Mech. Engrg* **193**, 2051–2067.

S. Zonca, C. Vergara and L. Formaggia (2018), An unfitted formulation for the interaction of an incompressible fluid with a thick structure via an XFEM/DG approach, *SIAM J. Sci. Comput.* **40**, B59–B84.